

THE SOLVENT CAGE EFFECT: USING MICROVISCOSITY TO PREDICT THE
RECOMBINATION EFFICIENCY OF GEMINATE RADICALS FORMED BY THE
PHOTOLYSIS OF THE MO-MO BOND OF $CP'_2MO_2(CO)_6$

by

JUSTIN THOMAS BARRY

A DISSERTATION

Presented to the Department of Chemistry and Biochemistry
and the Graduate School of the University of Oregon
in partial fulfillment of the requirements
for the degree of
Doctor of Philosophy

June 2018

DISSERTATION APPROVAL PAGE

Student: Justin Thomas Barry

Title: The Solvent Cage Effect: Using Microviscosity to Predict the Recombination Efficiency of Geminate Radicals Formed by the Photolysis of the Mo-Mo Bond of $\text{Cp}'_2\text{Mo}_2(\text{CO})_6$

This dissertation has been accepted and approved in partial fulfillment of the requirements for the Doctor of Philosophy degree in the Department of Chemistry and Biochemistry by:

Dr. Michael D. Pluth	Chairperson
Dr. David R. Tyler	Advisor
Dr. James E. Hutchison	Core Member
Dr. Bruce P. Branchaud	Core Member
Dr. Miriam Deutsch	Institutional Representative

and

Dr. Sara D. Hodges	Interim Vice Provost and Dean of the Graduate School
--------------------	--

Original approval signatures are on file with the University of Oregon Graduate School.

Degree awarded June 2018

© 2018 Justin Thomas Barry

DISSERTATION ABSTRACT

Justin Thomas Barry

Doctor of Philosophy

Department of Chemistry and Biochemistry

June 2018

Title: The Solvent Cage Effect: Using Microviscosity to Predict the Recombination Efficiency of Geminate Radicals Formed by the Photolysis of the Mo-Mo Bond of $\text{Cp}'_2\text{Mo}_2(\text{CO})_6$

Radicals are core reactive species that occur in almost every subfield of chemistry. In particular, solution phase radicals find their way into biochemistry (e.g. vitamin B₁₂), and in polymer chemistry (e.g. radical polymerizations) just to name a few. Yet, given the proliferation of radical chemistry, there are still fundamental aspects of it that are poorly understood.

This dissertation probed factors that influence the solvent cage effect. The solvent cage effect is where two radicals are held in close proximity to one another and prevented from easily escaping (to form free radicals) by a cage of solvent molecules. A convenient metric of the solvent cage effect is the radical recombination efficiency (F_{CP}). Typically, F_{CP} correlates with the bulk viscosity of the solution, however, this parameter only produces qualitative assessments. This dissertation outlines a method to *quantitatively* predict F_{CP} using the *microviscosity*. This microviscosity dependence holds for non-polar, aromatic, polar, and hydrogen-bonding solvents, along with solutions that contain polymers. Microviscosity is a great metric because it addresses an underlying reason for the solvent cage effect, the strength of the cage.

Not only does the strength of the solvent cage around the radical pair affect F_{CP} ,

but so does the identity of the radicals themselves. That is, the strength of the solvent cage is one piece to forming a total predictive model. F_{cP} for the $Cp^*_2Mo_2(CO)_6$ dimer also varies with the wavelength of irradiation. Identifying the mechanism by which this wavelength dependence occurs may also provide another factor to include in an overall model of the solvent cage effect. Also, an attempt at synthesizing an asymmetric molybdenum dimer was performed. This asymmetric dimer would allow the study of solvent caged radical pairs that are different from each other.

Predicting the photochemical cage pair recombination efficiency (F_{cP}) is the major topic of this dissertation. However, there is also the collisional cage recombination efficiency (F_c'). This is where *free* radicals come together in what is called a collisional solvent cage pair. A method and values of F_c' are detailed later in this dissertation.

This dissertation contains previously published and unpublished co-authored material.

CURRICULUM VITAE

NAME OF AUTHOR: Justin Thomas Barry

GRADUATE AND UNDERGRADUATE SCHOOLS ATTENDED:

University of Oregon, Eugene OR
Southern Oregon University, Ashland OR

DEGREES AWARDED:

Doctor of Philosophy, Chemistry, 2018, University of Oregon
Master of Science, Chemistry of Polymers and Coatings, 2012, University of Oregon
Bachelor of Science, ACS Biochemistry, 2011, Southern Oregon University

AREAS OF SPECIAL INTEREST:

Photochemistry
Inorganic Chemistry
Organometallic Chemistry
Polymer Chemistry

PROFESSIONAL EXPERIENCE:

Teaching Assistant for University of Oregon Materials Science Institute Masters
Polymer and Coatings Laboratory

Teaching Assistant for University of Oregon Organic Chemistry Laboratory

Teaching Assistant for University of Oregon Honors General Chemistry Lecture

Teaching Assistant for University of Oregon Instrumental Analysis Laboratory

Intern Chemist for Momentive Specialty Chemicals Adhesive Division

GRANTS, AWARDS, AND HONORS:

Graduate Student Award for Excellence in the Teaching of Chemistry, University
of Oregon, 2013-2014

College of Arts and Sciences Dissertation Research Fellowship, University of Oregon, 2017

PUBLICATIONS:

- (1) Barry, J. T.; Berg, D. J.; Tyler, D. R. Radical Cage Effects: The Prediction of Radical Cage Pair Recombination Efficiencies Using Microviscosity Across a Range of Solvent Types. *J. Am. Chem. Soc.* **2017**, *139*, 14399–14405.
- (2) Barry, J. T.; Berg, D. J.; Tyler, D. R. Radical Cage Effects: Comparison of Solvent Bulk Viscosity and Microviscosity in Predicting the Recombination Efficiencies of Radical Cage Pairs. *J. Am. Chem. Soc.* **2016**, *138*, 9389–9392.
- (3) Kendall, A. J.; Barry, J. T.; Seidenkranz, D. T.; Ryerson, A.; Hiatt, C.; Salazar, C. A.; Bryant, D. J.; Tyler, D. R. Highly Efficient Biphasic Ozonolysis of Alkenes Using a High-Throughput Film-Shear Flow Reactor. *Tetrahedron Lett.* **2016**, *57*, 1342–1345.

ACKNOWLEDGMENTS

Graduate school would have been a bitter journey without the support and the friendship of so many people. My family was truly the best support system that I could have ever hoped for. My parents never doubted my potential and were always encouraging. My sister Nichole and brother-in-law Marshall helped by commiserating about their physics graduate school, turns out graduate school is tough in every subject. My girlfriend Emily, thank you for listening to so much chemistry over the years, without you I wouldn't have made it.

Within graduate school I was very lucky to have so many friends and frenemies. When I joined the Tyler lab, I was thrilled to have the support and friendship of Sarah Brady, Chantal Balesdent, Bryan Nell, Emma Downs, and Alex Kendall. After I joined, I was very lucky to hang with the new crew of Adrian Henle, Dan Seidenkranz, and Stephanie Nappa. There are so many fond memories and stories with these people who made work always feel like a second home. Professor Tyler had an immense impact on my academic career by being a great PI as well as a friend. The Tyler lab was also fortunate enough to have many wonderful undergraduate researchers. Although I was technically their mentor, I always learned something new from each of them.

I am very appreciative to the committee that I had. Professors Mike Pluth, Jim Hutchison, Bruce Branchaud, and Miriam Deutsch always had their doors and ears open to me and for that, I am grateful. I would like to acknowledge the National Science Foundation for funding that made my dissertation research possible.

Dedicated to my family; David, Lisa, Nichole, Marshall, and Emily.

TABLE OF CONTENTS

Chapter	Page
I. SOLVENT CAGE EFFECTS FROM METAL BASED RADICALS	1
1.1. Introduction.....	1
1.2. Describing the Solvent Cage Effect with Kinetic Terms.....	2
1.3. Measuring F_{cP} with Bulk Photolysis.....	4
1.4. F_{cP} Dependence on Mass and Size of the Radical	8
1.5. Spin-Orbit Coupling in Metal Based Radicals.....	14
1.6. Primary and Secondary Solvent Cages	18
1.7. Bridge.....	21
II. RADICAL CAGE EFFECTS: COMPARISON OF SOLVENT BULK VISCOSITY AND MICROVISCOSITY IN PREDICTING THE RECOMBINATION EFFICIENCIES OF RADICAL CAGE PAIRS	23
2.1. Introduction.....	23
2.2. Results and Discussion	25
2.3. Conclusions.....	30
2.4. Bridge.....	31
III. RADICAL CAGE EFFECTS: THE PREDICTION OF RADICAL CAGE PAIR RECOMBINATION EFFICIENCIES USING MICROVISCOSITY ACROSS A RANGE OF SOLVENT TYPES	32

Chapter	Page
3.1. Introduction.....	32
3.2. Methods.....	35
3.3. Results and Discussion	39
3.4. Conclusions.....	52
3.5. Bridge.....	53
IV. WAVELENGTH DEPENDENCE OF RECOMBINATION EFFICIENCIES OF RADICAL CAGE PAIRS GENERATED FROM $CP_2'MO_2(CO)_6$ DIMER	54
4.1. Introduction.....	54
4.2. Results.....	56
4.3. Discussion and Conclusions	59
4.4. Bridge.....	61
V. PROGRESS TOWARDS AN ASYMMETRIC MOLYBDENUM DIMER TO STUDY SIZE AND MASS DEPENDENCE ON F_{CP} OF ASSYMETRIC RADICAL PAIRS IN A SOLVENT CAGE	62
5.1. Introduction.....	62
5.2. Synthesis	69
5.3. Summary	82
5.4. Bridge.....	83

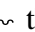
Chapter	Page
VI. A COMPARISON OF PHOTOCHEMICAL AND COLLISIONAL CAGE	
RECOMBINATION EFFICIENCIES	84
6.1. Introduction.....	84
6.2. Results.....	89
6.3. Discussion	94
6.4. Concluding Summary	98
APPENDICES	100
A. SUPPORTING INFORMATION FOR CHAPTER I.....	100
B. SUPPORTING INFORMATION FOR CHAPTER II.....	112
C. SUPPORTING INFORMATION FOR CHAPTER III	122
D. SUPPORTING INFORMATION FOR CHAPTER V	132
E. SUPPORTING INFORMATION FOR CHAPTER VI	139
F. CRYSTAL STRUCTURES	145
REFERENCES CITED.....	168

LIST OF FIGURES

Figure	Page
1.1. F_{CP} dependence on bulk viscosity for two $Cp'_2M_2(CO)_6$ dimers (where $M = Mo, W$). Paraffin oil/ <i>n</i> -hexane/ CCl_4 solvent system at $23\text{ }^\circ C$, $h\nu$ at 550 nm, with error $\pm 2\sigma$	7
1.2. Plot of F_{CP} vs bulk viscosity for the functionalized $(R_3SiOCH_2CH_2Cp)_2Mo_2(CO)_6$ dimers (R identity indicated by legend). Mineral oil/ <i>n</i> -hexane/ CCl_4 solvent system at $23 \pm 1\text{ }^\circ C$, $h\nu$ at 540 nm, with error $\pm 1\sigma$	10
1.3. Plot of $F_{CP}^{-1}-1$ vs $mass^{0.5}/radius^2$ for the functionalized $(R_3SiOCH_2CH_2Cp)_2Mo_2(CO)_6$ dimers. Dashed lines follow along the same identity of R-group on the dimer. Solid lines are linear best-fit. Mineral oil/ <i>n</i> -hexane/ CCl_4 solvent system at $23 \pm 1\text{ }^\circ C$, $h\nu$ at 540 nm.....	11
1.4. Plot of $F_{CP}^{-1}-1$ vs $mass^{0.5}/(effective\ radius)^2$ for molybdenum dimers 6-6 , 7-7 , and 8-8 (see Scheme 1.6). ³⁷ (Hexanes/squalane (viscogen)/ CCl_4 solvent system with $h\nu = 546\text{ nm}$.).....	13
1.5. Plot of F_{CP} vs viscosity for $Cp'_2W_2(CO)_6$, $Cp'_2Mo_2(CO)_6$ and $(Me_3SiOCH_2CH_2Cp)_2Mo_2(CO)_6$ in hexane/mineral oil/ CCl_4 at $23 \pm 1\text{ }^\circ C$, error $\pm 1\sigma$	14
1.6. Plot of Φ_{Obs} vs bulk viscosity for three organometallic complexes. Filled symbols and solid best-fit lines represent data collected in the presence of 2.0 M 1-chlorobenzene. Open symbols and dashed best-fit lines represent data	

Figure	Page
collected in the presence of 2.0 M 1-iodobenzene. (<i>n</i> -hexane, squalane/CCl ₄)	16
1.7. A comparison of what the reaction coordinate may look like for both a Mo-Mo and a W-W bond. The energies of the two cage pairs are shown as equal to assist in the comparison	17
2.1. Plot of cage recombination efficiency (F_{cP}) as a function of solvent system bulk viscosity (cP). Each sample contains 20 wt% CCl ₄ ; error bars are 1 σ ; and the curves are only a visual guide.....	27
2.2. Cage recombination efficiency (F_{cP}) plotted as a function of microviscosity ($1/D$). Each sample contains 20 wt% CCl ₄ , error bars are 1 σ ; and the curves are only a visual guide	29
3.1. A plot of F_{cP} as a function of bulk viscosity (cP). Each sample contains 20 wt% CCl ₄ ; error bars are 1 σ ; curves are only a visual aid. The toluene/polystyrene data has been truncated for clarity, see Figure C.6.....	41
3.2. A plot of F_{cP} as a function of microviscosity. Each sample contains 20 wt% CCl ₄ ; error bars are 1 σ ; a single curve is used as a visual aid	43
3.3. A plot of F_{cP} as a function of bulk viscosity (cP). Each sample contains 20 wt% CCl ₄ ; error bars are 1 σ ; curves are only a visual aid.	45
3.4. A plot of F_{cP} as a function of microviscosity. Each sample contains 20 wt% CCl ₄ ; error bars are 1 σ ; a single curve is used as a visual aid. This plot contains all of the solvent systems tested in this study	46
3.5. A plot of Φ_{obsd} as a function of polarity ($E_{(NR)}$, see 3.3 Methods, Determination	

Figure	Page
of Solvent Polarity). Error bars are 1σ	47
3.6. Monomer and excimer fluorescence of pyrene at different viscosities. Solvent system is hexane/paraffin with CCl_4 constant at 20 wt%. Concentration of pyrene is constant between samples at 10 mM ($25.0 \text{ }^\circ\text{C} \pm 0.05 \text{ }^\circ\text{C}$)	49
3.7. A plot of F_{CP} as a function ratio of monomer fluorescence to excimer fluorescence. Each sample contains 20 wt% CCl_4 ; error bars are 1σ ; curves are only a visual aid	50
4.1. Plot of intensity of the 200 W high pressure mercury arc lamp vs wavelength selected on monochrometer (blue dashed trace). Electronic spectrum of $\text{Cp}'_2\text{Mo}_2(\text{CO})_6$ dimer also plotted (green trace). Selected wavelengths for irradiation are red circles on green trace.....	57
4.2. Plot of F_{CP} vs bulk viscosity with irradiation at different wavelengths for the $\text{Cp}'_2\text{Mo}_2(\text{CO})_6$ dimer. The 505 nm data set contains two more points off scale at 10.0 and 20.6 cP. (<i>n</i> -hexane/paraffin oil/ CCl_4 solvent system at $25 \pm 0.1 \text{ }^\circ\text{C}$).....	58
4.3. Solvent molecules (white circles) participating in intermolecular vibrational energy transfer (blue dashed lines) from the radical pair (red circles). Secondary solvent cage shows the solvent molecule (green circle) separating the radical pair.....	60
5.1. Electronic spectrum of both the $\text{Cp}'_2\text{Mo}_2(\text{CO})_6$ dimer and $\text{Cp}'\text{Mo}-\text{Cl}(\text{CO})_3$	63
5.2. ^1H -NMR of the $\text{Cp}'_2\text{Mo}_2(\text{CO})_6$ dimer (in CDCl_3 , not T1 optimized, Acros).....	64
5.3. Infrared spectrum of $\text{Cp}'_2\text{Mo}_2(\text{CO})_6$ dimer (in DCM, solvent subtracted)	64

Figure	Page
5.4. Examples of organometallic molecules where photolysis results in a solvent caged radical pair that contains two different sized radicals. (Bond breaking indicated by red bond with  through it).....	66
5.5. ¹ H-NMR of complex [17]	73
5.6. FT-IR spectrum of [17] (solvent subtracted from DCM)	74
5.7. Monitoring the reaction of Scheme 11 by FT-IR.....	79
6.1. Plot of rate vs rate ² /[CCl ₄] ² for solution set 1 (error ±1σ). Solution properties; $\eta = 0.853 \pm 0.003$ cp, $D = 1.58 \pm 0.06 \times 10^{-9}$ m ² /s, slope of best-fit = -2.846.....	90
6.2. Plot of rate vs rate ² /[CCl ₄] ² for solution set 2 (error ±1σ). Solution properties; $\eta = 7.06 \pm 0.02$ cp, $D = 0.32 \pm 0.03 \times 10^{-9}$ m ² ·s ⁻¹ , slope of best-fit line = -3.3974.....	91
6.3. Plot of inverse bulk viscosity (cP ⁻¹) vs k_D (determined by k_d molarity) values for a set of different neat solvents (one data point omitted). (best-fit: $f(x) = (4.1586 \times 10^9)(x) + (5.5843 \times 10^9)$, error bars ± 1σ).....	94

LIST OF TABLES

Table	Page
1.1. Primary (F_{c1}), secondary (F_{c2}), net (F_{cP}) recombination efficiencies for (RCp) ₂ Mo ₂ (CO) ₆ dimer, where R = -CH ₂ CH ₂ N(CH ₃)C(O)(CH ₂) _n CH ₃ (see Scheme 1.6)	20
2.1. Solvents and viscosogens used in this study	28
3.1. Properties of the DMF/CCl ₄ mixed solvent systems	47
4.1. Wavelengths of irradiation with energy conversion	60
6.1. Properties of solutions used in this study.....	90
6.2. Approximated values of k_D using either bulk viscosity (η) or diffusion coefficient (D). F_c' is calculated using these values	93
6.3. F_c' values calculated using experimental k_d values.....	94
6.4. Compilation of collisional cage recombination (F_c') values for two solutions of differing bulk viscosity (η). Compared with the photochemical cage recombination efficiency (F_{cP}).....	95

LIST OF SCHEMES

Scheme	Page
1.1. Mechanistic model of the solvent cage effect. Radicals are generated from the generic molecule R-R by photolysis	3
1.2. Photolysis of the $\text{Cp}'_2\text{Mo}_2(\text{CO})_6$ dimer homolytically splits the Mo-Mo bond.....	5
1.3. Mechanistic model of the solvent cage effect with a radical trap.....	5
1.4. Molybdenum dimer with ligand modifications to increase size and mass	9
1.5. In-cage trapping of the molybdenum-centered radical by an amide-H atom. R-groups vary in length as $\text{R} = -(\text{CH}_2)_n\text{CH}_3$ with ($n = 3, 8, 13, 18$)	12
1.6. Functionalized molybdenum dimer with methyl groups in place of amide-H atoms from Scheme 1.5.....	13
1.7. Photolysis of a generic R-R dimer that results in an initial triplet state	15
1.8. Mechanistic model for primary and secondary solvent cage effects	19
1.9. Full scheme for the solvent cage effect including photochemical geminate and collisional non-geminate radical pairs. Secondary radical pairs are indicated by a solvent molecule (S) between the two radicals. Non-geminate radical pairs are indicated by the mis-match color scheme (green and red) of the radicals. Misalignment situations are indicated by the orientation of the radical (\bullet)	22
2.1. Photodissociation of a general molecule (R-R) that results in a radical cage pair	25
2.2. Photolysis of $\text{Cp}'_2\text{Mo}_2(\text{CO})_6$ results in a caged radical pair.....	26

Scheme	Page
3.1. Photodissociation of a general Molecule (R-R) results in a radical cage pair	33
3.2. Photochemical production of caged radicals and subsequent trapping by CCl ₄	37
4.1. Conceptual diagram of the two halves [CpM(CO) ₃] of a Cp ₂ M ₂ (CO) ₆ dimer to illustrate the electronic transitions (M = Mo, or W). Green arrows represent the electronic transitions	55
5.1. Restrosynthesis of an asymmetric dimer using the “cation/anion” approach.....	67
5.2. Generation of molybdenum dimers using the “one electron oxidation” method.....	68
5.3. “Photochemical cross-over” method of synthesizing an asymmetric dimer	69
5.4. Synthetic route to the anion complex [15].....	70
5.5. Synthetic route to a “cation” complex	71
5.6. Final synthetic step of the “cation/anion” method to form an asymmetric dimer complex [17]	73
5.7. Electron transfer between the “cation” and “anion” resulting in both symmetric and asymmetric dimer products	75
5.8. Literature synthesis of a mixed ligand dimer.....	76
5.9. Synthesis of anion [20] and bromide [21] complexes	76
5.10. Reaction conditions according to literature procedure	77
5.11. Reaction of a bromide complex [23] with a substituted cyclopentadiene ligand with an anion complex [22]	78

Scheme	Page
5.12. Fast halogen exchange leads to a scrambling of the initial reactants, generating three potential reaction pairs. In this case, only the cyclopentadiene substituted molybdenum(0) anion and molybdenum(II) bromide react quickly and for the observed $\text{Cp}_2\text{Mo}_2(\text{CO})_6$ dimer	81
6.1. Cross-over experiment using azomethanes in either the gas-phase or in a solution of isooctane	85
6.2. Mechanistic model of the geminate photochemical cage effect	86
6.3. Expanded mechanistic model of the solvent cage effect that includes a primary and secondary solvent caged radical pair.....	87
6.4. Mechanistic model of the solvent cage effect with a smaller concentration of radical trap (CCl_4) than in Scheme 6.2	88
6.5. Full scheme for the solvent cage effect including photochemical geminate and collisional non geminate radical pairs. Secondary radical pairs are indicated by a solvent molecule (S) between the two radicals. Non-geminate radical pairs are indicated by the mis-match color scheme (green and red) of the radicals. Radical dots indicate whether there is correct or incorrect orientation for recombination	97

CHAPTER I

SOLVENT CAGE EFFECTS FROM METAL BASED RADICALS

Justin T. Barry, David R. Tyler*

Department of Chemistry and Biochemistry, University of Oregon, Eugene, OR

97403-1253

Chapter I of my dissertation will be an introduction into the field of solvent cage effects using metal based radicals. This chapter will introduce the body of research on solvent cage effects that has been produced in the Tyler lab. This will frame the majority of the work of this dissertation in the historical context of the project. A brief introduction into photochemical kinetics with derivations is included as Appendix A.

Chapter I will be published as a peer-reviewed review of solvent cage effects with the co-authorship of David R. Tyler. Chapters II and III were also produced with the co-authorship of David R. Tyler, as well as, Daniel J. Berg. Chapter VI will be published as a peer-reviewed research article with the co-authorship of David R. Tyler.

1.1. Introduction

Solvent “cage effects” have a major impact on chemical reactivity and chemical kinetics in nearly all fields of chemistry. For example, in organic chemistry, cage effects

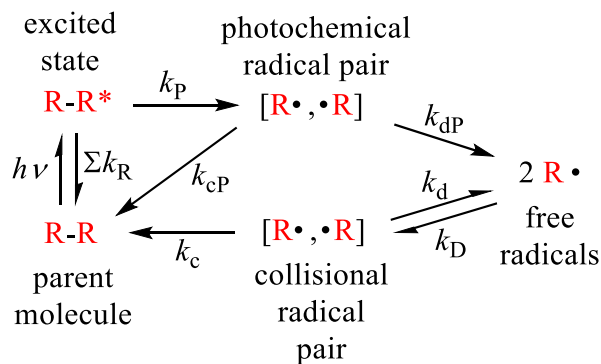
are necessary to explain such fundamental phenomena as magnetic isotope^{1,2} and CIDNP effects^{3,4}, rate-viscosity correlations⁵, and regio- and stereo-chemical control.^{6,7} In polymer chemistry, they explain the subtleties of radical polymerization kinetics.⁸⁻¹³ In biochemistry, cage effects are pervasive, as in the reactions of photosynthetic model complexes and the reactions of hemes with O₂.¹⁴ In inorganic chemistry, to give just one example of many, they are necessary to explain electron transfer reactions.¹⁵⁻¹⁸ The caging phenomenon is not limited to solutions but has also been observed on surfaces¹⁹, solids²⁰, and multicomponent systems such as micelles.²¹ Despite the major impacts that solvent cage effects have on chemical reactivity, it is surprising that many basic properties of the cage effect remained unknown for so long and that practically no quantitative predictive knowledge of the cage effect was available.

This dissertation describes the results of fundamental investigations into the solvent cage effect with the goal of better understanding every major molecular and environmental parameter that may influence the solvent cage effect. Understanding each parameter that impacts the solvent cage effect will yield a model that can quantitatively predict the magnitude of this effect.

1.2. Describing the Solvent Cage Effect with Kinetic Terms

Kinetic terms of the solvent cage effect will be introduced first so a convenient definition may be defined later (Scheme 1.1). Radical cage pairs are generated by the homolytic cleavage of a generic molecule by photolysis. Light energy is used to generate an excited state (R-R*) from a parent molecule (R-R). This excited state may relax to the

ground state (Σk_R , sum of all relaxation processes) or homolytically cleave (k_P) to generate a photochemical radical pair ($R\cdot, \cdot R$). This *geminate* radical pair is initially held together by a cage of solvent molecules. The two radicals may either recombine (k_{cP}) or diffuse out of the solvent cage (k_{dP}) to become free radicals. These free radicals can diffuse (k_D) and encounter other free radicals. These two radicals that encounter each other form a collisional radical pair, meaning they did not originate photochemically from the same molecule. Again the solvent holds them in a cage and they may combine (k_c) or diffuse (k_d) out of this collisional solvent cage. Note that, if a particular species arises directly from a photochemical event, a subscript “P” denotes so in the kinetic term (hence k_{dP} vs k_d). A convenient definition to describe the solvent cage effect is the photochemical recombination efficiency (F_{cP} , eq 1).



Scheme 1.1. Mechanistic model of the solvent cage effect. Radicals are generated from the generic molecule R-R by photolysis.

$$F_{cP} = \frac{k_{cP}}{(k_{cP} + k_{dP})} \quad (1)$$

This photochemical recombination efficiency denotes the amount of geminate radical pairs that recombine to form the original parent molecule. The collisional radical

pair also has a recombination efficiency (F_c , eq 2). The two different recombination efficiencies (F_{cP} and F_c) aren't necessarily the same value. Chapter VI of this dissertation investigates the relationship between F_{cP} and F_c . It is worth noting that both of these “recombination” efficiencies (F_{cP} and F_c) are different from an “initiator” efficiency (f) in polymer kinetics. Polymer chemists are more concerned with the generation of free radicals for radical polymerization and this initiator efficiency can be thought of as a “cage-escape” efficiency.

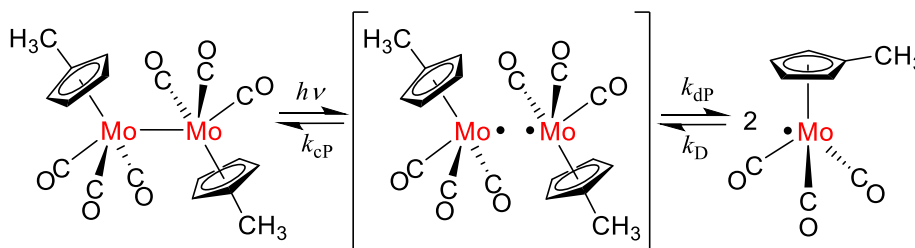
$$F_c = \frac{k_c}{(k_1 + k_d)} \quad (2)$$

1.3. Measuring F_{cP} with Bulk Photolysis

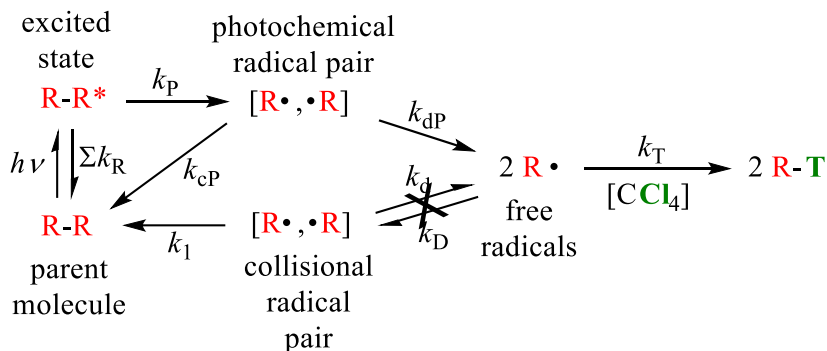
The measurement of F_{cP} is usually considered arduous. For instance, the F_c values for the reversible thermolysis of diacyl peroxides were measured using the randomization rate of labeled oxygen-18.²² Fortunately, a newer method for measuring F_{cP} was developed where the classical isotopic labeling experiment was not necessary.²³ This newer method makes use of the well-known photochemistry of a $Cp'_2M_2(CO)_6$ dimer (where $M = Mo$ or W , and $Cp' = \eta^5\text{-CH}_3\text{C}_5\text{H}_4$, Scheme 1.2). The irradiation of this $Cp'_2M_2(CO)_6$ dimer homolytically splits the metal-metal bond to form radicals. Common spectroscopic techniques can be used to directly observe the kinetics of this M-M bond breaking/forming as opposed to using mass spectrometry to identify isotopic distributions. This is how radical cage pairs are generated to study solvent cage effects. Because there are two recombination efficiencies (F_{cP} and F_c), a radical trap is added to

capture any free radicals that are produced (Scheme 1.3). The radical trap CCl_4 reacts irreversibly with any free radicals that are produced by creating a metal-chloride bond. This prevents any collisional radical pairs from being formed (Scheme 1.3).

Conveniently, the rate constant for radical trapping (k_T) is slow enough on the time scale of radical diffusion that no “in-cage” trapping occurs.²³ In-cage trapping would be the reaction of a CCl_4 molecule (that is part of the immediate solvent cage) with a caged radical. In-cage trapping severely complicates the kinetics of the experiments because the concentration dependence on CCl_4 tends to dominate.²⁴ The $\cdot\text{CCl}_3$ radicals do not react further with any metal species.



Scheme 1.2. Photolysis of the $\text{Cp}'_2\text{Mo}_2(\text{CO})_6$ dimer homolytically splits the Mo-Mo bond.



Scheme 1.3. Mechanistic model of the solvent cage effect with a radical trap.

The *strength* of the solvent cage is ultimately what prevents radicals from easily escaping each other (k_{dP} , Scheme 1.3). Conversely, a weaker solvent cage increases the probability that a radical will escape the solvent cage and become a free radical. Increasing the bulk viscosity (η) of the solvent system creates a stronger solvent cage, with bulk viscosity being the solution's resistance to flow (measured in centipoise, cP). If the solvent itself becomes more resistant to flow, fewer radicals are able to escape and more recombination occurs. Briefly, the determination of F_{cP} will use bulk viscosity to change k_{dP} . The relevant photochemical kinetic equations to reach F_{cP} with kinetic data are eq 3 and 4 (the derivation of these equations is included in Appendix A). Briefly, to obtain F_{cP} , the “quantum yield of the pair” (ϕ_{pair}) must be determined and then eq 3 may be used to calculate F_{cP} (Φ_{Obs} is the observed quantum yield during the experiment, see Appendix A).

$$\Phi_{Obs} = (1 - F_{cP})\phi_{pair} \quad (3)$$

$$\frac{1}{\Phi_{Obs}} = \frac{1}{\phi_{pair}} \left(1 + k_{cP}\eta \right) \quad (4)$$

To determine ϕ_{pair} , measurements of Φ_{Obs} are made at differing bulk viscosities. The viscosity of the solution may be augmented by increasing the volume percentage of a viscosity enhancer (viscogen). The choice of viscogen must be done with care to prevent selective solvation. This is a situation where the solvent cage around the caged radical pair is not representative of the bulk solution. A common system would be the solvent *n*-hexane, paraffin oil as the viscogen, and CCl_4 as the radical trapping agent. A plot of Φ_{Obs}^{-1} vs bulk viscosity (η) can then be extrapolated to the y-intercept to yield ϕ_{pair} (eq 4).

The y-intercept is at infinite fluidity and at this point $\Phi_{\text{Obs}} = \phi_{\text{pair}}$. Finally, Φ_{Obs} and ϕ_{pair} are used with eq 3 to calculate F_{cP} . A plot of F_{cP} vs bulk viscosity (Figure 1.1) illustrates the differences between a $\text{Cp}'_2\text{Mo}_2(\text{CO})_6$ dimer and a $\text{Cp}'_2\text{W}_2(\text{CO})_6$ dimer.²³ The best-fit line for this F_{cP} –bulk viscosity relationship is logarithmic in nature (the reason for this particular line-shape is discussed in section 3.4).

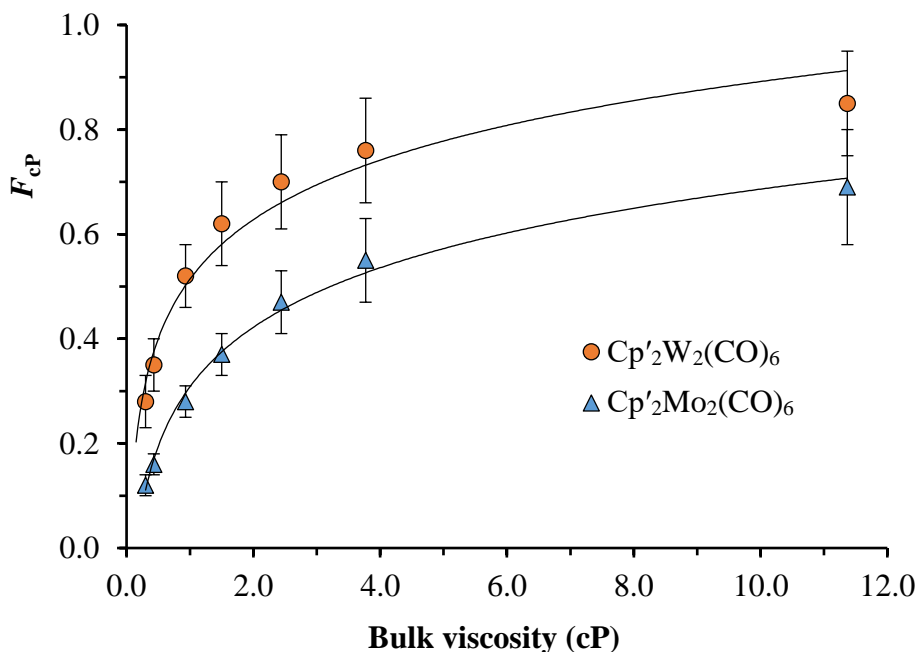


Figure 1.1. F_{cP} dependence on bulk viscosity for two $\text{Cp}'_2\text{M}_2(\text{CO})_6$ dimers (where $\text{M} = \text{Mo}$, or W). Paraffin oil/*n*-hexane/ CCl_4 solvent system at 23 °C, $h\nu$ at 550 nm, with error $\pm 2\sigma$.²³

The values of F_{cP} for the $\text{Cp}'_2\text{W}_2(\text{CO})_6$ dimer are significantly higher than those of the $\text{Cp}'_2\text{Mo}_2(\text{CO})_6$ dimer. There are multiple factors that may be responsible for this. Again, the complete goal would be to understand every aspect that affects the solvent cage effect. There is a significant difference in the bond dissociation energy vs excitation energy between the two dimers ($h\nu = 52$ kcal/mol at 550 nm; $D_{\text{w-w}} \approx 56$ kcal/mol²⁵;

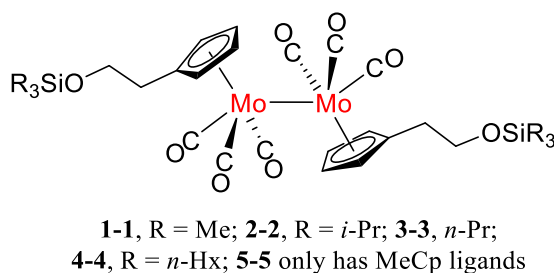
$D_{\text{Mo-Mo}} \approx 32 \text{ kcal/mol}^{26}$). In systems with organic based radicals, the difference between excitation energy and bond dissociation energy is converted to translational energy of the radical. This would lead to more cage escape (k_{dP}) for the molybdenum radicals. There is also an increase in spin-orbit coupling from molybdenum to tungsten that may potentially play a factor (this will be tested later in section 1.5).²³ Lastly, a prediction from Noyes is that the size and mass of a radical greatly affect its recombination efficiency.^{27,28} The larger mass of the tungsten radical would lower k_{dP} and hence raise F_{CP} .

1.4. F_{CP} Dependence on Mass and Size of the Radical

There are many different sized radicals that can range from the hydrogen radical of 1 Da to polymer radicals that are 10^6 Da.²⁹ Some theoretical basis from Noyes postulated that the solvent cage effect is dependent on both the mass and size of the radical.^{27,28,30} Testing the dependence of F_{CP} on mass and volume was an attractive next step that could lend answers to the discrepancy in F_{CP} values between $\text{Cp}'_2\text{W}_2(\text{CO})_6$ and $\text{Cp}'_2\text{Mo}_2(\text{CO})_6$ dimers. Synthetic additions to a Cp ligand on a metal-metal dimer would increase both mass and volume. From the previous experiments with $\text{Cp}'_2\text{W}_2(\text{CO})_6$ and $\text{Cp}'_2\text{Mo}_2(\text{CO})_6$ dimers, it became apparent that the identity of the bond that was breaking had to be constant in order to isolate mass and size dependence. The molybdenum based dimer was chosen to continue these experiments due to its ease of synthesis.

A variety of molybdenum based dimers were synthesized to test mass and size affects (Scheme 1.4).³¹⁻³³ The ethyl spacer between the cyclopentadiene ligand and the

modified silyl group isolates the Mo-Mo bond. This made all of the derivatives (**1-1** → **5-5**) have nearly the same electronic spectrum (changes in the electronic spectrum would change the energy required to irradiate). Thus the experimental conditions are unchanged from the prior experiments for this new series of molecules. These new molecules were easily synthesized using the $(\text{HOCH}_2\text{CH}_2\text{Cp})_2\text{Mo}_2(\text{CO})_6$ dimer as the starting point.^{34,35} The alcohol group of this dimer allows a functionalization handle.



Scheme 1.4. Molybdenum dimer with ligand modifications to increase size and mass.³³

The recombination efficiency was measured for all of these new molybdenum dimers. Plots of F_{cP} vs bulk viscosity show the same dependence on bulk viscosity as demonstrated before (Figure 1.2). From the plot it is difficult to immediately see exactly how size and mass affect F_{cP} . A change in how the data is plotted may give more insight. Noyes predicted in his mathematical model that F_{cP} will increase as radical size (r) increases and as radical mass (m) decreases. The formula may be written as $k_{\text{dP}}/k_{\text{cP}} \propto m^{0.5}/r^2$ ($k_{\text{dP}}/k_{\text{cP}}$ is equal to $F_{\text{cP}}^{-1}-1$). A plot of F_{cP} vs $m^{0.5}/r^2$ shows the expected relationship from theory (Figure 1.3). The linear best-fit lines all follow to the origin, a requirement of the Noyes' theory.³³ This experimental work neatly compliments the theoretical work of Noyes.

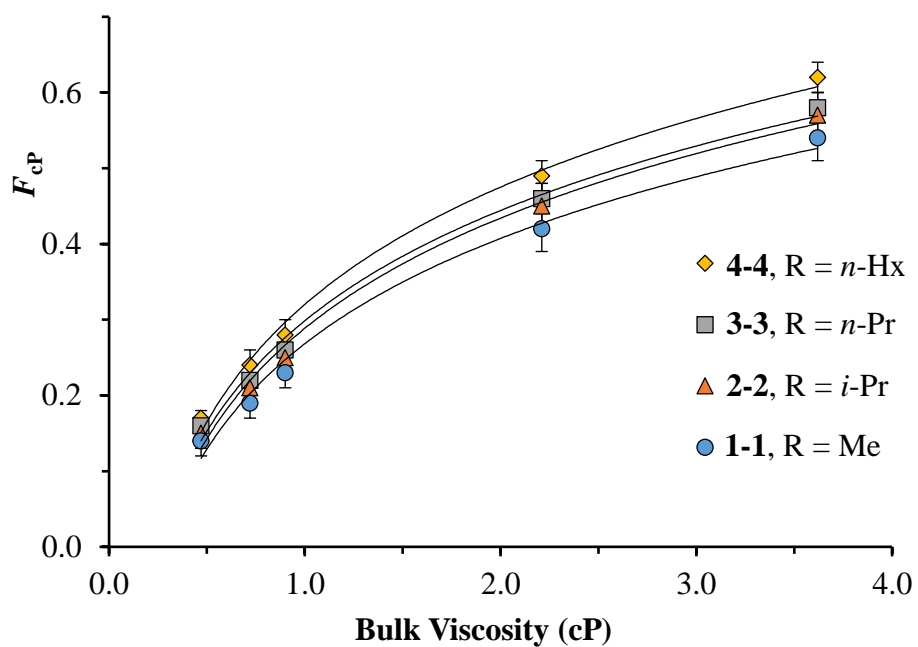


Figure 1.2. Plot of F_{cp} vs bulk viscosity for the functionalized $(R_3SiOCH_2CH_2Cp)_2Mo_2(CO)_6$ dimers (R identity indicated by legend). Mineral oil/*n*-hexane/ CCl_4 solvent system at 23 ± 1 °C, $h\nu$ at 540 nm, with error $\pm 1\sigma$.³³

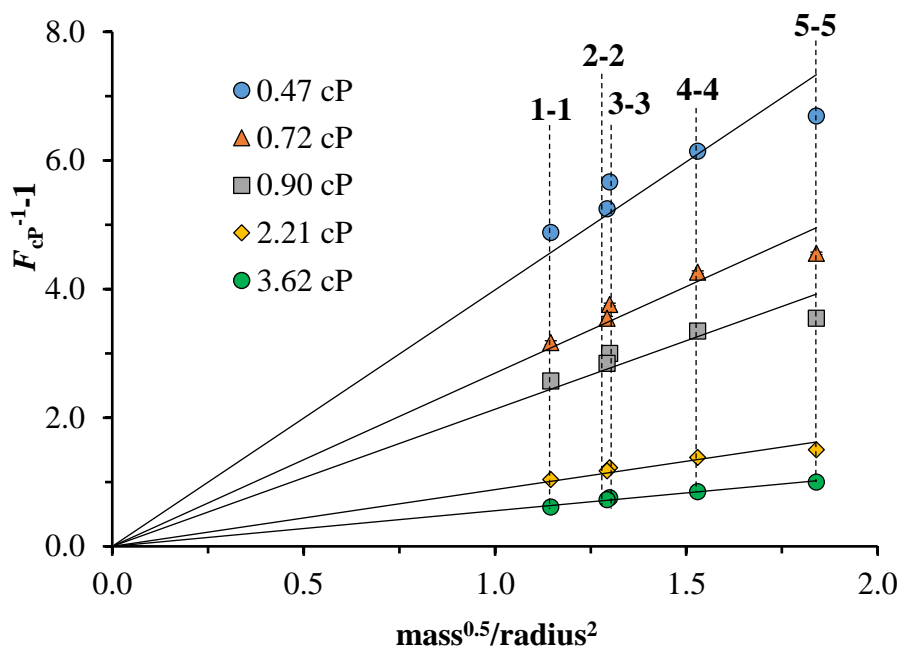
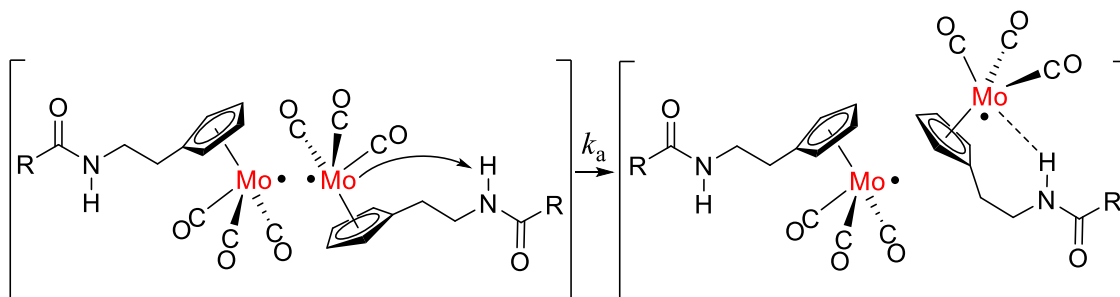


Figure 1.3. Plot of $F_{cp}^{-1}-1$ vs $mass^{0.5}/radius^2$ for the functionalized $(R_3SiOCH_2CH_2Cp)_2Mo_2(CO)_6$ dimers. Dashed lines follow along the same identity of R-group on the dimer. Solid lines are linear best-fit. Mineral oil/*n*-hexane/ CCl_4 solvent system at 23 ± 1 °C, $h\nu$ at 540 nm.³³

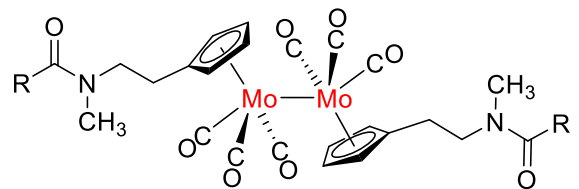
The functionalization of the molybdenum dimer with greater size and mass was continued to further probe the relationship of F_{cp} with mass and radius of the radical. This further experimental work was done to ensure the generality of the $F_{cp} \propto m^{0.5}/r^2$ relationship. Due to their ease of synthesis, amide functionalized molybdenum dimers were made (Scheme 1.5).^{36,37} Measured F_{cp} values for these dimers were nearly identical regardless of the size of the R group (Scheme 1.5).³⁸ This was very surprising considering the initial success of the silyl functionalized molybdenum dimers (Scheme 1.4). It was hypothesized that an agostic interaction between the N-H of the amide and the molybdenum radical was forming a stable six-membered ring (Scheme 1.5).³⁸ The F_{cp} values would thus be independent of the size of the R groups.

If this agostic interaction is indeed affecting F_{cP} , this type of strategy would be useful in adding photodegradable Mo-Mo bonds into polymers. Essentially the polymer backbone acts as an extremely large R-group and inhibits cage escape (photochemical degradation of the polymer). With an agostic interaction, the F_{cP} values would be independent of the large R-group and result in a much faster photodegradation of the polymer.



Scheme 1.5. In-cage trapping of the molybdenum-centered radical by an amide-H atom.³⁸ R-groups vary in length as $R = -(CH_2)_nCH_3$ with ($n = 3, 8, 13, 18$).

To test this hypothesis, the amide-H atoms were replaced with methyl groups (Scheme 1.6).³⁸ There should be no agostic interaction between the methyl group and a molybdenum radical. The F_{cP} values for these complexes were again measured and a plot of $F_{cP}^{-1} - 1$ vs $m^{0.5}/r^2$ (where r is the effective radius of a sphere with the same volume as the radical). This compares nicely to the previously observed data for the silyl complexes (Scheme 1.4). The F_{cP} values changed as a function of their mass and radius. The radicals themselves are considerably different from spherical, hence using the radical's radius was inappropriate. However, using either the surface area or the "effective radius" of a sphere (that has the same volume as the radical) worked well (Figure 1.4). This presented a nice modification to the Noyes theory (using a spheres radius) to a molecular shape of any size (surface area).



R = $-(\text{CH}_2)_n\text{CH}_3$ with $n = 3$ (**6-6**), 8 (**7-7**) and 18 (**8-8**)

Scheme 1.6. Functionalized molybdenum dimer with methyl groups in place of amide-H atoms from Scheme 1.5.³⁸

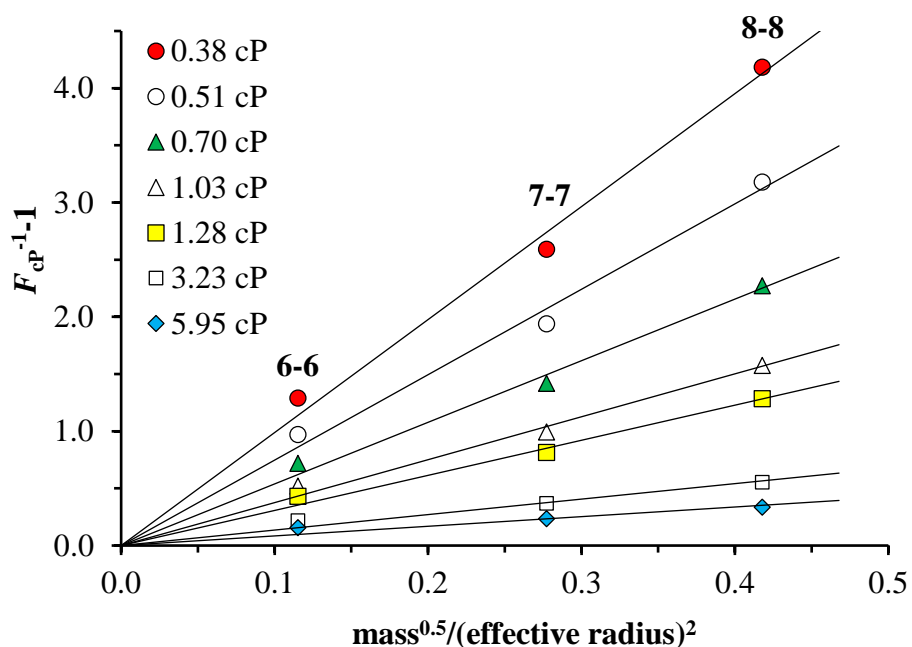


Figure 1.4. Plot of $F_{\text{CP}}^{-1}-1$ vs $\text{mass}^{0.5}/(\text{effective radius})^2$ for molybdenum dimers **6-6**, **7-7**, and **8-8** (see Scheme 1.6).³⁸ (Hexanes/squalane (viscogen)/ CCl_4 solvent system with $h\nu = 546$ nm.)

It is possible that this newly confirmed relationship of $F_{\text{CP}} \propto m^{0.5}/r^2$ can now explain why F_{CP} is much larger for the $\text{Cp}'_2\text{W}_2(\text{CO})_6$ dimer compared to the $\text{Cp}'_2\text{Mo}_2(\text{CO})_6$ dimer (Figure 1.1)? A plot of F_{CP} vs bulk viscosity of $\text{Cp}'_2\text{W}_2(\text{CO})_6$, $\text{Cp}'_2\text{Mo}_2(\text{CO})_6$, and **1-1** showed this is not the case (Figure 1.5). $\text{Cp}'_2\text{W}_2(\text{CO})_6$ and **1-1** are plotted together because the resulting radicals have similar mass (347 and 361 Da, respectively). Clearly from the graph, the tungsten dimer has a much higher F_{CP} even

when compared against a similar sized molybdenum dimer. A plot of $F_{\text{CP}}^{-1}-1$ vs $\text{mass}^{0.5}/\text{radius}^2$ for the tungsten dimer also did not clarify the discrepancy. From this, it was concluded that either spin-orbit coupling or the difference in bond dissociation energy is the reason for the difference in F_{CP} and not radical size or mass.

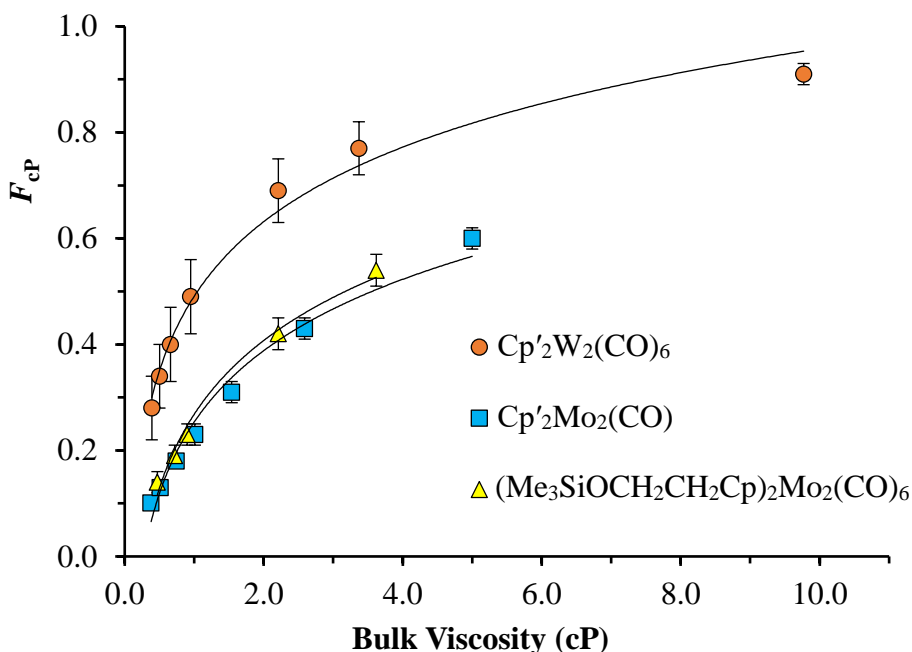


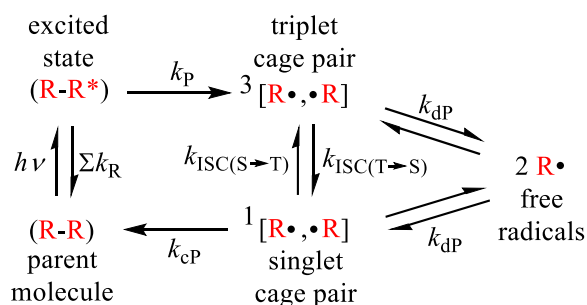
Figure 1.5. Plot of F_{CP} vs viscosity for $\text{Cp}'_2\text{W}_2(\text{CO})_6$, $\text{Cp}'_2\text{Mo}_2(\text{CO})_6$ and $(\text{Me}_3\text{SiOCH}_2\text{CH}_2\text{Cp})_2\text{Mo}_2(\text{CO})_6$ in hexane/mineral oil/ CCl_4 at 23 ± 1 °C, error $\pm 1\sigma$.³³

1.5. Spin-Orbit Coupling in Metal Based Radicals

Spin-orbit coupling to explain the discrepancy between F_{CP} of $\text{Cp}'_2\text{W}_2(\text{CO})_6$ and $\text{Cp}'_2\text{Mo}_2(\text{CO})_6$ was further tested. This could also demonstrate how the difference between 2nd and 3rd row transition metal spin-orbit coupling can have an effect on reactivity. An increase in spin-orbit coupling would facilitate intersystem crossing (ISC). Classically, the homolytic cleavage of a bond results in an initial triplet state that must

intersystem cross to a singlet state before recombination can occur (Scheme 1.7).³

Perhaps there is a “spin-barrier” to recombination for the molybdenum dimers that results in a much lower F_{cP} than the tungsten dimers. This would occur if the rate of triplet to singlet intersystem crossing [$k_{ISC(T\rightarrow S)}$] is slow compared to the recombination rate (k_{cP}) for the molybdenum dimers. Spin-barriers for carbon based radicals are fairly common but for metal based radicals it is generally assumed that there is no spin-barrier because the transition metal radical acts as the heavy atom. However, that train of thought doesn’t limit the postulation that spin barriers can occur at metal based radicals.³⁹



Scheme 1.7. Photolysis of a generic R-R dimer that results in an initial triplet state.⁴⁰

The possible spin-barrier was probed using heavy atoms. Spin-orbit coupling rate constants are influenced by high nuclear charge (Z) atoms near them (“heavy atom effect”).⁴⁰ This can occur when the heavy atom is a component of the molecule in question or part of the solute/solvent. Hence, if a spin-barrier is present, the Φ_{Obs} will change if the system contains a heavy atom. The heavy atom probe 1-iodobenzene was added to solutions and tested by bulk photolysis and using femtosecond transient absorption spectroscopy (2.0 M iodobenzene was calculated to be sufficient to cause a change in Φ_{Obs}).⁴⁰ Controls with 1-chlorobenzene were also conducted. Φ_{Obs} did not

change with the addition of 1-iodobenzene for $\text{Cp}'_2\text{Mo}_2(\text{CO})_6$, $\text{Cp}'_2\text{Fe}_2(\text{CO})_4$, or $\text{Cp}^*_2\text{TiCl}_2$ ($\text{Cp}^* = \eta^5\text{-(CH}_3)_5\text{C}_5$, Figure 1.6). Photolysis of $\text{Cp}^*_2\text{TiCl}_2$ produces a metal based radical $[\text{Cp}^*\text{TiCl}_2]\cdot$ and a carbon based radical $\cdot[\text{Cp}^*]$. Because there was no change in Φ_{Obs} , there is no spin-barrier for recombination in these transition metal complexes.

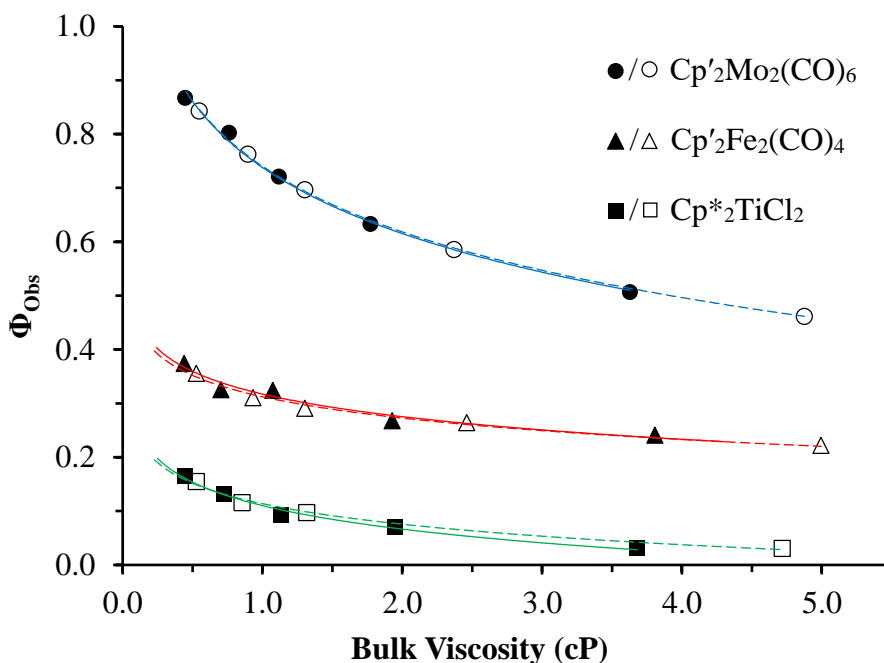


Figure 1.6. Plot of Φ_{Obs} vs bulk viscosity for three organometallic complexes. Filled symbols and solid best-fit lines represent data collected in the presence of 2.0 M 1-chlorobenzene. Open symbols and dashed best-fit lines represent data collected in the presence of 2.0 M 1-iodobenzene. (*n*-hexane, squalane/ CCl_4)⁴⁰

Explaining the difference of F_{CP} for $\text{Cp}'_2\text{Mo}_2(\text{CO})_6$ and $\text{Cp}'_2\text{W}_2(\text{CO})_6$ cannot be done with the spin-orbit coupling or with the differences in mass of the radicals. There is a significant difference between bond dissociation energy and the excitation energy ($h\nu = 52 \text{ kcal/mol}$; $D_{\text{w-w}} \sim 56 \text{ kcal/mol}$ ²⁵; $D_{\text{Mo-Mo}} \sim 32 \text{ kcal/mol}$ ²⁶). For the photochemical homolysis of I_2 , excess energy may be converted to kinetic energy of the atoms as

evidenced by the Φ_{Obs} dependence on wavelength of irradiation.^{27,28,30} However this assessment may not be true for multiatomic radicals where excess energy is rapidly lost to the solvent through vibrational modes.⁴¹ Instead, the larger F_{CP} values for $\text{Cp}'_2\text{W}_2(\text{CO})_6$ may reflect the increased driving force to recombination when compared to Mo radicals (Figure 1.7).³³ Consequently there would be a lower activation barrier and recombination would be much more probable.

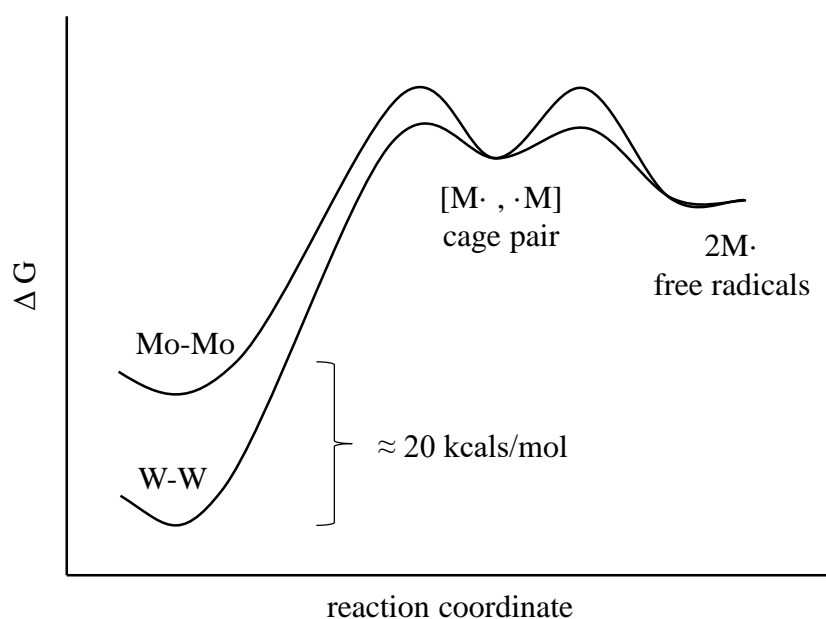


Figure 1.7. A comparison of what the reaction coordinate may look like for both a Mo-Mo and a W-W bond. The energies of the two cage pairs are shown as equal to assist in the comparison.³³

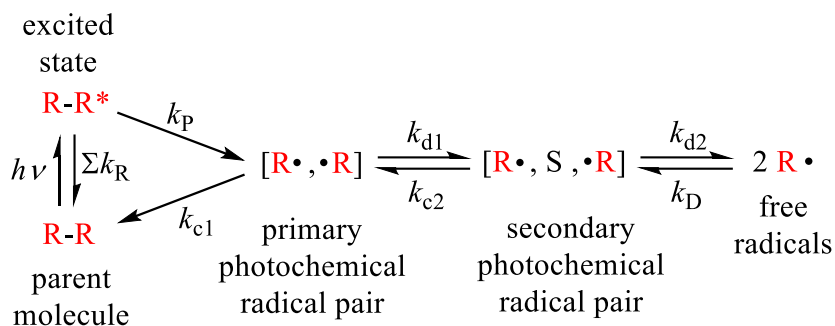
1.6. Primary and Secondary Solvent Cages

Although bulk photolysis yields wonderful kinetic data to get F_{CP} , the ultra-fast dynamics of the radical cage effect are quite hidden. The $Cp'_2Mo_2(CO)_6$ dimer contains two major features in its electronic spectrum, a $d\pi \rightarrow \sigma^*$ at 515 nm and a much more intense $\sigma \rightarrow \sigma^*$ at 319 nm. This lends the molecule to two-color femtosecond pump-probe transient absorption spectroscopy. The radical cage pairs may be generated by pumping at 515 nm and the reaction kinetics may be probed at 400 nm. The photochemistry of the $Cp'_2Mo_2(CO)_6$ dimer is well known at both of these wavelengths.^{42,43} The use of femtosecond spectroscopy allows the observation of the earliest moments of the solvent cage effect (the appropriate kinetics derivations and experimental setup are outside the scope of this introduction and are fully described elsewhere⁴²).

When molybdenum dimers of increasing size and mass were measured using the two-color femtosecond pump-probe transient absorption method, the cage recombination efficiencies were essentially the same. In contrast, the bulk photolysis method showed increases of F_{CP} with increasing size and mass. It soon became apparent that the femtosecond spectroscopy method was measuring a primary cage recombination efficiencies (Scheme 1.8). A secondary cage occurs when a solvent molecule(s) occupies the space between two geminate radicals. In other words, a radical escapes the primary cage but is still caged nearby in the secondary cage. A secondary cage effect is when geminate radicals recombine to reform the parent molecule even after a primary cage escape. There are recombination efficiencies for both the primary (F_{c1} , eq 5) and the

secondary solvent cage (F_{c2} , eq 6) with the original F_{cP} being the net cage recombination of the two.

By measuring F_{c1} with femtosecond spectroscopy, and measuring F_{cP} by bulk photolysis, F_{c2} may be calculated. This was done for a series of molybdenum dimers with increasing size and mass (Table 1.1). Primary recombination efficiencies are unaffected by the radical size whereas secondary cage effects are dominated by the radicals size and mass.



Scheme 1.8. Mechanistic model for primary and secondary solvent cage effects.⁴⁴

$$F_{c1} = \frac{k_{c1}}{(k_{c1} + k_{d1})} \quad (5)$$

$$F_{c2} = \frac{k_{c2}}{(k_{c2} + k_{d2})} \quad (6)$$

Table 1.1. Primary (F_{c1}), secondary (F_{c2}), net (F_{cP}) recombination efficiencies for $(RCp)_2Mo_2(CO)_6$ dimer, where $R = -CH_2CH_2N(CH_3)C(O)(CH_2)_nCH_3$ (see Scheme 1.6).⁴⁴

Cp ligand	F_{c1}	F_{cP}	F_{c2}
$n = 18$	0.43 ± 0.02	0.70 ± 0.04	0.68
$n = 13$	0.44 ± 0.01	0.59 ± 0.04	0.45
$n = 8$	0.42 ± 0.03	0.48 ± 0.03	0.22
$n = 3$	0.42 ± 0.02	0.42 ± 0.03	0.0
$Cp' = \eta^5\text{-CH}_3\text{C}_5\text{H}_4$	0.31 ± 0.01	0.31 ± 0.03	0.0

The ultra-fast kinetics lead to some intriguing observations regarding the primary solvent cage effect. The typical lifetime of a primary geminate radical pair is 5 ps or less.^{42,43} The rotational correlation time for a small molybdenum dimer $[Cp'_2Mo_2(CO)_6]$ is 36 ps.⁴³ This means that for a primary geminate radical pair, there is no rotation of the radical. This means that in the primary cage, the radical orbitals are correctly aligned for recombination. In the secondary cage, there is enough time for the radicals to rotate and cause misalignment. Misaligned orbitals do not have sufficient orbital orientation to recombine. This has major implications for radicals that don't originate from the same dimer and instead randomly encounter another free radical (collisional cage pairs). Collisional cage pairs are more likely to be misaligned, disfavoring recombination. If this is the case, then the photochemical recombination efficiency (F_{cP}) will be larger than the collisional recombination efficiency ($F_{c'}$) because more primary collisional the radical pairs has a mis-orientation of radical orbitals.

The overall scheme that includes primary, secondary, collisional, and mis-aligned radical pairs begins to get fairly complex (Scheme 1.9) when a radical trap is not present

to capture free radicals. Theoretically, why F_{cP} is much greater than F_c' can be easily explained by the population difference between the primary photochemical radical pair $[R\cdot, \cdot R]$ and the primary collisional radical pair $[R\cdot, \cdot R]$ (Scheme 1.9). The primary photochemical radical pair $[R\cdot, \cdot R]$ begins after photolysis whereas the primary collisional radical pair $[R\cdot, \cdot R]$ starts from the secondary collisional radical pair $[R\cdot, S, \cdot R]$. Experimental results comparing F_{cP} and F_c' are presented in Chapter VI.

1.7. Bridge

This introduction sets the stage for my dissertation with known factors that affect the solvent cage effect as well as a few unknowns. The goal of the project is to understand every factor that influences F_{cP} so that a quantitative model may be constructed. First, the fact that solutions with the same bulk viscosity have different solvent cage effects is thoroughly investigated (Chapter II and III). This is especially the case when a large viscogen is used (such as a polymer) or switching the base solvent (*n*-hexane to tetrahydrofuran).

CHAPTER II

RADICAL CAGE EFFECTS: COMPARISON OF SOLVENT
BULK VISCOSITY AND MICROVISCOSITY IN PREDICTING
THE RECOMBINATION EFFICIENCIES OF RADICAL CAGE
PAIRS

Justin T. Barry, Daniel J. Berg, David R. Tyler*

Department of Chemistry and Biochemistry, University of Oregon, Eugene, OR

97403-1253

Chapter II of my dissertation is a modified form of a published paper. Reproduced with permission from *J. Am. Chem. Soc.* **2016**, *138*, 9389–9392. Copyright 2016 American Chemical Society. I developed the experimental design, did the majority of the experiments, and wrote the manuscript. This work was co-authored with David R. Tyler and Daniel J. Berg. The contents on the published supporting information are provided as Appendix B.

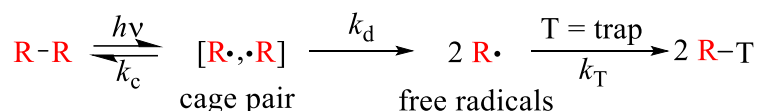
2.1. Introduction

A goal of our research is to uncover the underlying principles that govern radical cage effects so we can understand radical reactivity better. We report here that solvent microviscosity is more appropriate than macroviscosity (bulk viscosity) for describing the “strength” of the solvent cage and for quantifying the recombination efficiency of radical

cage pairs. The term “radical cage effect” refers to the phenomenon that the probability of recombination of a radical pair is greater in solution than in the gas phase.¹⁻³ The origin of this effect is the solvent “cage,” a term introduced by Franck and Rabinowitch in 1934 for a hole in the solvent that temporarily traps a pair of reactive molecules causing them to remain as colliding neighbors for a short period of time before random motion allows their separation (Scheme 2.1).^{4,5} Radical cage effects have an enormous impact on chemical reactivity in solution.^{6,7} In particular, they are necessary to explain a host of kinetic observations and fundamental reaction phenomena. For example, cage effects are necessary to explain magnetic isotope^{8,9} and CIDNP^{10,11} effects, rate-viscosity correlations,¹² variations in products and yields as a function of medium,^{13,14} variations in quantum yields as a function of medium,¹⁵ and regio- and stereochemical control.¹⁶⁻¹⁸ Examples of important reactions where cage effects are necessary to explain the kinetics include the initiation, propagation, and termination steps of radical polymerization reactions,¹⁹⁻²⁴ the reactions of coenzyme B₁₂ and its model complexes,^{8,25-29} the reactions of hemes with O₂,³⁰ and various electron transfer reactions.³¹⁻³⁴ New observations of cage effects and their impact on reactivity are reported regularly.³⁵⁻⁵⁶

With reference to the radical cage pair formed by the bond homolysis in Scheme 2.1, the “cage recombination efficiency” (F_{cP}) is defined as $F_{cP} = k_c / (k_c + k_d)$.⁵⁷ For quantitative purposes (e.g., in radical polymerization initiator kinetics) it is necessary to know the value of F_{cP} . Although F_{cP} is intuitively related to the viscosity of the solution, numerous studies have shown that bulk viscosity is utterly inadequate for predicting the value of F_{cP} and, in general, for quantitatively describing how solvents affect the dynamics of the cage effect.^{4,6} As shown below, F_{cP} for the same radical cage

pair can have remarkably different values in different solvents having the same bulk viscosity.⁵⁸ Various models have been proposed that attempt to quantify F_{cP} and the cage effect in terms of solvent parameters other than bulk viscosity. For example, models involving internal pressure, cohesive energy density, and solvent density have all been proposed.^{59–61} However, all of these models inadequately rely on bulk solvent parameters. Furthermore, several of these parameters are exceedingly complex and not conveniently measured. As a result, there is still no good model that adequately relates the strength of the solvent cage to the physical properties of the solvent.⁵⁹



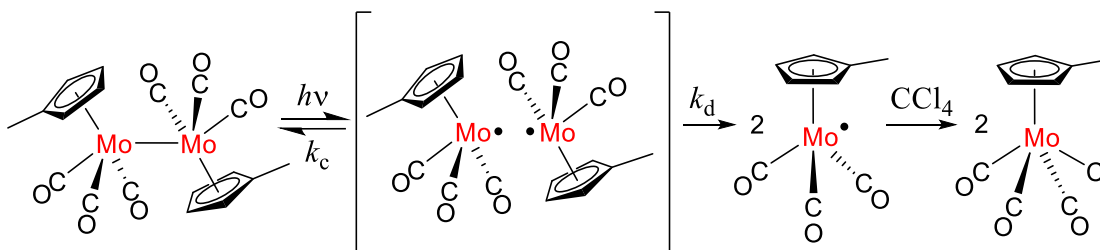
Scheme 2.1. Photodissociation of a general molecule (R-R) that results in a radical cage pair.

2.2. Results and Discussion

Because the solvent cage effect is a localized phenomenon, we hypothesized that local viscosity (i.e., microviscosity) is more appropriate than bulk viscosity for describing the cage effect and, in particular, for predicting F_{cP} . In this communication, we present the results of a study that tested the hypothesis that microviscosity is a more appropriate predictor of F_{cP} than macroviscosity.

Solvent-caged radical pairs were generated by irradiation ($\lambda = 532 \text{ nm}$) of the $\text{Cp}'_2\text{Mo}_2(\text{CO})_6$ molecule ($\text{Cp}' = \eta^5\text{-CH}_3\text{C}_5\text{H}_4$) in the solvent systems described below (Scheme 2.2).^{58,62–67} Prior work in our laboratory established methods for measuring F_{cP}

for photochemically generated radical cage pairs.^{58,67-69} In brief, the quantum yields for the reaction of $\text{Cp}'_2\text{Mo}_2(\text{CO})_6$ with CCl_4 (Scheme 2.2) were measured as a function of solvent bulk viscosity. (The viscosity was changed by adding a viscogen to the solvent. In order to avoid selective solvation, the viscogen was chosen so that it has a similar chemical structure and composition to the solvent. For example, IR-grade paraffin oil was added to hexane to increase the bulk viscosity of the hexane solution.) From the resulting plots of quantum yields vs bulk viscosity (see Appendix B), it is possible to calculate F_{CP} as a function of bulk viscosity by the method reported in our prior papers.^{58,63,68}



Scheme 2.2. Photolysis of $\text{Cp}'_2\text{Mo}_2(\text{CO})_6$ results in a caged radical pair.

Plots of F_{CP} as a function of macroviscosity for five solvent systems are shown in Figure 2.1. The five solvent systems (solvent/viscogen) are (1) hexane/paraffin oil; (2) hexane/polybutenes ($M_n = 3200$); (3) toluene/1,1-bis(3,4-dimethylphenyl)ethane (abbreviated “DXE”); (4) toluene/polystyrene ($M_w = 45,000$); and (5) hexamethyldisiloxane/poly(dimethylsiloxane) ($M_w = 3780$) (abbreviated HMDS and PDMS, respectively). CCl_4 (20% by weight) was added to each sample as the radical trapping agent (Scheme 2.2).⁷⁰ Note in the figure that, at any selected bulk viscosity, the F_{CP} values in the five solvent systems are all different. These results illustrate the point

made above that F_{cP} can be dramatically different in different solvent systems with the same macroviscosity.

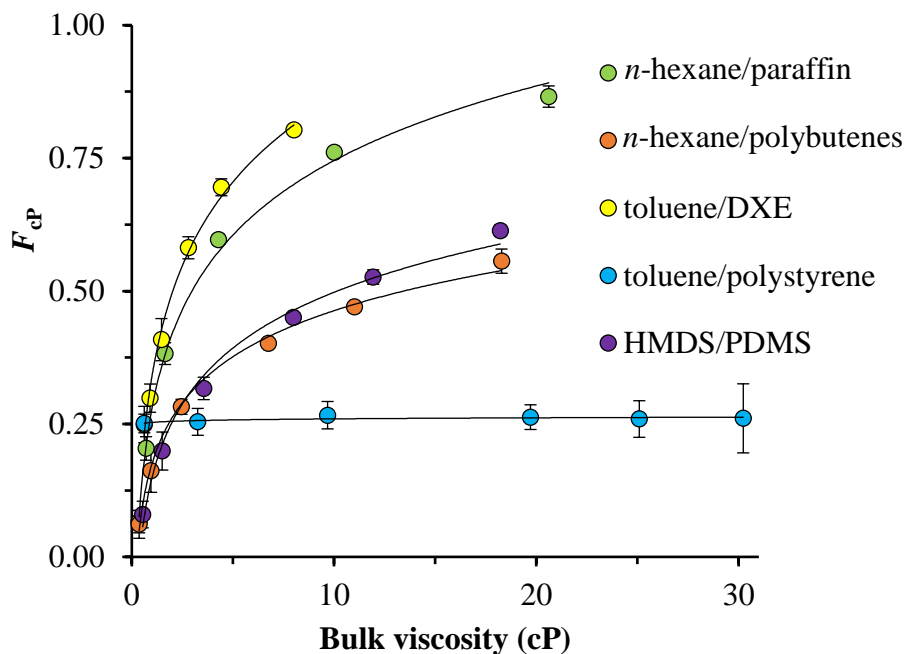


Figure 2.1. Plot of cage recombination efficiency (F_{cP}) as a function of solvent system bulk viscosity (cP). Each sample contains 20 wt% CCl_4 ; error bars are 1σ ; and the curves are only a visual guide.

To investigate the hypothesis that microviscosity is a better parameter for describing and interpreting F_{cP} , it was necessary to find a measurable solvent property that tracks with microviscosity. In studies of biological molecules (e.g., protein folding studies), there is a general consensus that rotational diffusion coefficients, obtained from NMR T_1 measurements, are correlated with the local viscosity of the solvent environment.⁷¹ For technical reasons, T_1 measurements were not possible with the molecules and radicals used in this study.⁷² However, other studies have shown that rotational and translational diffusion coefficients can be interchanged when probing the

microenvironment of biological molecules,⁷³⁻⁷⁶ and therefore we used translational diffusion coefficients.⁷⁷

The translational diffusion coefficients of the radicals in the five solvent systems used in this study were measured using NMR diffusion ordered spectroscopy (DOSY) (Table 2.1). More specifically, the translational diffusion coefficients were measured using a stable organometallic surrogate for the highly reactive [Cp'Mo(CO)₃] radicals. (C₆H₆)Cr(CO)₃ was chosen as the probe because F_{CP} is related to the radical mass and size according to the Noyes equation ($F_{CP} \propto \text{mass}^{0.5}/\text{radius}^2$), and the Cp'Mo(CO)₃ and (C₆H₆)Cr(CO)₃ species are reasonably similar in mass and size.^{58,78,79} (The relevant physical parameters for (C₆H₆)Cr(CO)₃ and the [Cp'Mo(CO)₃] radical are presented in the Appendix A, along with a more detailed justification for using (C₆H₆)Cr(CO)₃ as a surrogate for [Cp'Mo(CO)₃] radical.) According to the Stokes-Einstein equation,⁸⁰ viscosity is inversely proportional to the translation diffusion coefficient (D) so $1/D$ was taken as the solvent parameter representing microviscosity.⁸¹

Table 2.1. Solvents and viscogens used in this study.^a

solvent	viscogen	bulk viscosity range (cP)	microviscosity range (x10 ⁹ s/m ²)
<i>n</i> -hexane	paraffin oil	0.36-20.61	0.28-6.08
	poly(butenes)	0.36-18.27	0.28-2.31
toluene	DXE	0.61-8.02	0.57-5.05
	poly(styrene)	0.62-30.22	0.61-0.83
HMDS	PDMS	0.54-18.21	0.41-1.94

^aEach sample contained 20 wt % CCl₄

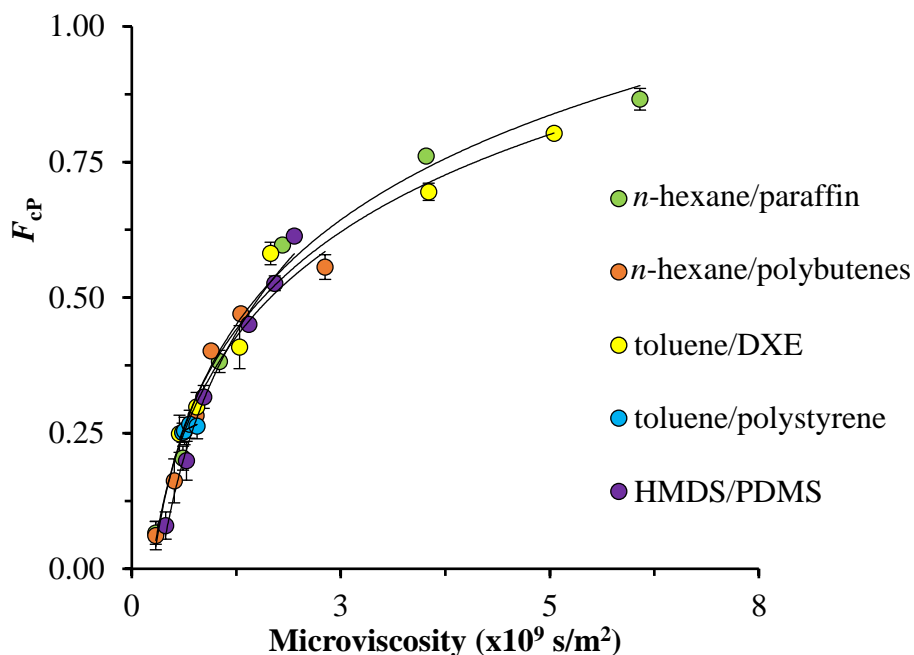


Figure 2.2. Cage recombination efficiency (F_{cp}) plotted as a function of microviscosity ($1/D$). Each sample contains 20 wt% CCl_4 , error bars are 1σ ; and the curves are only a visual guide.

The F_{cp} values in the five solvent systems in Figure 2.1 are shown replotted as a function of the microviscosity ($1/D$) in Figure 2.2. *Note that the F_{cp} values for all five solvent systems are nearly the same for identical values of the microviscosity.* This result shows that microviscosity provides the best correlation to date between the solvent and the value of F_{cp} . Restated, the microviscosity is the parameter of choice when probing solvent effects on the radical cage effect.

Radical-radical recombination requires that the two radicals have the correct orbital orientation to react. Therefore, it might seem that, in addition to being a function of $1/D$, the microviscosity should also be a function of a parameter related to the rate of radical rotation such as the rotational correlation time, τ_c . However, as noted above, studies of biological molecules have shown that the rotational and translational diffusion

coefficients can be used interchangeably to probe the microenvironment of biological molecules. Thus, in a description of microviscosity involving both $1/D$ and τ_c , the τ_c term can be written as a function of D to yield an expression for microviscosity involving only D .

2.3. Conclusion

In conclusion, the experiments reported here suggest that for nonpolar solvent systems quantitative discussions pertaining to F_{cP} should be based on microviscosity rather than bulk viscosity. In essence, if the translational diffusion coefficient for a particular radical in a cage pair is known then an accurate cage recombination efficiency is predictable, independent of the solvent system. This predictive power will be useful wherever quantitative knowledge of radical reactivity is necessary. It is noted that the method described above can be applied in reverse. That is, if F_{cP} is known then the diffusion coefficient of the molecule can be determined; in turn, the microviscosity of the local environment around the caged molecules can be probed. This reverse application would provide a method for determining the microviscosity in complex systems such as active sites of enzymes or in heterogeneous reactions. Polar solvent systems and hydrogen-bonding solvent systems are currently being investigated in our laboratory to determine if the results obtained above with nonpolar solvents are also applicable in these types of solvents.

2.4. Bridge

Using microviscosity to predict F_{cP} in non-polar systems led to the next series of experiments detailed in Chapter III. The question becomes “does microviscosity also dictate F_{cP} in polar solvent systems?” It is unclear from the reported data above that the microviscosity of the solvent cage could be accurately determined using the surrogate probe in polar solvents.

The microviscosity was determined by using a diffusion coefficient from DOSY-NMR. A complimentary technique would be useful if performing DOSY was not an option. For instance, if solvent peaks overlap with the probe molecule. A fluorescence method using pyrene as the probe molecule is explored in Chapter III.

CHAPTER III

RADICAL CAGE EFFECTS: THE PREDICTION OF RADICAL CAGE PAIR RECOMBINATION EFFICIENCIES USING MICROVISCOSITY ACROSS A RANGE OF SOLVENT TYPES

Justin T. Barry, Daniel J. Berg, David R. Tyler*

Department of Chemistry and Biochemistry, University of Oregon, Eugene, OR

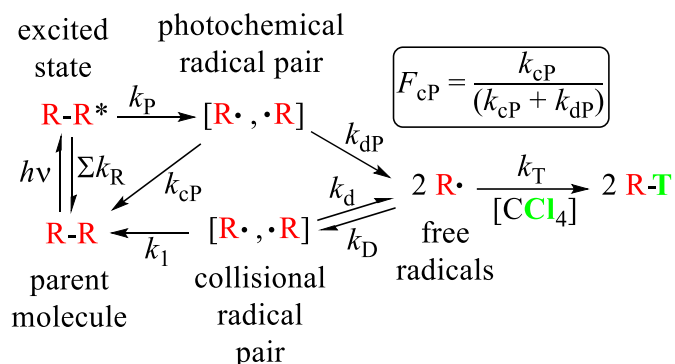
97403-1253

Chapter III of my dissertation is a modified form of a published paper. Reproduced with permission from *J. Am. Chem. Soc.* **2017**, *139*, 14399-14405. Copyright 2017 American Chemical Society. I developed the experimental design, did the majority of the experiments, and wrote the manuscript. This work was co-authored with David R. Tyler and Daniel J. Berg. The contents on the published supporting information are provided as Appendix C.

3.2. Introduction

Homolysis of a covalent bond in solution produces radicals that are initially held close together by a solvent “cage” before they can diffuse apart. In comparison to a gas-phase reaction, the solvent cage increases the probability that the newly formed radicals will recombine to form the original covalent bond. This phenomenon was first explained

in 1934 by Franck and Rabinowitch, who described the solvent cage as a hole in the solvent that temporarily traps two reactive molecules together until random motion allows their separation (Scheme 3.1).¹⁻³ The “radical cage effect” successfully explains many aspects of radical chemistry, including magnetic isotope effects,^{4,5} radical polymerization kinetics,⁶⁻¹² cobalamin reactivity,¹³ product distributions in photochemistry,¹⁴ stereochemistry of rearrangements,^{15,16} the reactivity of halogenase analogues,¹⁷ and chemically induced dynamic nuclear polarization effects (CIDNP).^{18,19} In addition to the solution phase, the cage effect has been observed to occur in solid state films,^{20,21} inside micelles,²² as well as in compressed and supercritical gases.²³ New reports of the radical cage effect appear frequently in the literature.²⁴⁻⁴⁷



Scheme 3.1. Photodissociation of a general Molecule (R-R) results in a radical cage pair.

A mechanistic model for the photolysis of a bond and the formation of a radical cage pair is shown in Scheme 3.1. In quantitative terms, the “cage recombination efficiency,” denoted by F_c , is defined as $F_c = k_c/(k_c + k_d)$. An important point is that F_c for a photochemically formed cage pair does not necessarily equal F_c for the same cage pair formed by thermolysis or by diffusional collision of two free radicals.⁴⁸ In order to

differentiate these cases, the photochemical cage recombination efficiency is denoted F_{CP} . In order to quantitatively interpret many radical reactions, it is necessary to know or be able to predict F_{CP} . Unfortunately, such predictions are nearly impossible to make. Most studies have focused on using the solvent bulk viscosity as a means to predict F_{CP} . Intuitively, k_{dP} (Scheme 3.1) is dependent on the bulk viscosity. The rationale is that higher bulk viscosity forms a stronger solvent cage, which prevents facile diffusion. Overall, a stronger solvent cage would increase F_{CP} . However, numerous studies have shown that the solvent bulk viscosity is inadequate for quantitatively predicting F_{CP} .^{49,50} In particular, solvents with the same bulk viscosity can have drastically different F_{CP} values.⁵¹⁻⁵³ Other studies have investigated internal solvent pressure, cohesive energy density, and solvent density as a way to predict and interpret F_{CP} . These methods have likewise met with little success.⁵⁴⁻⁵⁶ Furthermore, many of these latter solvent properties are complex and not easily or conveniently measured.

Further complicating the study of the radical cage effect is the difficulty in determining F_{CP} for some systems.^{57,58} As a result, our lab developed a straightforward method for determining F_{CP} using a model system based on photolysis of the Mo-Mo bond in the $\text{Cp}'_2\text{Mo}_2(\text{CO})_6$ dimer ($\text{Cp}' = \eta^5\text{-CH}_3\text{C}_5\text{H}_4$).^{59,60} This model system allowed us to study the effect of radical mass, size, and shape on F_{CP} .⁵¹ The study reported here uses the $\text{Cp}'_2\text{Mo}_2(\text{CO})_6$ system to investigate if the solvent microenvironment is a better parameter than bulk viscosity for predicting F_{CP} values. A portion of this study has been previously communicated.⁵³

3.2. Methods

General Considerations

All manipulations were carried out in the absence of water and atmospheric oxygen using standard glovebox and Schlenk techniques. To prevent unwanted photochemistry, a glove box was fitted with dark shrouds and the lights replaced with deep-red (633 nm) light emitting diodes. A standard darkroom with a deep-red safety light was also used.

Solvent systems used in this study had to meet a number of criteria to be useful. They should: not undergo disproportionation reactions with $\text{Cp}'_2\text{Mo}_2(\text{CO})_6$; not overlap in the $^1\text{H-NMR}$ with $\text{C}_6\text{H}_6\text{Cr}(\text{CO})_3$; be miscible with the radical trapping agent CCl_4 at 20 vol%; and significantly perturb either bulk viscosity or microviscosity. Solvent systems are detailed in Table C.1 with ranges of both bulk viscosity and microviscosity, and with relevant M_w for polymeric high viscosity additives (“viscogens”).

Determination of Bulk Viscosity

A Gay-Lussac pycnometer was used to determine the density of the solutions. The pycnometer was previously calibrated with 18 M Ω water at 25.0 °C. Solvent systems and the pycnometer were temperature-equilibrated in a box that was regulated with a heat exchanger at 25.0 °C for at least 30 minutes prior to measurement. Three Ubbelohde viscometers with different kinematic viscosity ranges were used in this study (Cannon Instrument UB-50, UB-75, and UB-100). A temperature regulated water tank was used to partially submerge the viscometers (regulated at 25.0 °C). The viscometers

measured kinematic viscosity, which was converted to dynamic viscosity (referred to as bulk viscosity in this paper, and measured in centipoise, cP). The viscometers were calibrated using neat solvents of a varying and known viscosity (Table C.2, Figure C.1).

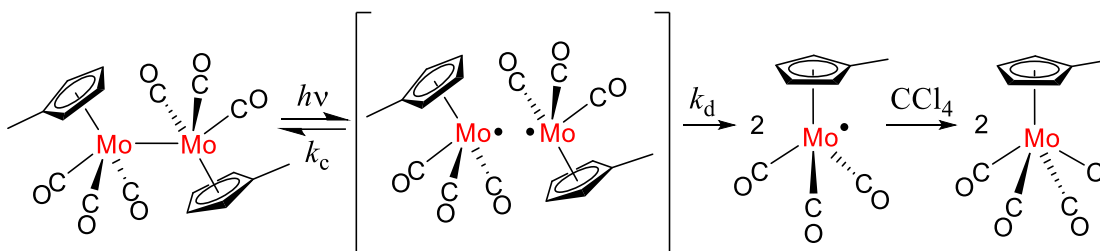
Photolysis Setup

An Oriel Merlin radiometry system was used to monitor the photoreaction of $\text{Cp}'_2\text{Mo}_2(\text{CO})_6$ in various solutions. The irradiation source was a modified 50 mW frequency doubled Nd:YAG diode laser pointer module (DPSS-5, 532 nm, Beam of Light Technologies) with a Oriel 100 mm², NIST-calibrated silicon photodiode (model 70356) detector.⁶¹ The beam was chopped with a five-blade chopper (Oriel model 75163) operating at 30.0 Hz to eliminate electrical line noise. A custom built water-jacketed cuvette-holder stir plate was regulated at 25.0 °C. The entire system was regulated at 25.0 °C using an air-flow radiator and water recirculator. Each sample was prepared in a darkened glovebox under an inert atmosphere before being transferred into a Schlenk UV-vis cell.

Determination of F_{CP}

In brief, finding F_{CP} involved measuring quantum yields for the disappearance of $\text{Cp}'_2\text{Mo}_2(\text{CO})_6$ as a function of solvent bulk viscosity. For the purposes of this work, all kinetic expressions and treatments are for a photochemical cage pair and not a thermally generated one.⁴⁸ When a $\text{Cp}'_2\text{Mo}_2(\text{CO})_6$ dimer is photolyzed at 532 nm, a radical cage pair is formed. The metal radicals may recombine (k_{CP}) or diffuse (k_{dP}) from the geminate radical cage. Diffusion out of the cage (k_{dP}) leads to trapping of the radical with CCl_4

(Scheme 3.2).⁵⁹ This reaction has been extensively studied with UV-vis and IR spectroscopy and shows no side reactivity.⁶² At a high enough concentration of CCl₄, collisional radical pairs produced by back diffusion (k_D , Scheme 3.1) are suppressed. The correct concentration of CCl₄ was previously determined.⁵¹ Radical trapping in the solvent cage does not occur, and only radicals that have diffused out of the cage are trapped (i.e., no “in-cage” trapping occurs).⁵¹ The [CCl₃] radicals produced do not react further with either the parent dimer or metal radicals.⁶³ Additionally, the multiplicity of the metal radicals has no effect on F_{CP} (i.e., there is no “spin barrier” to recombination).⁶⁴



Scheme 3.2. Photochemical production of caged radicals and subsequent trapping by CCl₄.

The observed quantum yield (Φ_{obsd} , for the disappearance of Cp'₂Mo₂(CO)₆) is given by eq 1. The linear portion of the absorbance slope (dA/dt) was used with the measured quantities of ϵ (extinction coeff.), volume, intensity, and the known path length of the cell. An example kinetic trace is shown as Figure C.2. The 100/%A term is a correction for nonabsorbance.

$$\Phi_{\text{obsd}} = \frac{-\left(\frac{dA}{dt}\right)(\text{volume})}{(\epsilon)(\text{pathlength})(\text{intensity})} \times \frac{100}{\%A} \quad (1)$$

Φ_{obsd} is related to the kinetic terms of Scheme 3.2 and to F_{CP} by eq 2.

$$\Phi_{\text{obsd}} = \phi_{\text{pair}} \left(\frac{k_{\text{dP}}}{k_{\text{cP}} + k_{\text{dP}}} \right) = \phi_{\text{pair}} (1 - F_{\text{cP}}) \quad (2)$$

Finding ϕ_{pair} will then yield the desired quantity F_{cP} . To find ϕ_{pair} , a further rearrangement is necessary to yield eq 3.

$$\left(\frac{1}{\Phi_{\text{obsd}}} \right) = \left(\frac{1}{\phi_{\text{pair}}} \right) \left(1 + \frac{k_{\text{cP}}}{k_{\text{dP}}} \right) \quad (3)$$

The term k_{dP} is inherently related to the bulk viscosity of the system. As the viscosity of the system decreases, k_{dP} becomes very large, and the term $(k_{\text{cP}}/k_{\text{dP}})$ becomes very small. If k_{cP} and ϕ_{pair} are assumed to be independent of bulk viscosity then the y-intercept of a plot of $1/\Phi_{\text{obsd}}$ versus viscosity is equal to ϕ_{pair} . See Figure C.3 for an example. Once ϕ_{pair} has been determined for a solvent system, Φ_{obsd} values are converted to F_{cP} using eq 2.

Excimer Fluorescence

Pyrene (Eastman Organic Chemicals, 98%) was first recrystallized from ethanol and then sublimed under reduced pressure. All samples were then manipulated in a dark, dry glovebox under inert atmosphere. Fluorescence measurements were conducted using a Quanta Master 40 spectrofluorometer (Photon Technology International) equipped with a Quantum Northwest TLC-50 temperature controller set at $25.0 \text{ }^{\circ}\text{C} \pm 0.05 \text{ }^{\circ}\text{C}$. Samples tested had a concentration of 10 mM pyrene. The excitation wavelength was 371 nm with an emission scan from 372-550 nm. See Figure 3.6 for a sample set of pyrene fluorescence spectra.

Determination of Diffusion Coefficient by NMR

NMR samples contained a flame sealed internal lock capillary of acetone- d_6 and were subsequently flame sealed under a blanket of argon. Diffusion ordered spectroscopy (DOSY) was performed on either a 500 or 600 MHz Bruker spectrometer (operating at ^1H 500.23 or 600.02 MHz, respectively) using the **ledbpgp2s** pulse sequence. See Figure C.4 for a sample spectrum. Pulse widths were individually calibrated to be 90° . A methanol temperature probe was used to confirm the internal temperature (25°C) of the probe prior to experimentation.⁶⁵

Determination of Solvent Polarity

Nile red was used to determine solvent polarity in mixed DMF/ CCl_4 solvents using known methods. See Figure C.5 for sample UV-vis spectra.^{66,67} The solvatochromic agent Betaine 30 was also investigated but it showed a limited solubility in CCl_4 despite literature to the contrary.⁶⁸ A Cary-60 UV-vis spectrophotometer was used to acquire spectra. The use of DMF/ CCl_4 is further discussed in Appendix C.

3.3. Results and Discussion

For many applications, one would like to be able to predict the value of F_{CP} for a given radical cage pair in a specific solvent. However, even if F_{CP} values are known for one solvent system, extending those results to another solvent system is impossible because different solvent systems having the same bulk viscosity typically do not have

the same F_{CP} values.⁵³ When starting this study, our hypothesis was that a solvent bulk property is unable to measure the “caging strength” of the solvent because the “caging strength” is a localized phenomenon. We reasoned that a local viscosity (i.e., microviscosity) would be more appropriate for predicting the strength of the solvent cage and hence F_{CP} .

To investigate our hypothesis, solvent systems with variable viscosity were designed. Specifically, the solvent systems consisted of a low viscosity component (e.g., *n*-hexane) and a high viscosity additive (e.g., paraffin). (All of the solvents systems also contained 20% CCl_4 as a radical trapping agent.) By increasing the percentage of the high viscosity additive (the “viscogen”), the bulk viscosity increased. The viscogen and low viscosity component were carefully chosen to prevent “selective solvation”; solvents and viscogens with very similar chemical structures were thus used. (It was initially hypothesized that selective solvation might affect the interpretation of the results.⁶⁹ However, as reported below, solvent systems having low- and high-viscosity components with significantly different polarities and structures did not adversely affect the correlation between F_{CP} and microviscosity.)

The initial solvent systems used in this study are listed on the right side of Figure 3.1. F_{CP} for the photochemical reaction in Scheme 3.2 was measured for each solvent system as a function of bulk viscosity (Figure 3.1). The different systems included nonpolar aromatics (toluene/1,1-bis(3,4-dimethylphenyl)ethane (DXE); toluene/polystyrene), aliphatics (*n*-hexane/paraffin; *n*-hexane/polybutenes), and a siloxane system (hexamethyldisiloxane (HMDS) /polydimethylsiloxane (PDMS)), along with one polar system (glyme/tetraglyme).

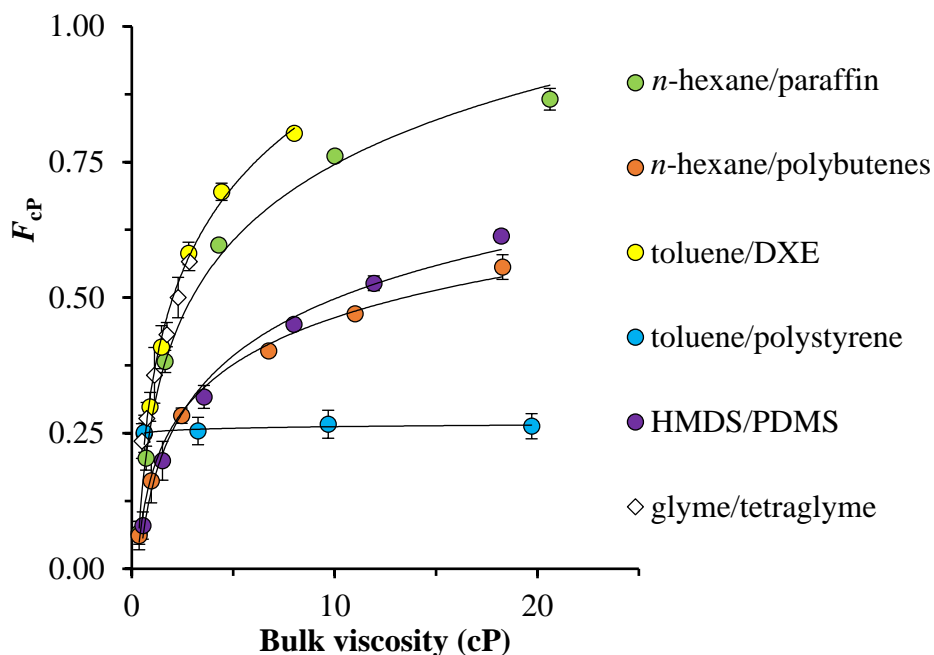


Figure 3.1. A plot of F_{CP} as a function of bulk viscosity (cP). Each sample contains 20 wt% CCl_4 ; error bars are 1σ ; curves are only a visual aid. The toluene/polystyrene data has been truncated for clarity, see Figure C.6.

The results in Figure 3.1 show that F_{CP} is not correlated to the bulk viscosity across different solvent systems. For example, if one looks at 5 cP, there are five different F_{CP} values for this bulk viscosity. Note that although the toluene/polystyrene solvent system shows a large increase in bulk viscosity there is only a minuscule change in F_{CP} . This result is interpreted as the polymer additive drastically changing the bulk viscosity but leaving the microenvironment around the radical cage pair unaffected. (Direct measurement of the microviscosity verified this interpretation, see below.)

Microviscosity Defined Using a Diffusion Coefficient

To test whether F_{CP} has a better correlation with microviscosity, it was first necessary to define a metric for microviscosity. In a previous paper, we developed the concept of using the diffusion coefficient of a probe molecule as a measurement of the microviscosity around that molecule.⁵³ In brief, according to the Stokes-Einstein equation (eq 4), viscosity (η) is proportional to $1/D$ (where D is the translational diffusion coefficient). It is important to note the viscosity (η) in this equation is the environment directly affecting the molecule whose translational diffusion coefficient (D) is being measured, i.e., the viscosity in the equation is the microviscosity.

$$D = \frac{k_{\text{B}}T}{6\pi\eta r} \quad (4)$$

An accurate measurement of microviscosity depends on an appropriate probe molecule. The radicals produced by photolysis in Scheme 3.2 are too short-lived to be directly observed using NMR. Therefore, a suitable surrogate molecule was required. Theoretical predictions by Noyes and experimental validation by our lab showed that $F_{\text{CP}} \propto \text{mass}^{0.5}/\text{radius}^2$ of the particles in the solvent cage.^{51,70,71} A suitable surrogate molecule, $\text{C}_6\text{H}_6\text{Cr}(\text{CO})_3$, closely meets the mass and radius required to mimic the $[\text{Cp}'\text{Mo}(\text{CO})_3]$ radicals.⁵³ (Note that all of the solvent systems studied are carefully selected to not have any overlapping NMR signals with the $\text{C}_6\text{H}_6\text{Cr}(\text{CO})_3$ probe molecule.) For each solvent system, diffusion coefficients of the $\text{C}_6\text{H}_6\text{Cr}(\text{CO})_3$ probe molecule were determined and then converted to a microviscosity by taking the reciprocal.

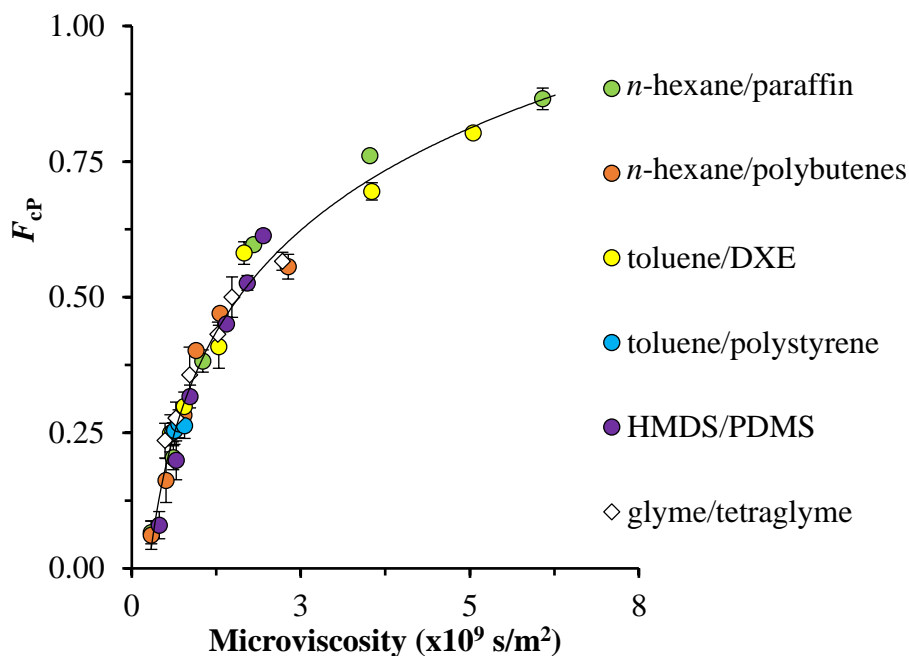


Figure 3.2. A plot of F_{CP} as a function of microviscosity. Each sample contains 20 wt% CCl_4 ; error bars are 1σ ; a single curve is used as a visual aid.

When F_{CP} is plotted as a function of microviscosity, all of the solvent systems fall on the same trend line (Figure 3.2). This plot spans solvent types from aliphatic to polar. Note that the toluene/polystyrene system shows that the microviscosity does not change, as predicted above. It is suggested that all of the F_{CP} values for that system are essentially the same because the microenvironments are the same at each bulk viscosity.

Mixed Solvent Systems and the Effect of Polarity

With the apparent validation of the hypothesis relating F_{CP} to microviscosity in solvent systems composed of similar solvents and viscogens, we wanted to test the limitations of the F_{CP} -microviscosity relationship by studying solvent systems with dissimilar solvents and viscogens. The dissimilar solvents could produce selective

solvation that would affect F_{CP} . The possibility of solvent interactions affecting F_{CP} was previously shown by our lab with [RCpMo(CO)₃] radicals forming agostic interactions with amide H-bonds.⁷² The practical importance of predicting F_{CP} values in mixed solvent systems cannot be overstated. For instance, radical polymerizations contain solvent as well as significant amounts of alkene monomer. Being able to predict F_{CP} in the polymerization reaction solution is critical when it comes to designing the polymerization process.

To test the limitations of our method, we studied three new mixed solvent systems where selective solvation could impact microviscosity. The three new solvent systems are listed in the legend of Figure 3.3, which shows the plots of F_{CP} vs bulk viscosity for the reaction in Scheme 3.2. As was the case in Figure 3.1, all of the new solvent systems show the general trend of increasing F_{CP} with increasing bulk viscosity. But, as was the case in Figure 3.1, it is impossible to predict F_{CP} values based on bulk viscosity. In contrast, in the plots of F_{CP} vs microviscosity (Figure C.7), all of the F_{CP} points fall on the same trend line.

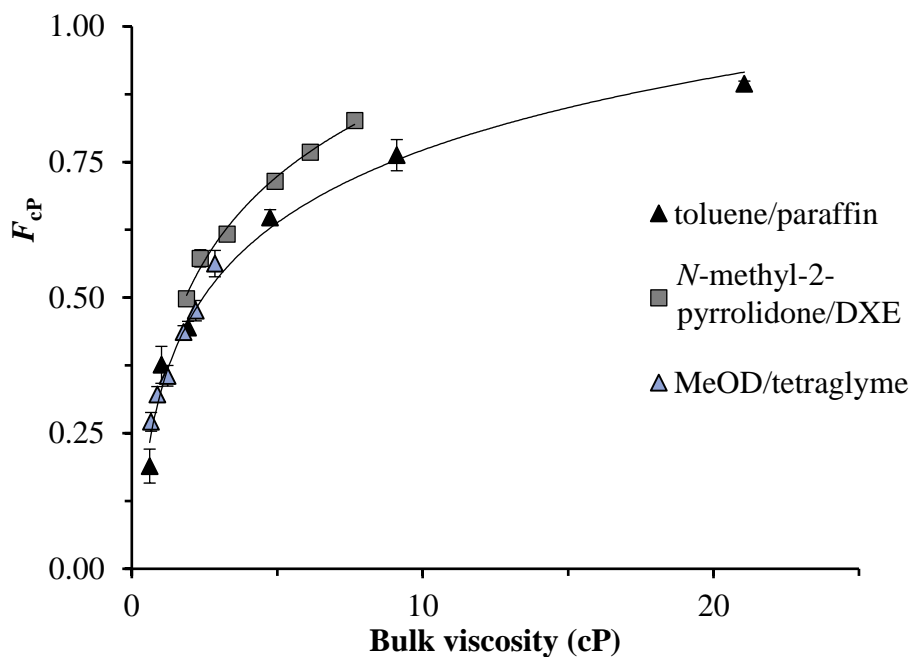


Figure 3.3. A plot of F_{cp} as a function of bulk viscosity (cP). Each sample contains 20 wt% CCl_4 ; error bars are 1σ ; curves are only a visual aid.

Furthermore, the curve in Figure C.7 is the same curve as that shown in Figure 3.2 (see Figure 3.4, which shows the results in Figure 3.2 and C.7 plotted together). The proposed interpretation is that because the microviscosity is a direct indication of the local environment around the solvent cage pair there is no need to differentiate solvents on the basis of polarity, hydrogen bonding ability, or other solvent properties.

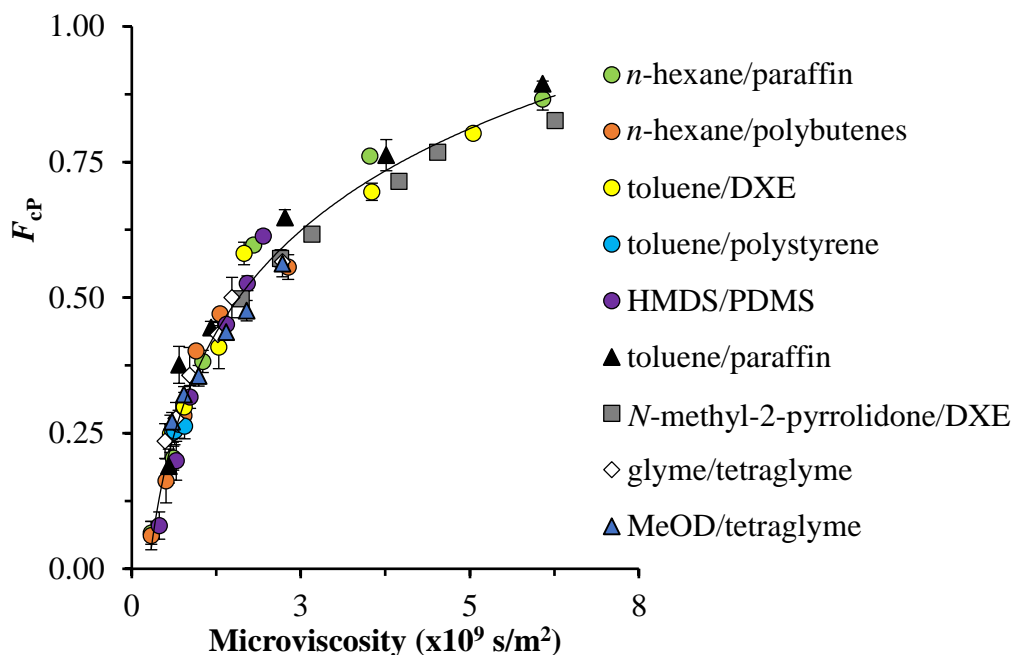


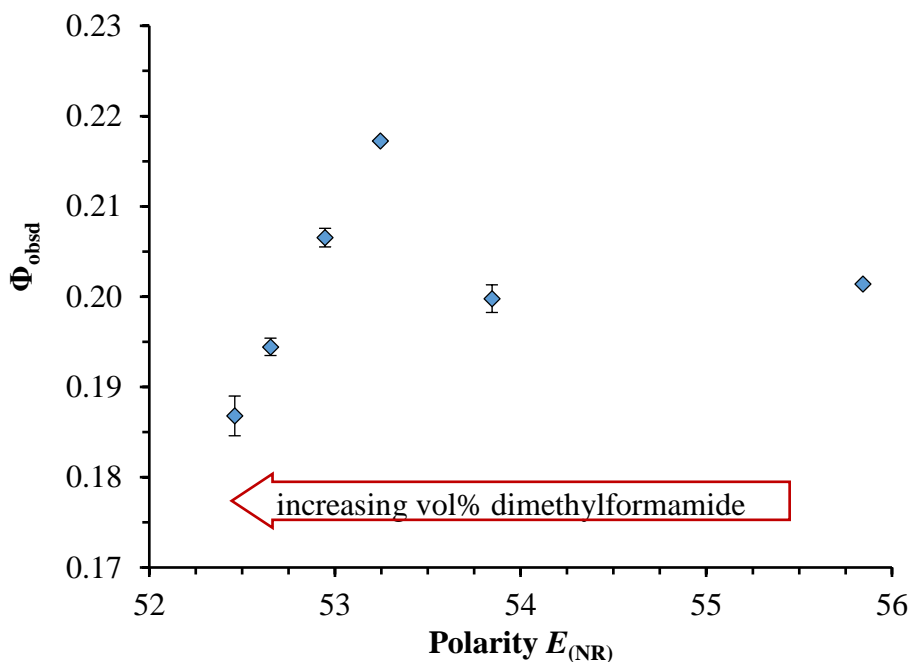
Figure 3.4. A plot of F_{cp} as a function of microviscosity. Each sample contains 20 wt% CCl_4 ; error bars are 1σ ; a single curve is used as a visual aid. This plot contains all of the solvent systems tested in this study.

Additional tests confirmed that polarity has little effect on F_{cp} . To probe the role of polarity, dimethylformamide was used as the solvent because of its similar bulk viscosity to CCl_4 , the radical trap used throughout this investigation (DMF 0.80 cP, CCl_4 0.90 cP).⁷³

A series of mixed solvent systems containing an increasing amount of DMF was made with the bulk viscosity and microviscosity being measured in the same way as described earlier (Table 3.1).

Table 3.1. Properties of the DMF/CCl₄ mixed solvent systems.

DMF (vol%)	CCl ₄ (vol%)	bulk viscosity (cP)	microviscosity (x 10 ⁹ s/m ²)	polarity ⁶⁶ $E_{(NR)}$
0	100	0.90	0.82	55.84
16	84	0.93	0.90	53.85
32	68	0.99	0.93	53.24
48	52	0.98	0.92	52.95
64	36	0.93	0.88	52.65
80	20	0.88	0.86	52.46

**Figure 3.5.** A plot of Φ_{obsd} as a function of polarity ($E_{(NR)}$, see 3.3 Methods, Determination of Solvent Polarity). Error bars are 1 σ .

The quantum yields for the DMF/CCl₄ solvent systems are presented in Figure 3.6. Note that Φ_{obsd} varies only slightly with polarity: the range of Φ_{obsd} is 0.19-0.22. For comparison, Φ_{obsd} for the *n*-hexane/paraffin solvent system is 0.10-0.65. Furthermore, there is only a small correlation of Φ_{obsd} with either bulk viscosity or microviscosity (Figure C.8-C.9). Because solvent polarity has only a minimal effect on

Φ_{obsd} , there will only be a minimal effect of polarity on F_{CP} . Generalizing this result, the mixed solvent systems of Figure C.7 would be expected to only depend on the microviscosity of the system, and indeed this is the case (Figure 3.4).

Microviscosity Defined with Excimer Fluorescence

To corroborate the microviscosity results obtained by NMR, another method for measuring microviscosity was also investigated that could rival the simplicity of DOSY. It is well-known that pyrene can form excimers in solution. The formation of the excimer is dependent on the concentration of pyrene, its diffusion coefficient, and the temperature of the solution (with more exact methods using all of these variables to measure systems as complicated as cellular membranes).^{74,75} To simplify the method, both concentration and temperature were held constant in our study. Consequently, the variability of excimer:monomer emission is only due to changes in the microviscosity of the solution (Figure 3.6). The monomer/excimer fluorescence ratio can therefore be used as an indication of the microviscosity.

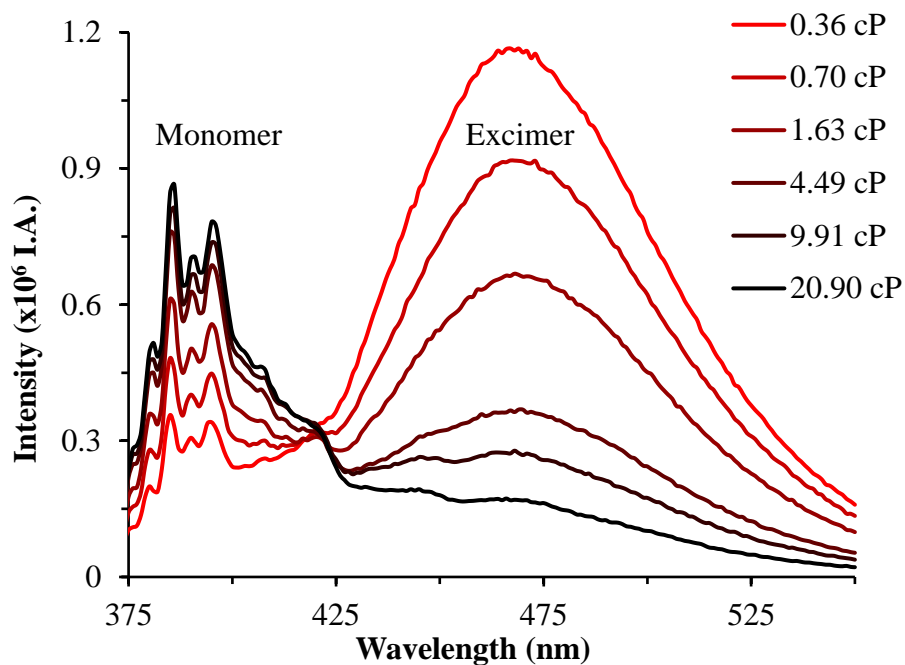


Figure 3.6. Monomer and excimer fluorescence of pyrene at different viscosities. Solvent system is hexane/paraffin with CCl_4 constant at 20 wt%. Concentration of pyrene is constant between samples at 10 mM ($25.0\text{ }^\circ\text{C} \pm 0.05\text{ }^\circ\text{C}$).

F_{CP} values for the photochemical reaction in Scheme 3.2 as a function of the pyrene monomer/excimer fluorescence ratio are shown in Figure 3.7. Note that unlike the plots in Figure 3.4, the curves in Figure 3.7 do not overlap.

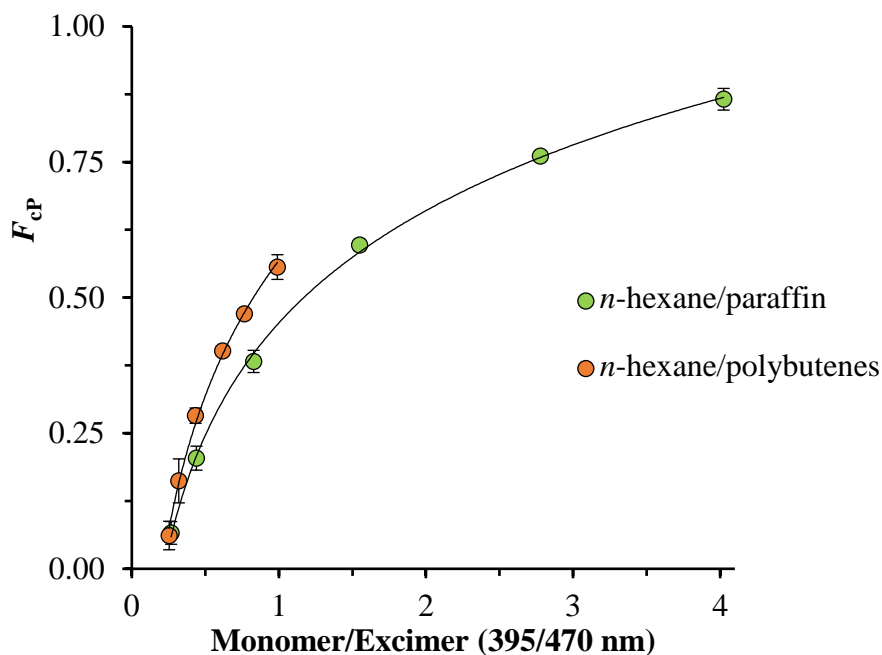


Figure 3.7. A plot of F_{cp} as a function ratio of monomer fluorescence to excimer fluorescence. Each sample contains 20 wt% CCl_4 ; error bars are 1σ ; curves are only a visual aid.

The deviation of the curves in Figure 3.7 may be caused by an intrinsic problem with the fluorescence method or it may be caused by an inappropriate probe molecule. Obviously, the pyrene probe molecule is significantly different in volume and mass compared to the $[\text{Cp}'\text{Mo}(\text{CO})_3]$ radicals produced by photolysis. Using the appropriate probe molecule was key to the success of the NMR method, and the unsuitability of the pyrene molecule may be responsible for the deviation in Figure 3.7. It is noted that we studied only two solvent systems in this experiment because significant quenching by CCl_4 occurred in all other solvent systems such that minimal excimer fluorescence was detected.⁷⁶ Because of the quenching and because of the poor performance of the pyrene probe, the fluorescence method was not pursued further.

Theoretical Basis for Microviscosity Dictating F_{cP} .

The results presented above suggest that microviscosity is a reasonable choice for a parameter that can be used to quantitatively predict F_{cP} . We rationalize the dependence of F_{cP} on microviscosity as follows. Algebraic manipulation of the equation for F_{cP} ($F_{cP} = k_{cP}/(k_{cP} + k_{dP})$), gives eq 5.

$$F_{cP} = \frac{1}{1 + \left(\frac{k_{dP}}{k_{cP}}\right)} \quad (5)$$

This equation can be further manipulated to contain only observables. The diffusion rate constant, k_{dP} , can be related to the diffusion coefficient, D , using the Smoluchowski equation ($k_{dP} \propto D$).⁷⁷ Likewise, because the recombination rate, k_{cP} , is critically dependent on the radicals' orbital alignment, k_{cP} is dependent on the rotational correlation time of the radicals ($k_{cP} \propto \tau_C$). (Fast radical rotation in the cage would misalign the orbitals and prevent recombination, which is why $k_{cP} \propto \tau_C$.) Eq 5 can therefore be rewritten as eq 6, in which a is a constant.

$$F_{cP} = \frac{1}{1 + \left(\frac{aD}{\tau_C}\right)} \quad (6)$$

Prior femtosecond pump-probe experiments by our lab showed that radical rotation does not occur on the time scale of primary geminate recombination.⁷⁸ This observation negates the need for τ_C in the equation for F_{cP} . Ignoring τ_C in eq 6 and using the relationship $\eta_{\text{micro}} \propto 1/D$ gives eq 7 (where c is a constant), an equation that yields the curve shape in Figure 3.4.

$$F_{\text{cP}} = \frac{1}{1 + \left(\frac{c}{\eta_{\text{micro}}}\right)} \quad (7)$$

3.4. Conclusions

The goal of this study was to find a method to quantitatively correlate F_{cP} values to the properties of the solvent system. Although bulk viscosity qualitatively correlates with cage recombination efficiency, the shortcomings of using bulk viscosity for quantitative work are well-known. The new method developed in this study employs microviscosity, a parameter straightforwardly measured using an NMR probe. As demonstrated herein, microviscosity provides a reliable correlation between the cage recombination efficiency in all categories of solvents, thus lending itself to quantitative predictions. The correlation between F_{cP} and microviscosity holds for a wide range of solvent systems, spanning nonpolar, polar, aromatic, and hydrogen bonding solvents. In addition, selective solvation from mixed-type solvent systems was shown to not significantly affect the predictive power of the method. It is important to emphasize the straightforwardness of the method: to predict F_{cP} of a particular radical, all that is needed is to measure the diffusion coefficient of an appropriate NMR probe.

Finally, it is noted that the correlation of microviscosity with F_{cP} appears to be attributable to the judicious selection of the probe molecule. The probe molecule must be a structurally similar mimic for the radicals. Probe molecules may be difficult to find for some radicals because closed shell analogues can potentially diffuse much faster than the radicals they intend to mimic.⁷⁹ But even in these cases, it may be possible to extract

meaningful results. An experimental and theoretical analysis by Strickrath et al. sought to resolve the difference between the diffusion rates of alkyl radicals produced from alkylcobalamin photodissociation and their closed shell mimics.⁸⁰

3.6. Bridge

The work presented in both Chapters II and III sought to define a parameter that could be used to predict F_{CP} in any solvent regardless of type. Microviscosity was the parameter that was most appropriate to do this.

An additional parameter that affects F_{CP} for the $\text{Cp}'_2\text{Mo}_2(\text{CO})_6$ dimer is the wavelength at which it is irradiated. Although this may be a specific case, the wavelength dependence of F_{CP} was investigated nonetheless in Chapter IV.

CHAPTER IV

WAVELENGTH DEPENDENCE OF RECOMBINATION
EFFICIENCIES OF RADICAL CAGE PAIRS GENERATED
FROM $\text{Cp}'_2\text{Mo}_2(\text{CO})_6$ DIMER

Justin T. Barry

Department of Chemistry and Biochemistry, University of Oregon, Eugene, OR

97403-1253

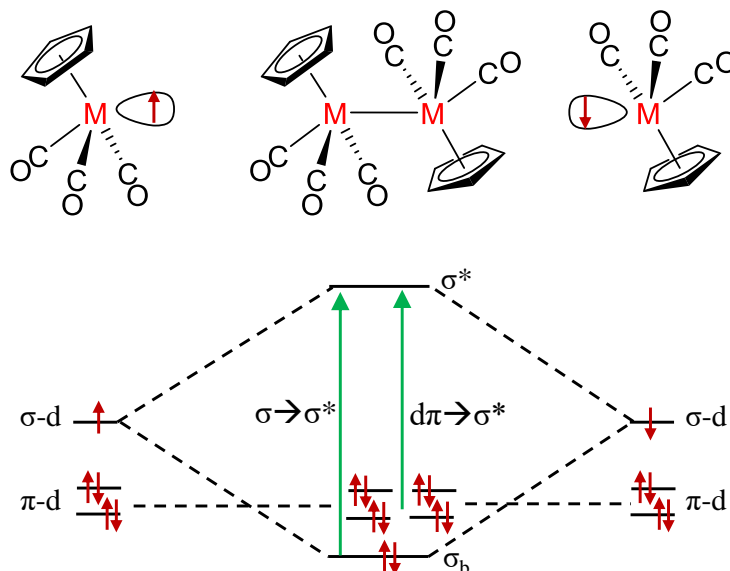
Chapter IV of my dissertation details experiments and investigations into the wavelength dependence on recombination efficiencies (F_{cP}) for the $\text{Cp}'_2\text{Mo}_2(\text{CO})_6$ dimer. This builds upon prior experimentation conducted in the Tyler lab. The goal of this research was to further build the understanding of what factors affect the solvent cage effect.

4.1. Introduction

The dependence of F_{cP} on microviscosity (discussed in Chapters 2 and 3) began with the observation that solvent systems with the same bulk viscosity didn't have the same recombination efficiency F_{cP} . Following up on observations that didn't fit a general hypothesis on F_{cP} led to very fruitful research. By following up on these discrepancies, it was discovered that *microviscosity* could accurately predict the solvent cage effect. The

wavelength dependence of F_{CP} for the $Cp'_2Mo_2(CO)_6$ dimer was selected as the next parameter for study.

For the $Cp'_2Mo_2(CO)_6$ dimer, there are two dominate electronic transitions ($d\pi \rightarrow \sigma^*$ at 505 nm, and $\sigma \rightarrow \sigma^*$ at 393 nm). Both of these homolyze the Mo-Mo bond to form a radical caged pair by promotion of an electron to the σ^* orbital (Scheme 4.1). It should be noted that irradiation at $\sigma \rightarrow \sigma^*$ (393 nm) results in a small amount of CO-loss product. This is most likely due to an overlap of a $d\pi \rightarrow \pi^*$ (CO) metal-to-ligand charge transfer band (MLCT) with the $\sigma \rightarrow \sigma^*$ band.¹ F_{CP} values for the $Cp'_2Mo_2(CO)_6$ have been experimentally shown to vary depending on the irradiation wavelength.² This was for samples with the same solvent system (hexane/squalane/ CCl_4), at the same bulk viscosity, and with the same identity of the dimer. (Bulk viscosity and the identity of the dimer can change the observed recombination efficiency.)^{3,4}



Scheme 4.1. Conceptual diagram of the two halves $[CpM(CO)_3]$ of a $Cp_2M_2(CO)_6$ dimer to illustrate the electronic transitions (M = Mo, or W).⁵ Green arrows represent the electronic transitions.

4.2. Results

The first step was to successfully repeat prior results and determine that F_{cP} does vary with wavelength.² An Oriel 200 W high pressure mercury arc lamp and a monochromator would be used to generate the irradiation wavelength (prior work was conducted using a 50 mW frequency doubled Nd:YAG diode laser at 532 nm).⁶ The experiment for determining F_{cP} was more challenging for this system due to the use of the mercury arc lamp. The intensity of light that is produced by the 200 W high pressure mercury arc lamp is ~6% of the output from the laser system. This means that the overall experiment for the data collection is much longer and introduces more error from temperature and power fluctuations (larger error bars in F_{cP} than previous experiments).

Another experimental difficulty was the mercury arc lamp contains very strong mercury-lines. These had to be considered when designing the experiment with a monochromator that has a bandpass. For instance, there is a strong 404.7 nm emission (“H-line”) for mercury. If the monochromator were set to 397 nm the majority of incoming irradiation on the sample would still be from the 404.7 nm line (because of the bandpass). The monochromator was rastered 1.0 nm at a time to determine the mercury lines and compared to the electronic spectrum of the $Cp'_2Mo_2(CO)_6$ dimer (Figure 4.1).

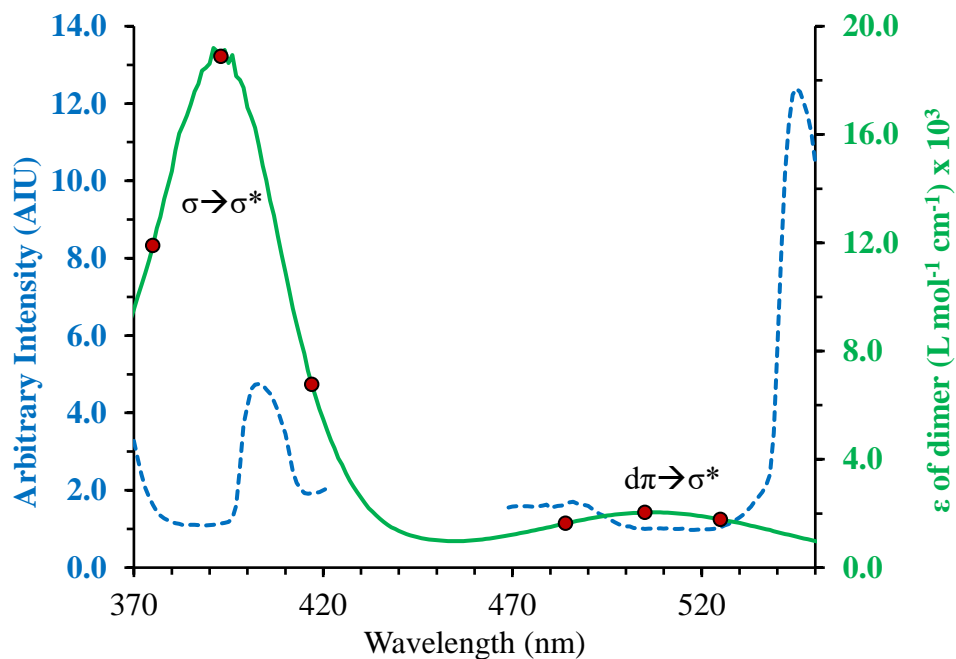
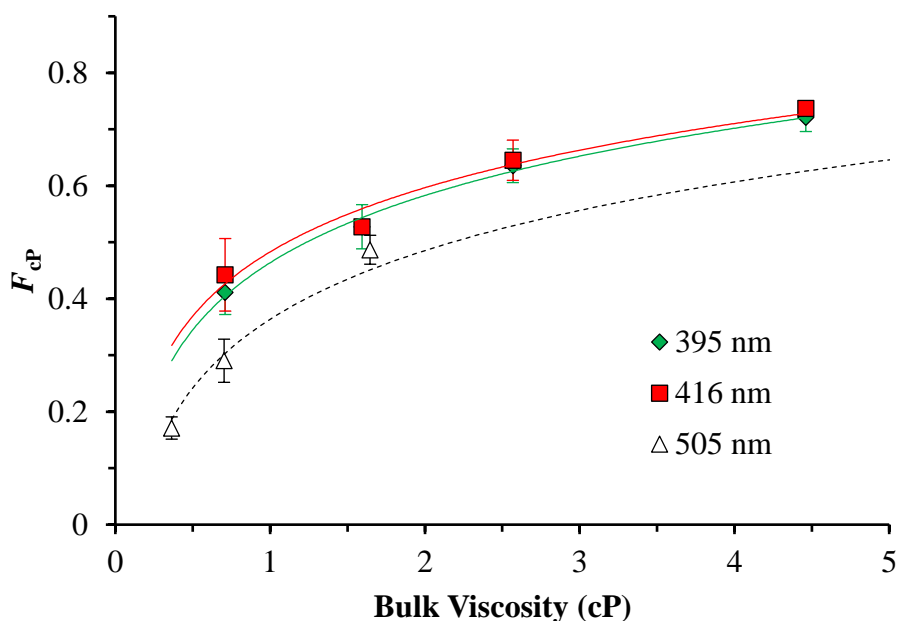


Figure 4.1. Plot of intensity of the 200 W high pressure mercury arc lamp vs wavelength selected on monochromator (blue dashed trace). Electronic spectrum of $\text{Cp}'_2\text{Mo}_2(\text{CO})_6$ dimer also plotted (green trace). Selected wavelengths for irradiation are red circles on solid green trace.

Six wavelengths were initially selected to irradiate (Figure 4.1, Table 4.1). Three wavelengths at each electronic transition were chosen. This was to test if the energy of excitation within the same electronic transition had an effect on F_{CP} . These three wavelengths in the same electronic transition only spanned an energy range of ~3 Kcal/mol whereas the difference between the two electronic transitions is ~10 Kcal/mol (Table 4.1). A preliminary set of data shows the expected reported relationship between wavelength of irradiation and F_{CP} (Figure 4.2).²

Table 4.1. Wavelengths of irradiation with energy conversion.

Transition	Wavelength (nm)	Energy (Kcal/mol)
$d\pi \rightarrow \sigma^*$	526	54.35
$d\pi \rightarrow \sigma^*$	505	56.61
$d\pi \rightarrow \sigma^*$	484	59.07
$\sigma \rightarrow \sigma^*$	416	68.73
$\sigma \rightarrow \sigma^*$	395	72.38
$\sigma \rightarrow \sigma^*$	374	76.45

**Figure 4.2.** Plot of F_{CP} vs bulk viscosity with irradiation at different wavelengths for the $Cp'_2Mo_2(CO)_6$ dimer. The 505 nm data set contains two more points off scale at 10.0 and 20.6 cP. Error $\pm 1\sigma$. (*n*-hexane/paraffin oil/ CCl_4 solvent system at 25 ± 0.1 °C)

From this preliminary set of data, the literature precedent was replicated. The best fit lines of the $\sigma \rightarrow \sigma^*$ transition at 395 and 416 nm are nearly the same while the best fit line of the $d\pi \rightarrow \sigma^*$ transition at 505 nm is significantly different from the other two wavelengths. In other words, irradiation at different electronic transitions changes F_{CP} ,

but changing wavelength within the same electronic transition doesn't change F_{CP} . Both this data and the literature example show that the higher the energy of the electronic transition, the greater the value of F_{CP} . Further work on this project was halted to construct a testable hypothesis after the successful replication of this data.

4.3. Discussion and Conclusions

Any excess energy that is not used to homolyze the Mo-Mo bond ($D_{Mo-Mo} \approx 35$ Kcal/mol) is left over for other processes. The λ_{max} between the two electronic transitions spans a difference of almost 16 Kcal/mol (505 nm = 56.61 Kcal/mol, 395 nm = 72.38 Kcal/mol). This excess energy and the fate of that energy may explain the discrepancy in the F_{CP} values. Dissipation of this energy as vibrational energy takes place in two stages.⁷ Intramolecular vibrational relaxation (IVR) occurs (10-0.1 ps) followed by intermolecular vibrational energy transfer (VET) to the solvent (1000-10 ps).⁷ Both of these processes must be considered because the lifetime of the primary radical cage is ≈ 5 ps.⁸

One proposed theory is that the excess energy is immediately transferred to the solvent that composes the cage around the radicals. This produces a locally "hot" environment of caging solvent molecules. This is expressed as either vibrational or translational motion in these solvent molecules. The microenvironment is ultimately responsible for the solvent cage effect (Chapters 2 and 3) and this translational motion would act to decrease the strength of the solvent cage. Therefore it would be expected

for F_{CP} to decrease with increasing excitation energy. This is the opposite of what is observed.

This hypothesis uses the classical view of just a primary solvent cage (Primary Solvent Cage, Figure 4.3). In this simplified model, the molecules directly participating in the solvent cage (blue dashed line, Figure 4.3) are being affected. If the primary cage for these radicals $[\text{Cp}'\text{Mo}(\text{CO})_3]\cdot$ is only 5 ps, then perhaps the intermolecular vibrational energy transfer actually occurs during the secondary solvent cage (Figure 4.3).

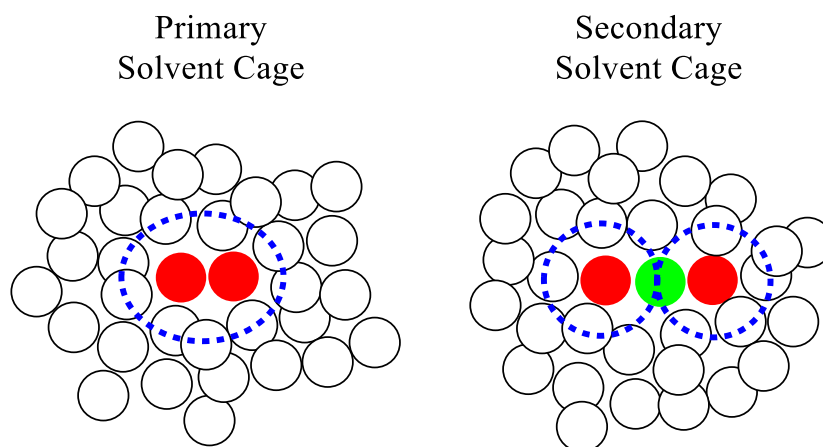


Figure 4.3. Solvent molecules (white circles) participating in intermolecular vibrational energy transfer (blue dashed lines) from the radical pair (red circles). Secondary solvent cage shows the solvent molecule (green circle) separating the radical pair.

The secondary solvent cage occurs when the radicals separate enough for a solvent molecule to enter between them. If this secondary cage is where intermolecular vibrational energy transfer occurs, then the solvent molecule(s) separating the two radicals (green circle, Figure 4.3) receives much more vibrational energy transfer than the solvent cage. This would lead to increased translational and rotational energy of this particular solvent molecule. These separating solvent molecules would then be more apt to leave and the geminate radicals would then enter back into the primary cage. The

overall affect would be the increase of F_{cP} , which is what is actually observed. A method to test this specific hypothesis is being developed.

The results of the prior chapter corroborate prior research on the wavelength dependent nature of F_{cP} for the $Cp_2Mo_2(CO)_6$ dimer. Unfortunately, no testable hypothesis was developed with our current methodology. Potentially further experimentation with femtosecond pump-probe spectroscopy may expand our understanding at different wavelengths. Although these techniques have been successfully used with the $Cp'_2Mo_2(CO)_6$ dimer, only pump experiments at the $d\pi \rightarrow \sigma^*$ transition were conducted. Ultrafast relaxations were observed using these experiments and were assigned to vibrational relaxation events.⁸ Perhaps irradiation at the $\sigma \rightarrow \sigma^*$ would dramatically change the magnitude of these vibrational relaxations and give experimental evidence for the hypothesis given.

4.4. Bridge

This chapter and prior chapters only examined the symmetrical $Cp'_2Mo_2(CO)_6$ dimer. Homolysis of this Mo-Mo bond would result in two caged radicals that are identical (both are $Cp'Mo(CO)_3$). An attempt to synthesize an asymmetric molybdenum dimer was conducted to test how asymmetrical radical pairs behave in solution. This is critical because radical caged pairs can be any size.

CHAPTER V

PROGRESS TOWARDS AN ASYMMETRIC MOLYBDENUM DIMER TO STUDY SIZE AND MASS DEPENDENCE ON F_{CP} OF ASSYMETRIC RADICAL PAIRS IN A SOLVENT CAGE

Justin T. Barry

Department of Chemistry and Biochemistry, University of Oregon, Eugene, OR

97403-1253

Chapter VI of my dissertation details the work completed towards the synthesis of an asymmetric molybdenum dimer of the type $R^1Cp(CO)_3Mo-Mo(CO)_3CpR^2$ (where $R^1 \neq R^2$). Although ultimately unsuccessful in the synthesis of an asymmetric molybdenum dimer using one particular method, two different synthetic methods and recommendations to apply to further research are made. Selected experimental details are contained in Appendix D.

5.1. Introduction

All of the previous chapters dealt with the photolysis of the molybdenum dimer $Cp'_2Mo_2(CO)_6$ (where $Cp' = \eta^5-CH_3C_5H_4$). This photolysis will split the Mo-Mo bond and generate two symmetrical molybdenum radicals that are initially caged together by the solvent. The convenience of using the $Cp'_2Mo_2(CO)_6$ cannot be overstated. In

photolysis, the dimer has two electronic transitions ($d\pi \rightarrow \sigma^*$ at 505 nm, and $\sigma \rightarrow \sigma^*$ at 393 nm) to allow photolysis at one wavelength and probing at the other (Figure 5.1). The homolysis reaction is concerted with no intermediates.¹ Once the radicals have escaped the solvent cage, they will then react irreversibly with CCl_4 .² This trapped radical $[\text{Cp}'\text{Mo}-\text{Cl}(\text{CO})_3]$ has an electronic transition that doesn't interfere with the transitions of $\text{Cp}'_2\text{Mo}_2(\text{CO})_6$ (Figure 5.1). Any resulting $\cdot\text{CCl}_3$ radicals (from the Cl abstraction) don't react further with any remaining molybdenum radicals (hexachloroethane has been observed).³ Furthermore the synthesis of the symmetrical dimer is relatively straightforward.^{4,5} Synthetic manipulation of the Cp' ligand doesn't alter the electronics of the Mo-Mo bond (critical for comparisons between different dimers). For characterization, the dimer is diamagnetic and yields NMR spectra (Figure 5.2), while the carbonyl ligands on the molybdenum offer a wonderful fingerprint using FT-IR (Figure 5.3).

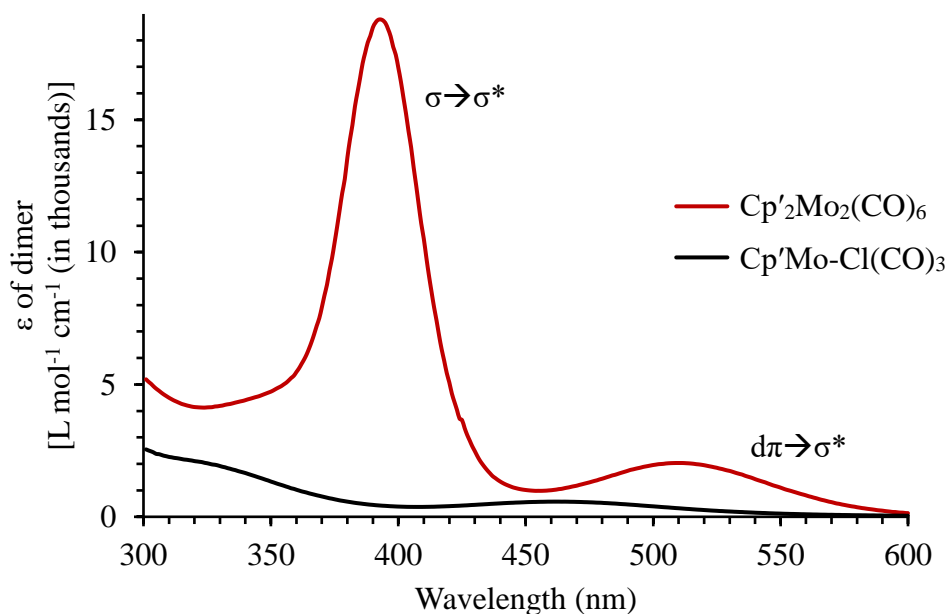


Figure 5.1. Electronic spectrum of both the $\text{Cp}'_2\text{Mo}_2(\text{CO})_6$ dimer and $\text{Cp}'\text{Mo}-\text{Cl}(\text{CO})_3$.

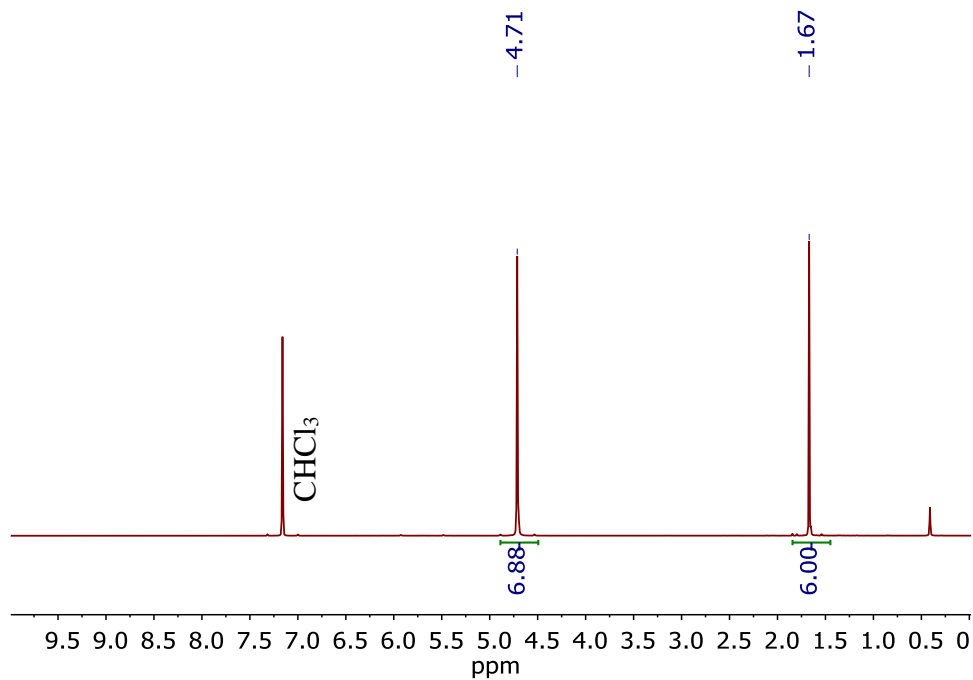


Figure 5.2. $^1\text{H-NMR}$ of the $\text{Cp}'_2\text{Mo}_2(\text{CO})_6$ dimer (in CDCl_3 , not T1 optimized, Acros).

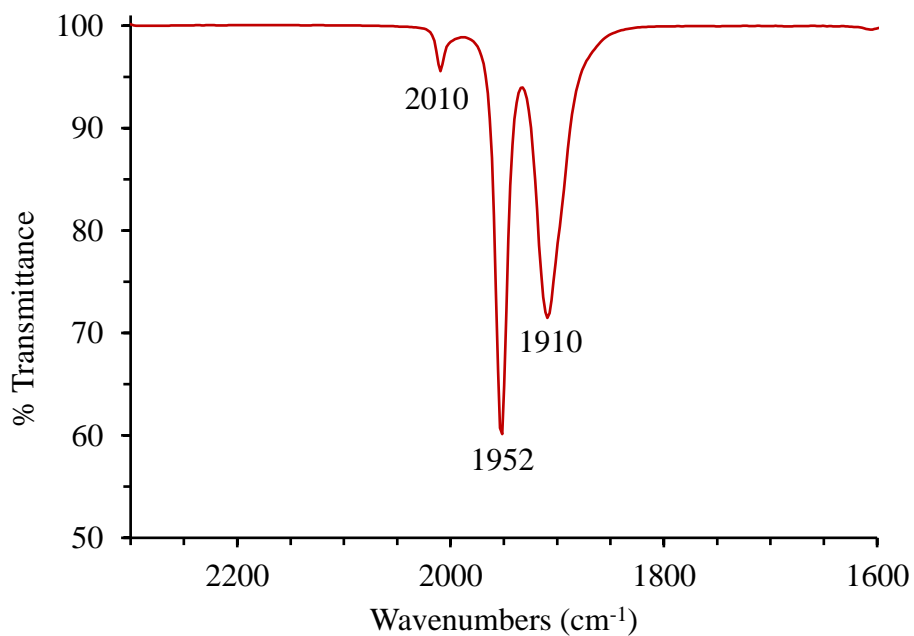


Figure 5.3. Infrared spectrum of $\text{Cp}'_2\text{Mo}_2(\text{CO})_6$ dimer (in DCM, solvent subtracted, Acros).

Many different symmetrical dimers have been produced by modification of the Cp' ligand and followed with characterization using NMR, FT-IR, and UV-vis. This has yielded many fruitful investigations of the radical cage effect. By modifying the Cp' ligand, the overall size and mass of the radical can be manipulated. This led to the first experimental validation of a prediction by Richard Noyes that $F_{CP} \propto \text{mass}^{0.5}/\text{radius}^2$ (mass and radius of the radical).⁶⁻⁸

Although a major breakthrough in our understanding of the radical cage effect for symmetrical radical pairs, how does this $F_{CP} \propto \text{mass}^{0.5}/\text{radius}^2$ relationship apply to asymmetrical radical pairs? In general, the situation of asymmetrical radical pairs is fairly common, with alkylcobalamins being a fervent area of study.⁹ These alkylcobalamins undergo photolysis to split the Co-R bond, producing a very large Co radical (with a large porphyrin-like ligand) and a very small alkyl radical (Figure 5.4). Two more examples of photochemically active organometallics are Cp_2TiCl_2 and a molybdenum dimer $\text{RCp}(\text{CO})_3\text{Mo-Mo}(\text{CO})_3\text{CpR}^2$ (Figure 5.4).

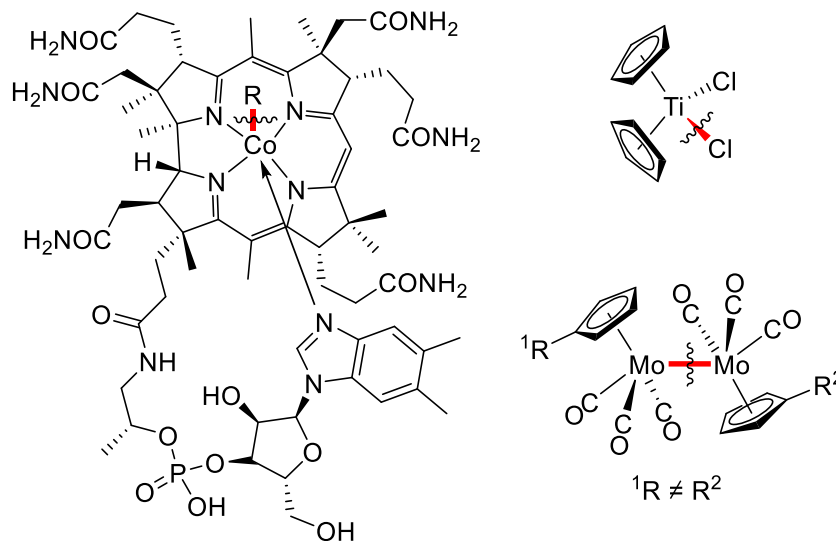
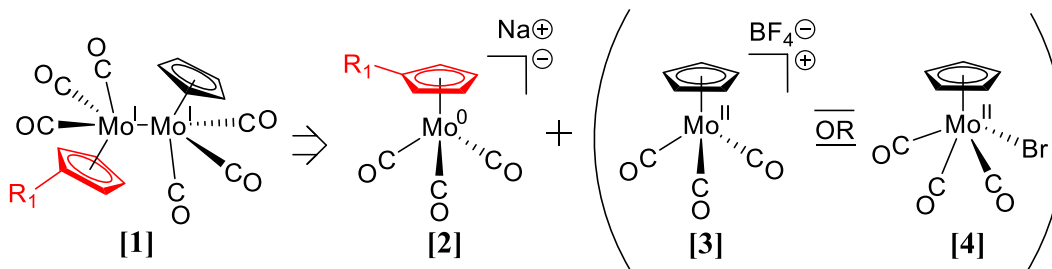


Figure 5.4. Examples of organometallic molecules where photolysis results in a solvent caged radical pair that contains two different sized radicals. (Bond breaking indicated by red bond with \sim through it)

The most attractive molecule to probe asymmetric radical pairs is the $\text{RCp}(\text{CO})_3\text{Mo}-\text{Mo}(\text{CO})_3\text{CpR}^2$. This molecule has all the properties of the symmetrical $\text{Cp}'_2\text{Mo}_2(\text{CO})_6$, and would allow direct comparisons with our prior results. In particular, the electronic transitions of the Mo-Mo bond remain unchanged and the same irradiation wavelength can be used (Chapter IV details the wavelength dependence of F_{CP}). This will actually make characterization of a true asymmetric dimer very difficult (same UV-vis and FT-IR of symmetric dimer).

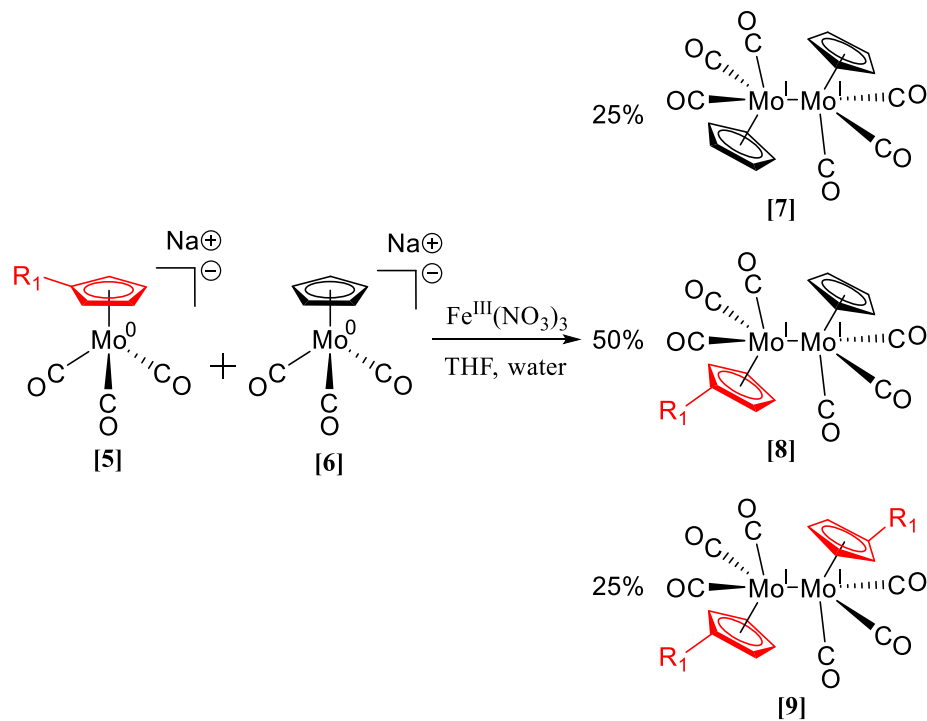
There are three readily conceivable ways of synthesizing an asymmetric dimer. The first method ([1], Scheme 5.1) can be retrosynthetically thought of as splitting the Mo-Mo bond into a molybdenum(0) anion and a molybdenum(II) cation ([2] and [3]/[4], respectively, Scheme 5.1). This will be called the “cation/anion” approach. Addition of these two components together should result in the coupling of both halves to yield the Mo(I) dimer ([1], Scheme 5.1, the substituted ligand will be color-coded red from now on

to add clarity).¹⁰ Additionally, there has been some literature precedent in generating asymmetrical dimers by using a molybdenum(II) bromide complex ([4]).^{11,12} However, these asymmetric dimers were fairly simple with only pentamethylcyclopentadiene and cyclopentadiene ligands shown to work.



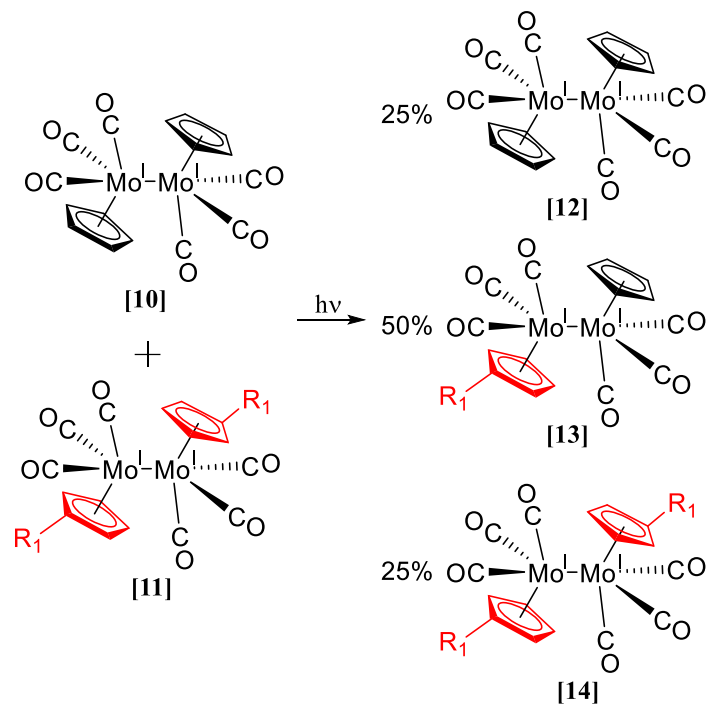
Scheme 5.1. Retrosynthesis of an asymmetric dimer using the “cation/anion” approach.

The second conceivable method is the “one electron oxidation” of a Mo(0) species to generate transient 17 electron molybdenum(I) complexes that then couple together in solution to form dimers (Scheme 5.2).^{5,13} Note that two different molybdenum(0) complexes ([5] and [6]) would have to be used to generate an asymmetric dimer ([8], Scheme 5.2). This results in a statistical distribution of both an asymmetric dimer and two symmetrical dimers ([7], and [9]). Both of these symmetrical dimers would have to be removed prior to photolysis experiments. This route is more traditional in the synthesis of symmetrical dimers. To make a symmetrical dimer, a single molybdenum(0) precursor is oxidized.



Scheme 5.2. Generation of molybdenum dimers using the “one electron oxidation” method.

The third and final type of synthesis would be irradiation of two symmetrical molybdenum dimers ([10], and [11], Scheme 5.3) in the absence of any radical trap. This would again provide a statistical distribution of the intended asymmetric dimer [13]. The starting symmetric dimers ([10] and [11]) would have to be available or synthesized using the “one electron oxidation” described above. This method is called the “photochemical cross-over”.



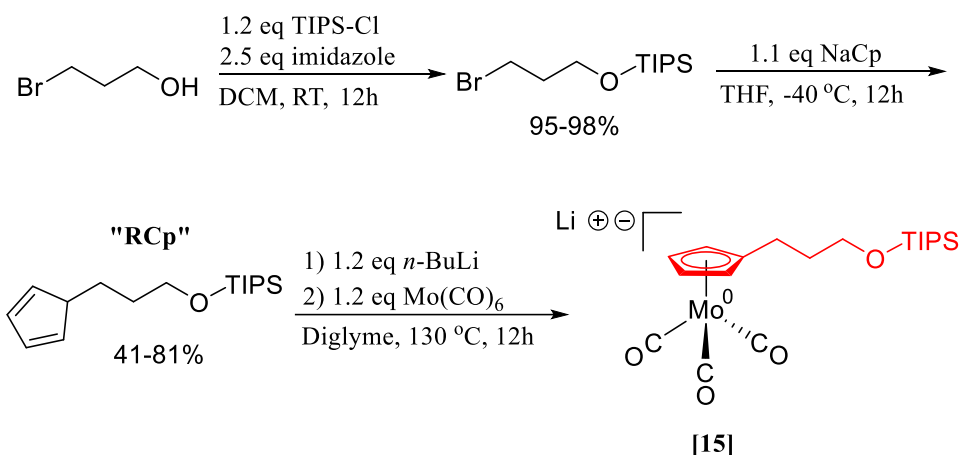
Scheme 5.3. “Photochemical cross-over” method of synthesizing an asymmetric dimer.

5.2. Synthesis

The first synthetic route attempted was the “cation/anion” method. This route had been previously investigated by our lab and had shown some promise.¹⁰ The “cation/anion” method would also produce only one product, whereas the other two methods the maximal theoretical yield can only be 50%. This product would also be much easier to purify by not being contaminated with other dimer species.

The first step is to synthetically modify one of the cyclopentadiene ligands on either the “anion” or the “cation”. The synthesis and purification of the cation is fairly challenging, so the anion was chosen to be modified. For symmetric dimers of various sizes, the ligand is typically modified with an alkyl chain ending in an alcohol. The dimer can then be subsequently modified with esterifications to form any size dimer

required. The same approach with an alcohol end group was attempted for the asymmetric dimer. A triisopropylsilyl (TIPS) ether was used to protect the alcohol of 3-bromo-1-propanol (Scheme 5.4). The bromide was attacked with sodium cyclopentadienide to generate the required ligand (**RCp**, Scheme 5.4). This was then deprotonated with *n*-BuLi and reacted with Mo(CO)₆ to form the anion ([**15**], Scheme 5.4, no yield, used *in situ*).

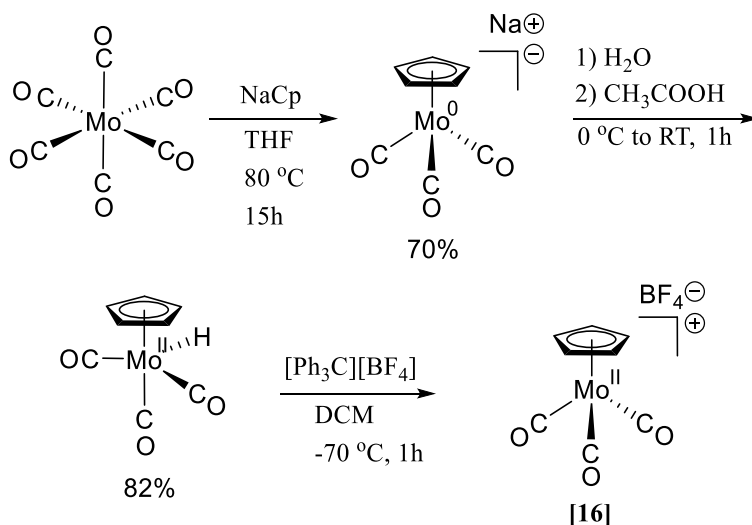


Scheme 5.4. Synthetic route to the anion complex [**15**].

It is worth noting some thoughts regarding the final reaction of Scheme 5.4. There was some confusion about the identity of free substituted cyclopentadiene (**RCp**) ligand. The **RCp** ligand readily undergoes a Diels-Alder to form an **RCp** dimer. The confusion originates because synthetic schemes only show the free substituted cyclopentadiene and never the Diels-Alder product (even if there was a work-up of the reaction where the Diels-Alder product inevitably formed). This **RCp** dimer cannot be deprotonated by the *n*-BuLi. This was confirmed by a control experiment of reacting dicyclopentadiene with *n*-BuLi followed by a quench with D₂O. If deprotonation of

dicyclopentadiene occurred, then deuteration would be readily apparent in the $^1\text{H-NMR}$. This was not the case. Cracking of the Diels-Alder RCp dimer with heat will release the free RCp to be deprotonated (hence using diglyme as a solvent and heating to $130\text{ }^\circ\text{C}$ in Scheme 5.4).

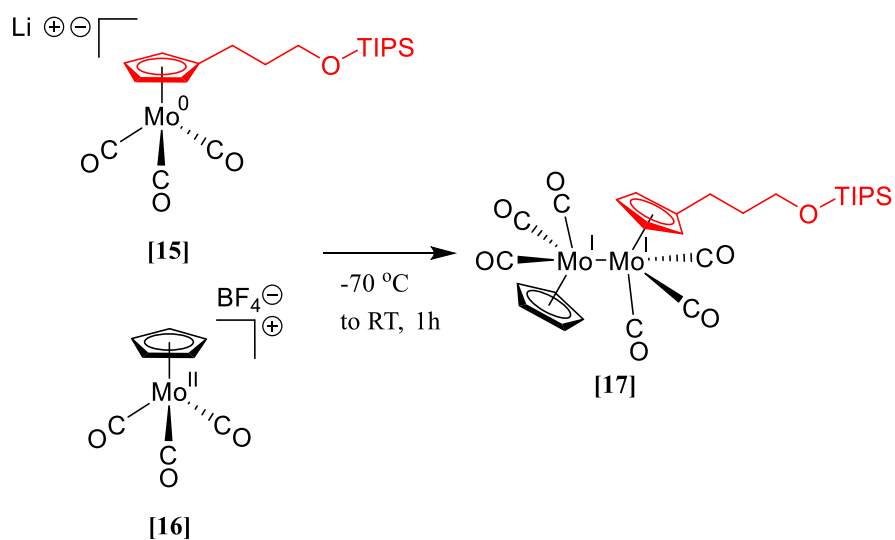
The synthesis of the “cation” begins with the reaction of $\text{Mo}(\text{CO})_6$ with sodium cyclopentadienide (Scheme 5.5). The product should look familiar because it is a $\text{NaCpMo}(\text{CO})_3$ “anion” (Scheme 5.4). This anion is then reacted with acetic acid, forming the yellow hydride complex in high yields. Finally, a hydride abstractor is added to remove a hydride and generate a molybdenum(II) complex. This forms the required “cation” complex ([16], Scheme 5.5, no yield because the complex is used *in situ* due to thermal instability¹⁴).



Scheme 5.5. Synthetic route to a “cation” complex.

The final step of the “anion/cation” method is the combination of the anion complex [15] and the cation complex [16]. (Scheme 5.6). Initially, it was believed that

only an asymmetric dimer was formed. Thin layer chromatography (TLC) separated multiple products that were consistent with a Mo-Mo dimer (determined by scraping off the spot of silica, dissolving in CHCl_3 , filtering and then UV-vis). Column chromatography in a dark glovebox was used in an attempt to purify. Only a very small amount of product was obtained. The resulting infrared and NMR spectra both are indicative of an asymmetric molybdenum dimer (Figure 5.5 and 5.6, respectively). Whether or not this is the intended asymmetric dimer is difficult to determine by NMR, FT-IR, and UV-vis. This is because the electronics of the Mo-Mo dimer are unchanged (no change in UV-vis or FT-IR), and a 1:1 distribution of symmetrical dimers would give identical integrals in the NMR. Crystallography would unambiguously determine the structure. Unfortunately, the relatively greasy triisopropylsilyl ether and the small amount of product made crystallization unsuccessful. Furthermore, it was discovered later that the typical deprotection step for silyl ethers (treatment with a fluoride source) degraded the Mo-Mo dimer. For these reasons the silyl ethers were abandoned as protecting groups.



Scheme 5.6. Final synthetic step of the "cation/anion" method to form an asymmetric dimer complex [17].

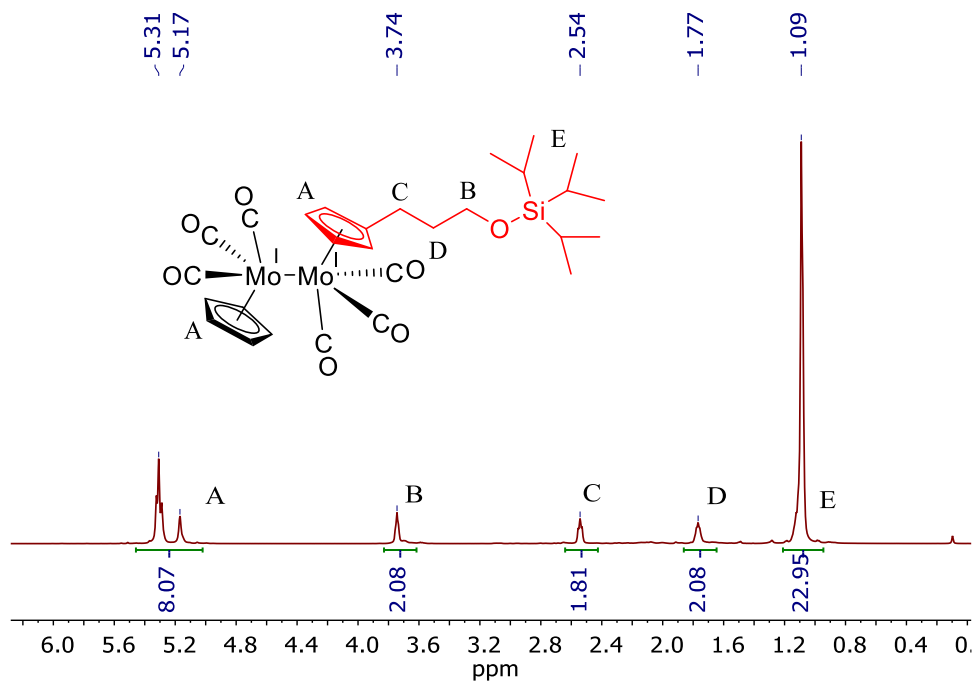


Figure 5.5. ¹H-NMR of complex [17].

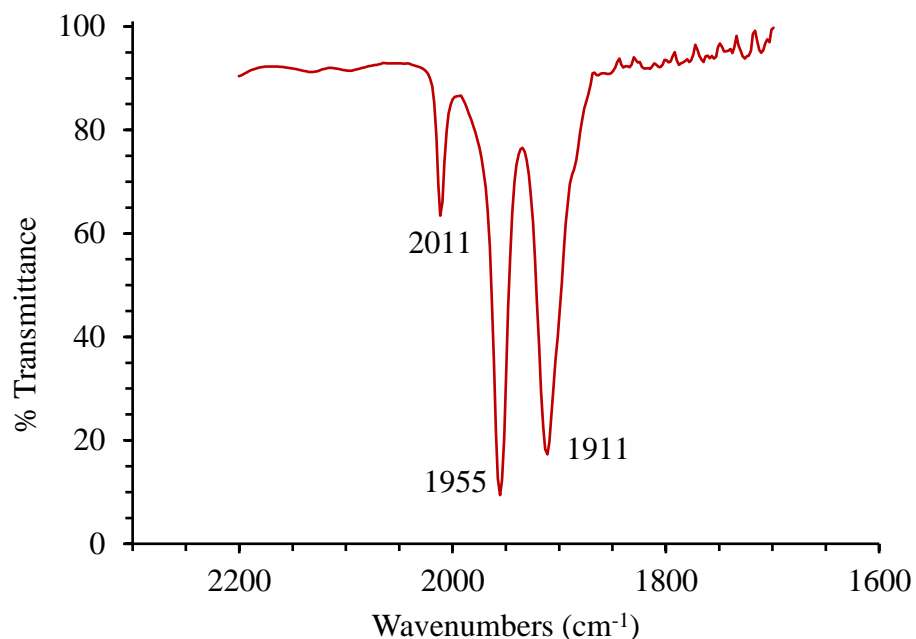
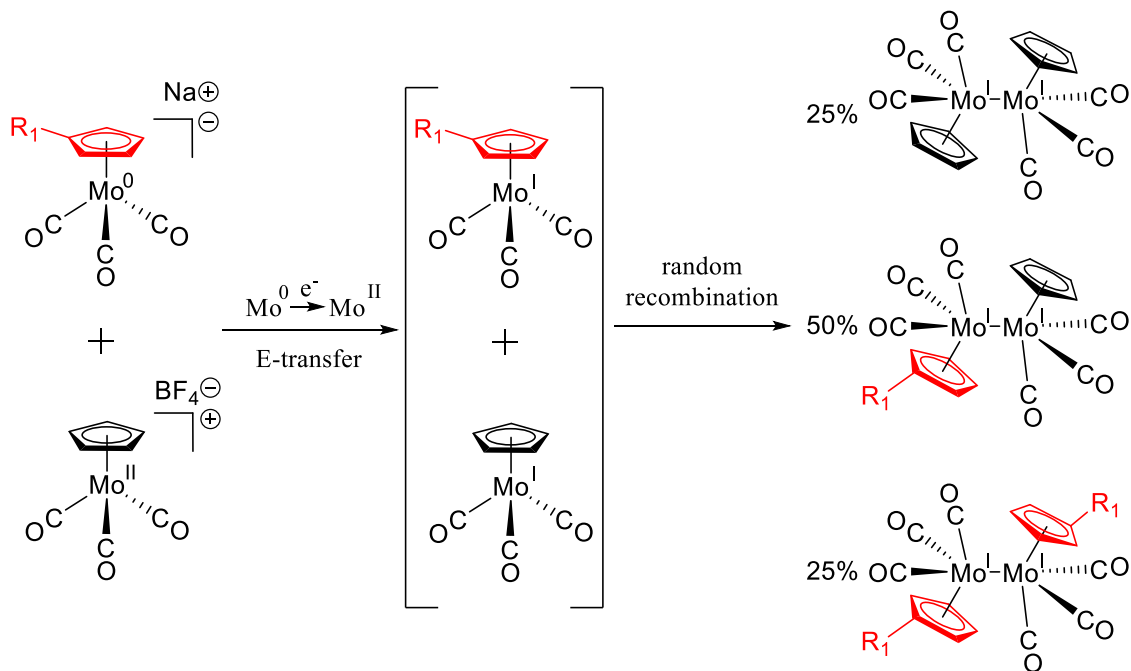


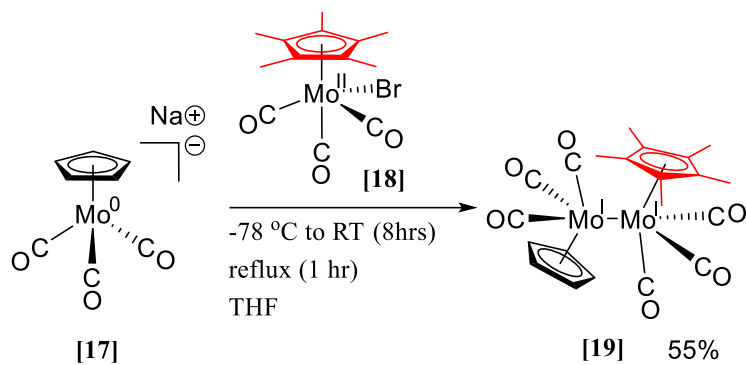
Figure 5.6. FT-IR spectrum of [17] (solvent subtracted from DCM).

Two things needed to happen to continue the “cation/anion” method. First, an acid sensitive 3,4-dihydro-2*H*-pyran (THP) protecting group was selected to replace the silyl ether protecting group. The THP group can be removed with acetic acid (which does not react with the dimer). Second, the thermal-instability of the tetrafluoroborate complex [16] prevented a thorough purification before its usage. This may have contributed to the low yields of the expected asymmetric dimer. Also, it is conceivable that electron transfer was occurring between the molybdenum(0) anion and the molybdenum(II) cation that would additionally lower yields (Scheme 5.7). This would also explain the observation of multiple Mo-Mo dimer products. This may have been testable by using a radical trap to capture a Mo(I) intermediate but was not attempted.

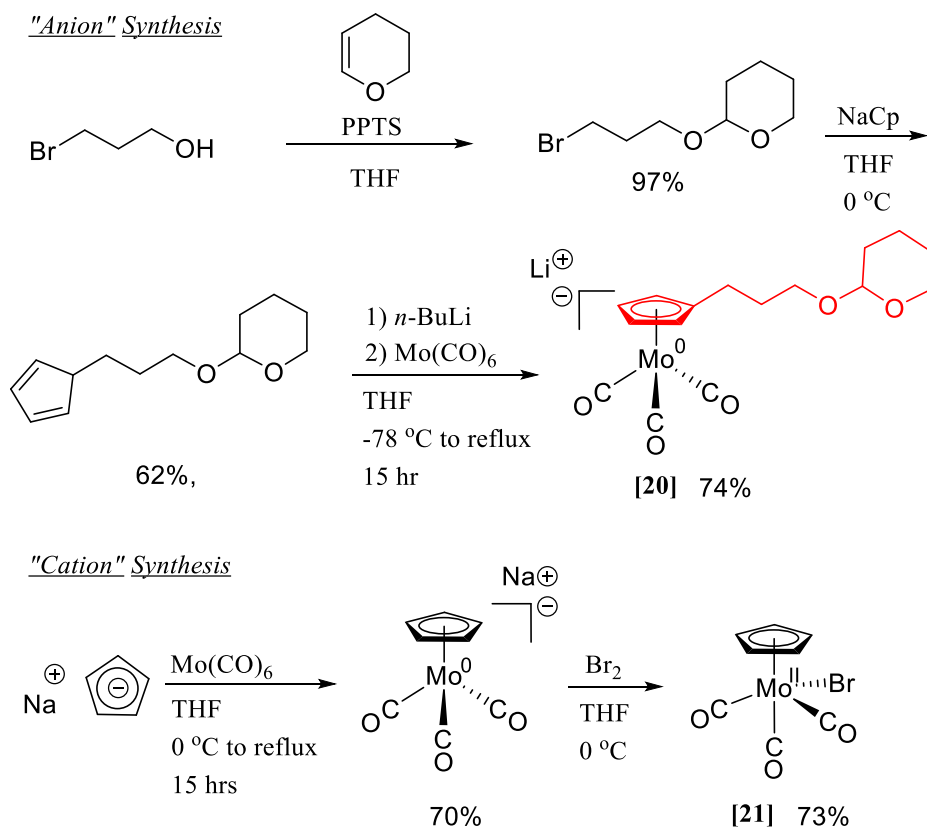


Scheme 5.7. Electron transfer between the “cation” and “anion” resulting in both symmetric and asymmetric dimer products.

A literature prep detailing the synthesis of an asymmetric dimer was found to circumvent issues with the tetrafluoroborate complex **[16]**.^{7,8} The synthesis involved the reaction between a molybdenum(0) **[17]** anion and a molybdenum(II) bromide **[18]** to produce an asymmetric dimer **[19]** (Scheme 5.8). The bromide complex **[18]** was much more thermally stable than the tetrafluoroborate complex **[16]**. This provided an attractive route to produce a simple asymmetric dimer. For our purposes, a protected alcohol would be required on the cyclopentadiene ligand. The synthetic route to obtain the appropriate anion (with a protected alcohol) and bromide complex are shown as Scheme 5.9.



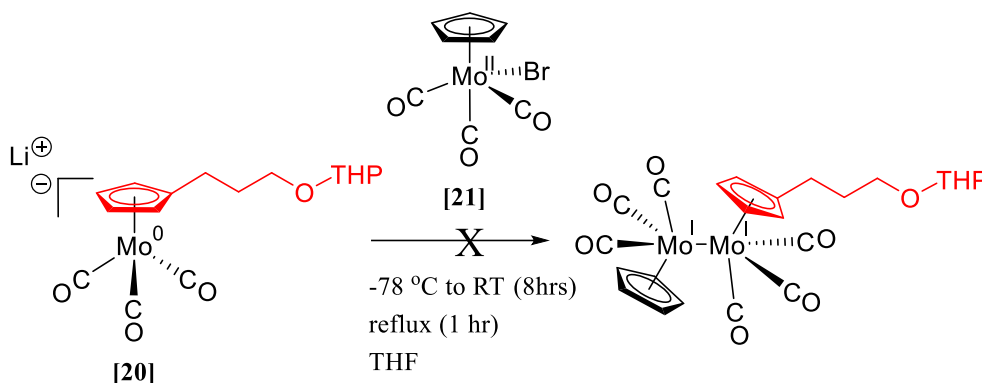
Scheme 5.8. Literature synthesis of a mixed ligand dimer.



Scheme 5.9. Synthesis of anion [20] and bromide [21] complexes.

The bromide complex proved to be thermally stable and could be obtained as a pure material. However, the first reaction conditions followed were those from literature

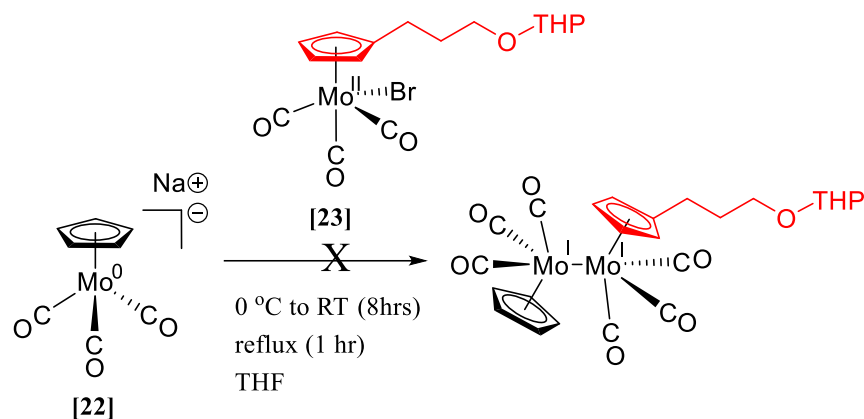
(Scheme 5.10), that is, complexes [20] and [21] were made and used without work up. The bromide complex [21] was subsequently cannulated into the [20] anion solution. The [20] anion complex featured the cyclopentadienide THP protected alcohol. The reaction was monitored by IR and stretches corresponding to a dimer complex were recorded. Upon careful crystallization and workup, only the symmetric $\text{Cp}_2\text{Mo}_2(\text{CO})_6$ dimer was shown in the NMR (no incorporation of the substituted cyclopentadiene ligand).



Scheme 5.10. Reaction conditions according to literature procedure.¹¹

It was postulated that the [20] anion had a reduced reactivity due to the substituted cyclopentadiene ligand and that the bromide complex reacted in some unknown fashion to produce a $\text{Cp}_2\text{Mo}_2(\text{CO})_6$ dimer. It is unknown how this transformation occurs. The literature prep had a sodium counterion for the [20] anion complex, our reaction instead had a lithium counterion. Perhaps the lack of solubility of the lithium bromide in THF was affecting the reaction. Therefore, complexes [22] and [23] were synthesized to address these concerns. As the previous reaction (Scheme 5.10) showed no change in the IR stretches until the reaction was brought to room temperature, future reactions were

begun at 0 °C instead of -78 °C. Again the [23] bromide complex was cannulated into the [22] anion solution (Scheme 5.11).



Scheme 5.11. Reaction of a bromide complex [23] with a substituted cyclopentadiene ligand with an anion complex [22].

Monitoring the reaction by IR over time showed the appearance of stretches indicating a Mo-Mo dimer (Figure 5.7). The reaction was worked up, and surprisingly, only the symmetric Cp₂Mo₂(CO)₆ dimer was isolated. If the reaction were to fail in a similar manner to the first attempt (Scheme 5.10), the symmetric molybdenum dimer with substituted cyclopentadiene ligands would be expected. The anion and bromide complexes used in this synthesis contained small amounts of impurities. More work was done to purify the starting materials and to try the reaction again.

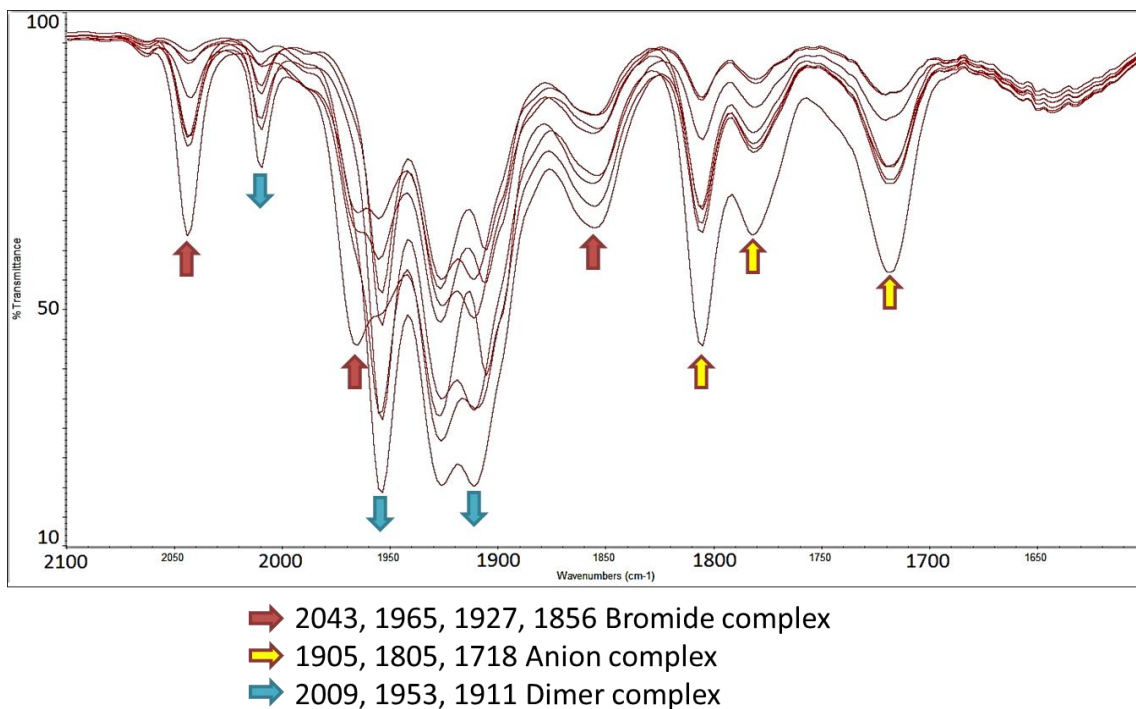


Figure 5.7. Monitoring the reaction of Scheme 11 by FT-IR.

In previous reactions, diglyme was used as a solvent primarily because the boiling point was high enough to retro-Diels-Alder any dimerized cyclopentadiene ligands. However this made the purification of the anions nearly impossible. Any diglyme left in the reaction would cause the complexes to oil instead of precipitate (most likely because the anion complex likes to co-precipitate with solvent molecules). This solvent issue was circumvented by the thermal cracking of the cyclopentadiene ligands immediately prior to a reaction. Purification procedures for the bromide and anion complexes were the slow addition of a saturated solution to hexane which caused precipitation of the complex. The purification of complexes incorporating the substituted cyclopentadiene proved the most difficult. Any THF or diglyme left from the reaction would cause the complex to oil. Instead, the THF was removed *in vacuo* and the complex dissolved in

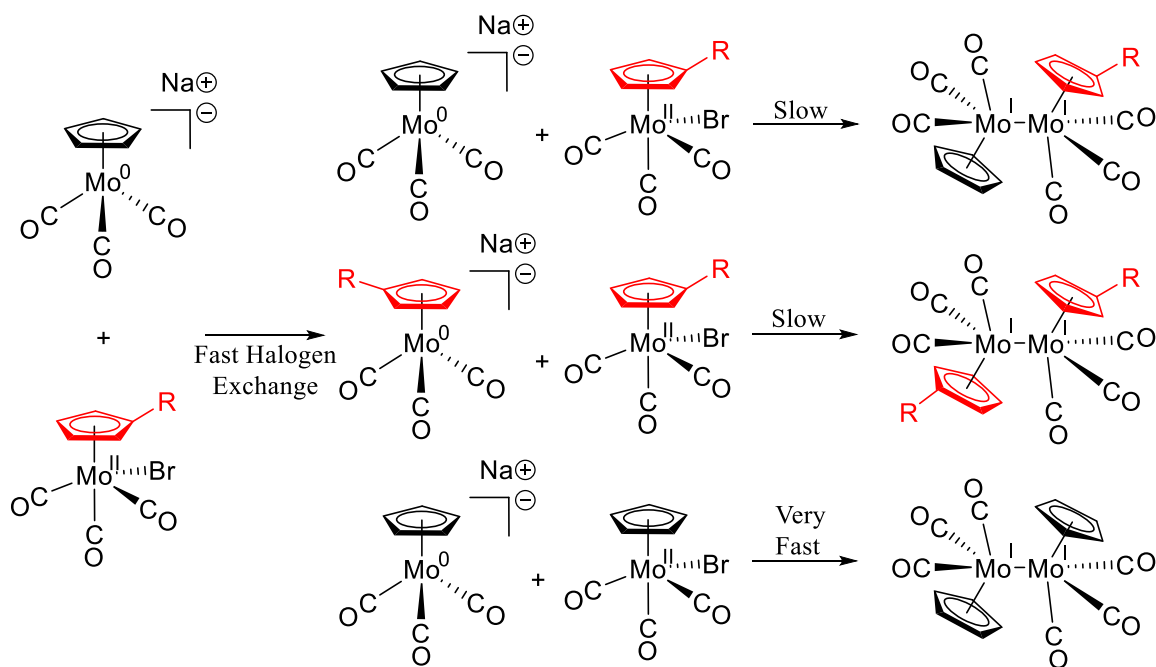
DCM before being adding to hexane. The subsequent infrared spectrum of the purified complexes was much cleaner and sharper.

With the purified complexes, the reaction between a bromide and anion complex was attempted again (Scheme 5.11). Again, only the symmetric $\text{Cp}_2\text{Mo}_2(\text{CO})_6$ dimer was shown to be isolated by NMR. The crude dimer product was serially recrystallized to see if any trace amount of asymmetric dimer was present. Both the supernatant and the crystallization showed no asymmetric dimer. Careful workup of the water and hexane washes from the initial crystallization of the reaction solution yielded no dimer. Unreacted $\text{NaCpMo}(\text{CO})_3$ anion was seen in the water layer by FT-IR (addition of the $\text{NaCpMo}(\text{CO})_3$ anion to water does not result in protonation to the hydride complex $\text{CpMoH}(\text{CO})_3$).

Reactions negating the reflux step were also performed. Here the idea was that the reflux was thermally scrambling an initially formed asymmetric dimer. The reaction proceeded slowly and no asymmetric dimer was isolated. Reactions were performed with different stoichiometric amounts including subsequent additions of bromide complex throughout the reaction progression, to no avail. A solution of bromide in THF was allowed to sit for seven days to check its stability. No dimer stretches or decomposition of the bromide complex was observed by IR.

The results from the reactions were both puzzling and disappointing. The substituted cyclopentadiene ligand may be preventing the intended reaction from occurring. The efficacy of the literature prep was called into question. The authors noted that performing the bromination of the anion complex at room temperature produced unintended dimer complexes (“*Cation Synthesis*”, Scheme 5.9). This is intuitively

correct from the reaction of an initially formed bromide complex $\text{CpMo}(\text{CO})_3\text{Br}$ with the remaining anion complex $\text{NaCpMo}(\text{CO})_3$ in solution. Indeed, in the initial synthesis of bromide complexes performed, a small amount of dimer was observed by FT-IR. The formation of the symmetrical $\text{Cp}_2\text{Mo}_2(\text{CO})_6$ dimer may be explained by the atom-transfer of the bromine between the molybdenum(0) and molybdenum(II) halide complexes (Scheme 5.12).¹⁵ Then only the non-substituted cyclopentadiene complexes show any reactivity to each other to produce the $\text{Cp}_2\text{Mo}_2(\text{CO})_6$ dimer (Scheme 5.12).



Scheme 5.12. Fast halogen exchange leads to a scrambling of the initial reactants, generating three potential reaction pairs. In this case, only the cyclopentadiene substituted molybdenum(0) anion and molybdenum(II) bromide react quickly and for the observed $\text{Cp}_2\text{Mo}_2(\text{CO})_6$ dimer.

5.3 Summary

The “cation/anion” method to forming an asymmetric dimer was overall low-yielding and produced many symmetric dimer products. If the “cation” were a molybdenum(II) bromide complex, the overall reaction only yielded a single symmetric $\text{Cp}_2\text{Mo}_2(\text{CO})_6$ dimer. This particular reaction was most disappointing because it had been shown to yield an asymmetric dimer (with significantly different cyclopentadiene ligands that attempted here). Initially, the reaction was seen as an attractive alternative to the route using the thermally unstable tetrafluoroborato complex as the cation. Some of the positive synthetic points are the discontinued use of diglyme, the use of an acid sensitive protecting group, and the purification protocol that were developed for the complexes.

It may be worthwhile to revisit the tetrafluoroborato route. Previously the route was used without purified starting materials or using the modifications listed above. It was always thought that the stoichiometry of the reaction was significantly different from the ideal 1:1 (because reagents were used *in situ*). Even though the reaction only produced a small amount of product, the $^1\text{H-NMR}$ indicated that a substituted ligand was incorporated in the correct stoichiometry.

The other two methods (“single electron oxidation”, and “photochemical cross-over”) were initially rejected because they produced multiple dimer products that would have to be separated. However, if these methods still produce the theoretical distribution of products (1 : 1, symmetric : asymmetric, Scheme 5.2 and 5.3) there may be enough product to separate with chromatography. As a proof of concept, a 1:1 mixture of

$\text{Cp}_2\text{Mo}_2(\text{CO})_6$ and $\text{MeCp}_2\text{Mo}_2(\text{CO})_6$ dimers were irradiated at 532 nm in THF. There was no visible change in the FT-IR and NMR as compared to the mixture. However in a GC-MS chromatogram, three peaks were found in a 1:2:1 ratio corresponding to $\text{Cp}_2\text{Mo}_2(\text{CO})_6$: $\text{MeCp}(\text{CO})_3\text{Mo-Mo}(\text{CO})_3\text{Cp}$: $\text{Cp}_2\text{Mo}_2(\text{CO})_6$ (confirmed by MS ions, and by “known addition”). Clearly separation by GC would not be an option for this project, however if the alkyl group were sufficiently large, separation by chromatography may be an option. Also the $\text{Cp}_2\text{Mo}_2(\text{CO})_6$ dimer is not very soluble in hexanes, so by solubilizing the crude product in hexanes there would only be a 1:2 ratio of symmetric and asymmetric dimer.

5.4. Bridge

This chapter focused on the synthesis of an asymmetric Mo-Mo dimer to probe the effects of an asymmetric radical pair in a solvent cage. Chapter VI returns to using the symmetrical $\text{Cp}'_2\text{Mo}_2(\text{CO})_6$ dimer to investigate whether the photochemical recombination efficiency (F_{cP}) is equal to the collisional recombination efficiency (F_c').

CHAPTER VI

A COMPARISON OF PHOTOCHEMICAL AND COLLISIONAL CAGE RECOMBINATION EFFICIENCIES

Justin T. Barry, David R. Tyler*

Department of Chemistry and Biochemistry, University of Oregon, Eugene, OR

97403-1253

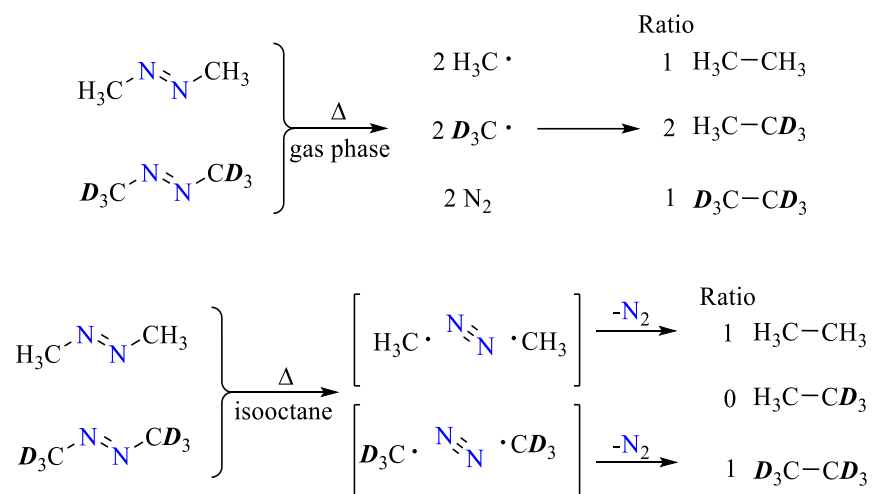
Chapter VI of my dissertation details experiments to determine the collisional cage recombination efficiency (F_c') of the $\text{Cp}'_2\text{Mo}_2(\text{CO})_6$ dimer. F_c' is then compared to the photochemical cage recombination efficiency (F_{cP}). The kinetic derivations used in this chapter are included as Appendix A and E. This chapter contains unpublished, and co-authored material with David R. Tyler.

6.1. Introduction

A cross-over experiment is the reaction of two similar but different reactants in a reaction mixture to aid in the determination of a mechanism.¹ Usually this is to determine if a mechanism involves a reactant breaking apart before recombining to form the product. These types of experiments also beautifully illustrate the effect of the solvent cage. For example, azomethane can thermally decompose into two methyl radicals with a molecule of dinitrogen separating them (Scheme 6.1).² The cross-over

experiment would have azomethane as well as azomethane- D_6 in equal quantities.

Heating this reaction in the gas phase produces crossover products in the ratio 1:2:1 of ethane, CH_3CD_3 , and ethane- D_6 (Scheme 6.1). If this experiment is done with isooctane as the solvent, there is nearly only non-crossover products of ethane and ethane- D_6 in a 1:1 mixture.

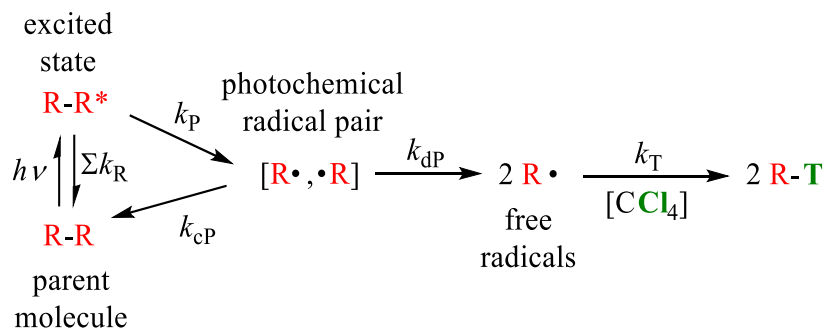


Scheme 6.1. Cross-over experiment using azomethanes in either the gas-phase or in a solution of isooctane.²

In the gas phase, nothing next to the radicals prevents diffusion away from their geminate counterpart. This results in a near random recombination of the radicals that produces the observed product distribution. In the solution-phase, isooctane acts as a cage around the newly formed radicals. This cage limits their diffusion away from each other, and the geminate radicals recombine without escaping this solvent cage. This results in nearly only ethane and ethane- D_6 . However, it was noted by the authors that there was still a 0.3% product of CH_3CD_3 .² This was the amount of radicals that successfully escaped the solvent cage and met a non-geminate radical that was

isotopically different. It is important to note that the solvent creates caging situations throughout the course of the entire reaction that limits diffusion. So there is both an initial solvent cage around the geminate radical pair and a non-geminate solvent cage around cross-over radical pair (collisional cage).

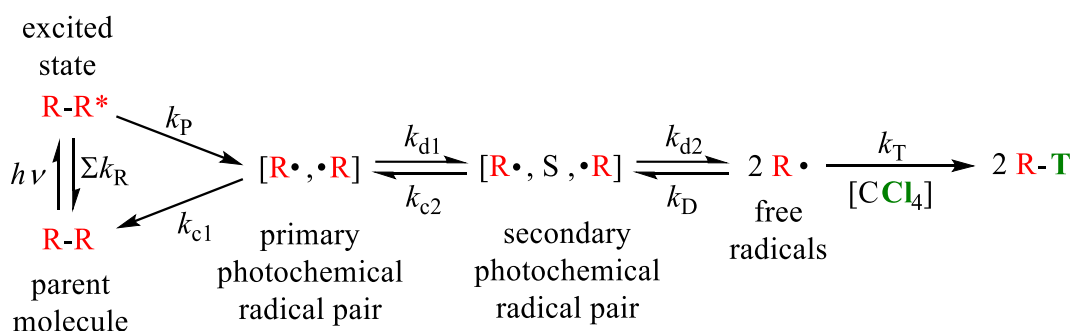
In our studies of the photochemical cage effect, (where radicals are generated photochemically and not thermally) there are also two solvent cages. These two cages are named as the photochemical cage (geminate) and the collisional cage effect (non-geminate radicals). A $\text{Cp}'_2\text{Mo}_2(\text{CO})_6$ dimer is irradiated to homolyze the Mo-Mo bond. This creates two geminate caged radicals. Briefly, to study the geminate cage, a large concentration of radical trap is added to solution to capture any free radicals that escape this geminate cage (Scheme 6.2). A kinetic derivation is then used to calculate the photochemical recombination efficiency (F_{cP} , eq 1) from the experimental kinetic data (derivation included in Appendix A).



Scheme 6.2. Mechanistic model of the geminate photochemical cage effect.

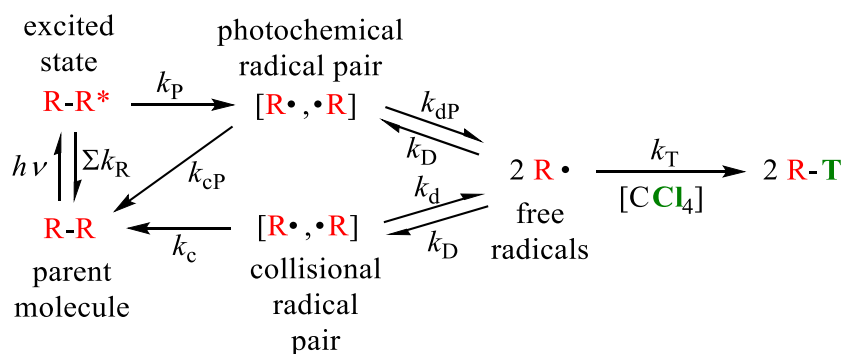
$$F_{\text{cP}} = \frac{k_{\text{cP}}}{(k_{\text{cP}} + k_{\text{dP}})} \quad (1)$$

This picture of a single cage followed by diffusion (k_{dP}) to become free radicals, is a simplified version of what actually happens. Instead this single cage picture can be further divided into two separate cages, a primary and a secondary photochemical solvent cage (Scheme 6.3). The secondary solvent cage differs considerably from the primary solvent cage. The primary solvent cage is relatively short-lived (5 ps).³ The radicals in this primary cage do not have enough time to rotate, such that their orbitals are correctly aligned for recombination (k_{c1}). Once a solvent molecule has intercalated between the two radicals, the secondary cage is formed. In this secondary cage there is sufficient time for the radicals to rotate and enter a misaligned configuration. If the misaligned radicals expel this solvent molecule and enter into the primary cage (k_{c2}), they cannot recombine (k_{c1}) because there is not sufficient bonding overlap of the orbitals. Since there are two geminate solvent cages, the definition of F_{cP} is a net recombination efficiency of both this primary and secondary solvent cage.⁴ Because it is the “net recombination efficiency” (F_{cP}) that is actually measured, it is conceptually valid to use the simple mechanistic model for the time being (Scheme 6.2).



Scheme 6.3. Expanded mechanistic model of the solvent cage effect that includes a primary and secondary solvent caged radical pair.

By using less radical trap, the overall simplified mechanistic model changes (Scheme 6.4). Now a population of free radicals builds up and collisional cages are formed. Collisional cages occur when free radicals meet each other and form non-geminate radical caged pairs. The collisional cage recombination efficiency (F_c' , eq 2) can be determined by using a kinetic derivation (eq 3) to isolate F_c' with measurable quantities (derivation included as Appendix E). The concentration of the radical trap (CCl_4) is varied while keeping both the microviscosity and concentration of the radical source $[\text{Cp}'_2\text{Mo}_2(\text{CO})_6]$ constant. The microviscosity of the solvent cage can dramatically change the strength of the solvent cage (and hence F_{cP}).^{5,6} Rates of the reaction will be used to determine F_c' , which are dependent on the irradiation intensity and the concentration of the absorbing species (as opposed to a quantum yield, Appendix A). To calculate F_c' , a plot of the rate vs $\text{rate}^2/[\text{CCl}_4]^2$ will give a slope of a best-fit line that can be used to determine F_c' (eq 4).



Scheme 6.4. Mechanistic model of the solvent cage effect with a smaller concentration of radical trap (CCl_4) than in Scheme 6.2.

$$F_c' = \frac{k_c}{(k_c + k_d)} \quad (2)$$

$$rate = \frac{a F_c' k_D}{2} - \frac{2rate^2 F_c' k_D}{k_T^2 [CCl_4]^2} \quad (3)$$

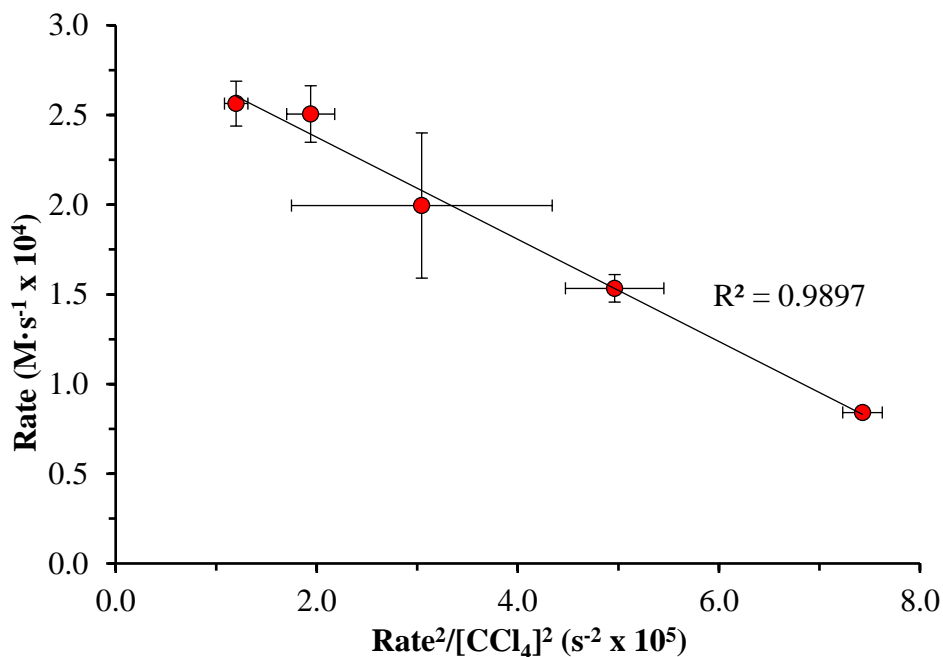
$$F_c' = \frac{-slope k_T^2}{2k_D} \quad (4)$$

6.2. Results

The concentration of CCl₄ is varied for two sets of solutions. One solution contains only *n*-decane and the other contains a mixture of *n*-decane and paraffin oil. Decane was specifically chosen because the bulk viscosity of *n*-decane is similar to CCl₄ (0.85 vs 0.90 cP, respectively). Paraffin oil was added to the second solution to change the bulk viscosity (and subsequently the microviscosity). The bulk viscosity, diffusion coefficient (*D*), and microviscosity of the solvent were measured using previously published methods (Table 6.1).^{5,6} Bulk photolysis was conducted and the rates of each sample set determined. This was plotted as rate vs rate²/[CCl₄]² for both sample sets (Figures 6.1-6.2).

Table 6.1. Properties of solutions used in this study.

Solution Set	Sample	[CCl ₄] (M)	Bulk Viscosity (cP)	Diffusion Coeff. (x10 ⁻⁹ m ² /s)	Microviscosity (x10 ⁹ s/m ²)
1	A	0.0098	0.851±0.003	1.56±0.02	0.640±0.007
	B	0.0218	0.856±0.005	1.52±0.02	0.657±0.009
	C	0.0391	0.850±0.002	1.58±0.02	0.632±0.008
	D	0.0570	0.850±0.001	1.58±0.02	0.632±0.008
	E	0.0741	0.859±0.004	1.67±0.02	0.597±0.006
	average			0.853±0.004	1.58±0.06
2	A	0.0227	7.058±0.003	0.369±0.006	2.71±0.04
	B	0.0416	7.062±0.005	0.300±0.004	3.33±0.04
	C	0.0624	7.046±0.002	0.320±0.002	3.12±0.02
	D	0.0844	7.036±0.002	0.313±0.003	3.19±0.03
	E	0.1030	7.055±0.003	0.293±0.003	3.42±0.04
	average			7.05±0.01	0.32±0.03

**Figure 6.1.** Plot of rate vs $\text{rate}^2/[\text{CCl}_4]^2$ for solution set 1 (error $\pm 1\sigma$). Solution properties; $\eta = 0.853 \pm 0.004$ cp, $D = 1.58 \pm 0.06 \times 10^{-9}$ m²/s, slope of best-fit = -2.846.

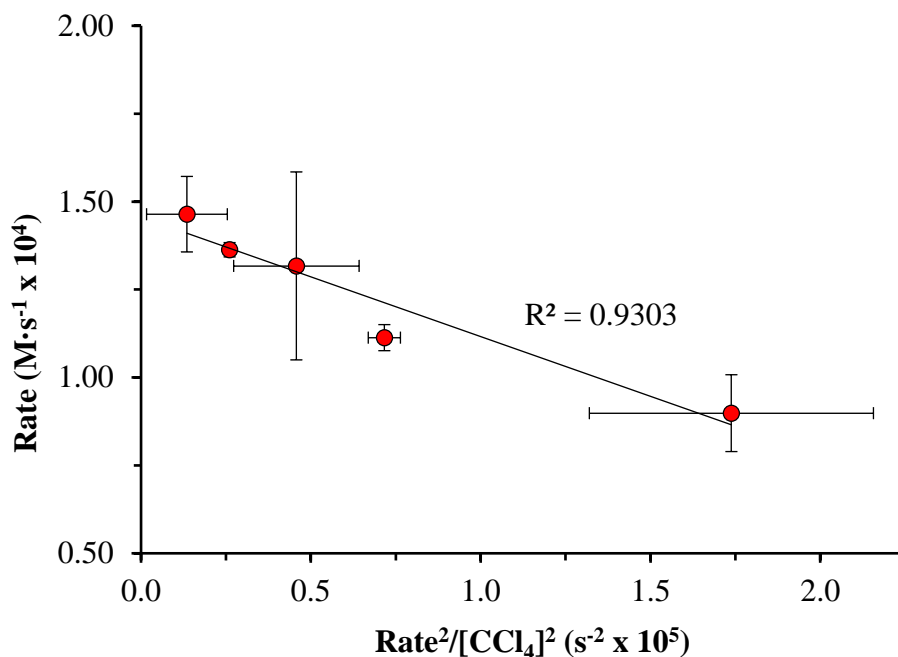


Figure 6.2. Plot of rate vs $\text{rate}^2/[\text{CCl}_4]^2$ for solution set 2 (error $\pm 1\sigma$). Solution properties; $\eta = 7.06 \pm 0.01$ cp, $D = 0.32 \pm 0.03 \times 10^{-9} \text{ m}^2 \cdot \text{s}^{-1}$, slope of best-fit line = -3.3974.

From eq 4, F_c' can be calculated using the slope of the best-fit lines (Figure 6.1-6.2), the rate constant for trapping of the radical (k_T) with CCl_4 , and with the bimolecular rate constant of diffusion (k_D) from the radical. The trapping rate constant is $2 \times 10^4 \text{ M}^{-1}\text{s}^{-1}$.⁷ Trapping rate constants tend to not vary considerably between different solvents and viscosities.⁸ However, k_D will vary considerably on the solvent and its viscosity. Due to this, k_D will be determined by three methods of approximation using either experimental diffusion coefficients, bulk viscosity, or k_d (unimolecular diffusion rate constant) values from prior femtosecond pump-probe spectroscopy experiments.⁹

For a diffusion-controlled reaction, the energy of activation (E_a) is very small. Hence in the Arrhenius equation (eq 5), the exponent becomes very small and $k \approx A$. This “A” is called the pre-exponential or frequency factor and relates to the frequency of

colliding reactive molecules and their orientation. From this frequency factor we can estimate the value of k_D .

$$k = A e^{-E_a/RT} \quad (5)$$

Calculation of k_D will be done using either the diffusion coefficients (D) or with the bulk viscosity (η) of the solution. The equation for using diffusion coefficients also requires the reaction distance ($r_A + r_B$, eq 6).¹⁰ This reaction distance can be approximated using the bond length of the Mo-Mo bond (3.2 Å). This bond length is unique in that it is more than twice the distance of the Pauli single-bond metal radii for molybdenum (1.371 Å).¹¹ An advantage of using bulk viscosity is the simplification of eq 6 using the Stokes-Einstein relation to yield eq 7 (no reaction distance needed).¹⁰ Both of these approximations were used to calculate k_D and then calculate F_c' (Table 6.2). This was done to facilitate the comparison of these two approximation formulae.

$$k_D = 4000 \pi L (r_A+r_B)(D_A+D_B) \quad (6)$$

$$k_D = \frac{8000RT}{3\eta} \quad (7)$$

Table 6.2. Approximated values of k_D using either bulk viscosity (η) or diffusion coefficient (D). F_c' is calculated using these values.

Solution Set	k_D from Bulk Viscosity ($M^{-1}\cdot s^{-1}$, x 10^9)	k_D from Diffusion Coeff. ($M^{-1}\cdot s^{-1}$, x 10^9)	F_c' using η	F_c' using D
1	7.75±0.04	7.7 ± 0.3	0.073	0.074
2	0.93±0.001	1.5± 0.1	0.726	0.438

The value of k_D may also be approximated by using experimentally determined k_d values determined by femtosecond pump-probe spectroscopy experiments.⁹ A plot of the inverse bulk viscosity (η , cP⁻¹) vs k_D for a set of different neat solvents yields a linear best-fit line (Figure 6.3).⁹ This proportionality between bulk viscosity and k_D is indicative of a diffusion controlled process.⁹ For solvent cage effects, we now know that a better metric for the bulk viscosity is the diffusion coefficient, and a more useful graph would be D vs. k_D .^{5,6} Using this best-fit line, and the measured bulk viscosity of the solutions, k_D is again approximated and the values of F_c' are calculated (Table 6.3).

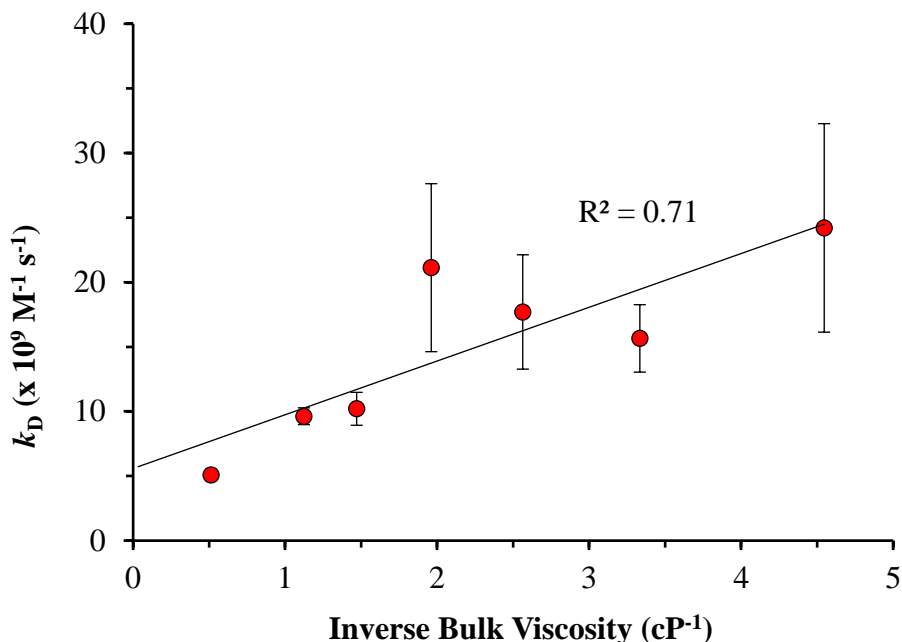


Figure 6.3. Plot of inverse bulk viscosity (cP^{-1}) vs k_D (determined by k_d molarity) values for a set of different neat solvents (one data point omitted).⁹ (best-fit: $f(x) = (4.1586 \times 10^9)(x) + (5.5843 \times 10^9)$, error bars $\pm 1\sigma$)

Table 6.3. F_c' values calculated using k_D from experimental k_d values.

Solution Set	Bulk Viscosity (cP)	k_D ($\text{M}^{-1}\cdot\text{s}^{-1}$, $\times 10^{10}$)	F_c'
1	0.853 ± 0.004	1.04596	0.054
2	7.05 ± 0.01	0.617417	0.110

6.3. Discussion

There are three F_c' values to consider, two that are calculated using approximated k_D values and one k_D value that is based on experimental data. All of these F_c' values show the same general trend, that F_c' increases with the strength of the solvent cage (Table 6.4). The strength of the solvent cage is indicated by either the increasing bulk viscosity of the solution or the decreasing diffusion coefficient of the probe molecule

through that solution. Also, with the exception of a single data point, all of the values of F_c' are significantly lower than the values for F_{cP} .

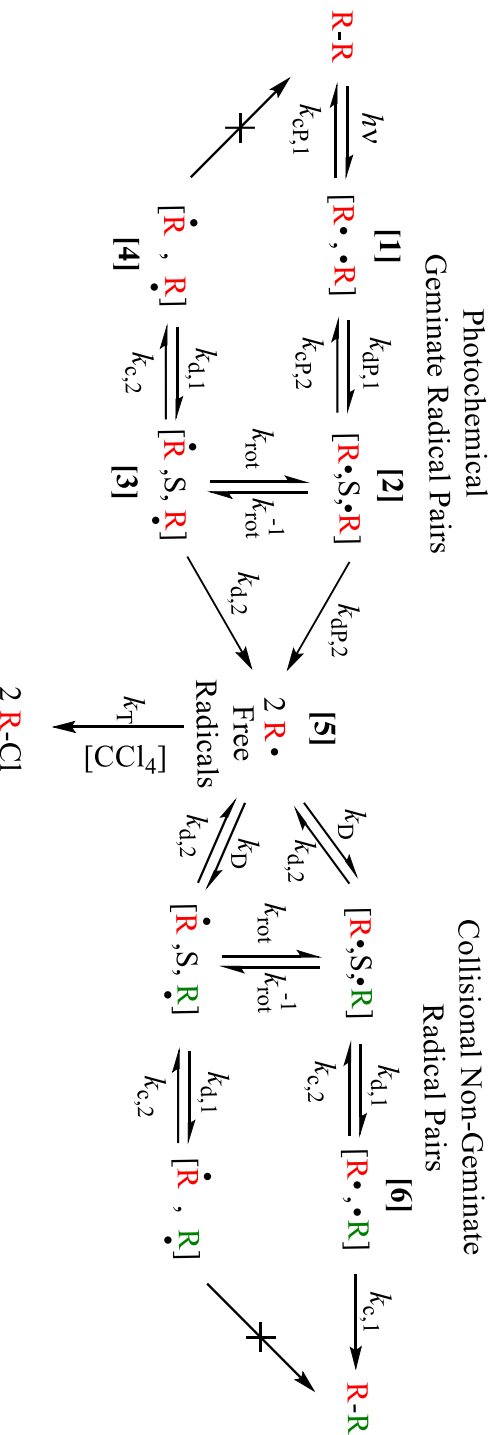
Table 6.4. Compilation of collisional cage recombination (F_c') values for two solutions of differing bulk viscosity (η). Compared with the photochemical cage recombination efficiency (F_{cP}).

Solution Set	Bulk Viscosity (cP)	Theoretical		Empirical	F_{cP}
		F_c' using k_D from η (eq 7)	F_c' using k_D from D (eq 6)	F_c' using k_d (Figure 6.4)	
1	0.853±0.004	0.073	0.074	0.054	0.18±0.03
2	7.05±0.01	0.726	0.438	0.110	0.65±0.02

The approximation formula using bulk viscosity (eq 7), gives a reasonable k_D value for 0.85 cP but not for 7.05 cP. This is most likely because the formula is only appropriate for lower viscosity ranges that correspond to most neat solvents. This may explain why the k_D from 0.85 cP is a more reasonable a value and compares well with the other approximation formula (eq 6).

The reason for the difference in values between F_{cP} and F_c' is intuitive. The difference may be explained when considering the orbital alignment necessary for recombination to occur along with a complete picture of the fate of the radicals (Scheme 6.5). Immediately following homolysis of the Mo-Mo bond, the radicals are in a primary solvent cage ([1], Scheme 6.5). These radicals have not had sufficient time to rotate, therefore the orbitals necessary to form a covalent bond are correctly oriented. That is, the primary cage lifetime (5 ps) is much shorter than rotation of the radical.⁹ Once the radicals separate far enough, a solvent molecule enters the space between them to create the secondary solvent cage ([2], Scheme 6.5). The lifetime of this cage is long enough that the radicals can now rotate and become misaligned ([3], Scheme 6.5). If

these misaligned radicals enter back into a primary cage ([4], Scheme 6.5) they will not have the proper orbital overlap to recombine. Once sufficient diffusion has occurred to create free radicals ([5], Scheme 6.5), collisional radical pairs can be made. To summarize, the photochemical geminate radical pairs start the entire process with proper orbital alignment to recombine in the primary solvent cage ([1], Scheme 6.5). In contrast, the collisional non-geminate pairs start as free radicals that have to both; 1) enter into the primary solvent cage with 2) the proper orbital alignment to recombine ([6], Scheme 6.5). Statistically speaking, there is a higher probability that photochemical geminate radical pairs meet both of these criteria and that the collisional non-geminate pairs do not. Hence F_{cP} being greater than F_c' .



Scheme 6.5. Full scheme for the solvent cage effect including photochemical geminate and collisional non-geminate radical pairs. Secondary radical pairs are indicated by a solvent molecule (S) between the two radicals. Non-geminate radical pairs are indicated by the mis-match color scheme (green and red) of the radicals. Radical dots indicate whether there is correct or incorrect orientation for recombination.

6.4. Concluding Summary

The goal of the entire project is to isolate individual parameters that have an impact on the solvent cage effect. These parameters together can create a quantitative and predictive model that can be used to determine F_{CP} *a priori*. So far the best single solvent parameter that can describe the solvent cage effect is the microviscosity (as felt by probe molecule that is similar in size and mass to the radicals being studied). The microviscosity holds for a wide range of solvents including solutions containing polymers.

However there are still some parameters in which the mechanism of action is poorly understood. The wavelength dependence of F_{CP} when using $Cp'_2Mo_2(CO)_6$ to generate radicals is one of these parameters that warrants further study. This wavelength dependence also extends further than the solvent cage effect and may answer some fundamental questions about the molecule dynamics of the $Cp'_2Mo_2(CO)_6$ dimer. Namely, what happens to the excess energy after the photochemical homolysis of the Mo-Mo bond?

Using symmetrical radicals pairs generated from $RCp_2Mo_2(CO)_6$, the theoretical relationship of $F_{CP} \propto \text{mass}^{0.5}/\text{radius}^2$ has been given experimental validation. The determination of an appropriate F_{CP} relationship to mass and radius of *asymmetrical* radical pairs is missing however. If the asymmetric $RCp(CO)_3Mo-Mo(CO)_3CpR^2$ dimer could be synthesized, the same experimental design used in the symmetrical $RCp_2Mo_2(CO)_6$ dimers could be applied. In many cases, solvent caged radical pairs are not symmetrical in size and mass.

Finally, the collisional cage recombination efficiency (F_c') was shown to be smaller than F_{CP} . The reason for this is difference is the collisional radical pair is more likely to be have misorientated orbitals in the primary solvent cage, than the photochemical radical pair. Also, F_c' was shown to increase with increasing strength of the solvent cage just like F_{CP} . The next step for this project would be to produce more data at different microviscosities to determine the curve shape of the best-fit line between F_c' vs microviscosity.

APPENDIX A

THE USE OF PHOTOCHEMICAL KINETICS TO REACH THE
DERIVATION OF F_{cP}

Justin T. Barry

Department of Chemistry and Biochemistry, University of Oregon, Eugene, OR
97403-1253

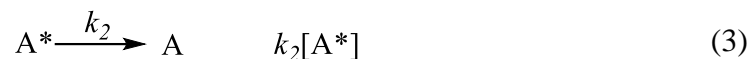
This appendix is intended to supplement the reader's knowledge of kinetics with photochemical kinetics. The goal is to work from some basics all the way up to the derivations used to determine an F_{cP} (see below for definition). The reader should be familiar with normal solution state kinetics (such as the steady-state approximation) before reading. If this is not the case, or a review of that material is necessary, the following cited publications are recommended.^{1,2}

A.1. Photochemical 1st Order Kinetics

Consider the simple reaction where a reactant A photochemically produces a product P (eq 1).



What is the rate of this reaction and how do we determine it experimentally? First, consider the elementary steps and their individual rate expressions (eq 2-4).



A^* represents the excited state of A . I_A is the absorbed intensity of light. This excited state can become product (k_3) or it can non-radiatively decay (k_2) to reform starting material. The expression for formation of product would be $k_3[A^*]$. Experimentally determining how much A^* is present in solution would be problematic because it is typically really short lived. So instead we assume that the concentration is not changing after a short period of time and steady-state to a more reasonable term (the arrow \Rightarrow denotes the final equation after algebraic manipulation of the immediately previous equation). From eq 6 we can isolate $[A^*]$ to get eq 7.

$$\text{Production rate of } A^*: \frac{d[A^*]}{dt} = I_A \quad (4)$$

$$\text{Consumption rate of } A^*: -\frac{d[A^*]}{dt} = k_2[A^*] + k_3[A^*] \quad (5)$$

$$I_A = k_2[A^*] + k_3[A^*] \quad (6)$$

$$\Rightarrow [A^*] = \frac{I_A}{k_2 + k_3} \quad (7)$$

Now we can use eq 7 in place of $[A^*]$ in the product rate expression (eq 4). This yields the following expression:

$$\frac{d[P]}{dt} = k_3[A^*] = k_3 \left(\frac{I_A}{k_2 + k_3} \right) \quad (8)$$

It can be difficult to use I_A if the intensity of the source varies slightly over time. Also, the comparison of two different rates from two different systems requires that the intensity and the concentration of absorbing species be the same. It is much more convenient to use a representation of the rate that is independent of intensity and concentration. We will define a quantum yield (Φ , phi) to do this:

$$\Phi = \text{quantum yield} = \frac{\text{rate}}{I_A} = \frac{\# \text{ of reactions that occur}}{\# \text{ of photons absorbed}} \quad (9)$$

This yields the following transformation to the final product rate expression (eq 10).

$$\begin{aligned} \text{If } \Phi &= \frac{\text{rate}}{I_A} \\ \text{And the rate is } &k_3 \left(\frac{I_A}{k_2 + k_3} \right) \\ \Rightarrow \Phi &= \frac{k_3}{k_2 + k_3} \end{aligned} \quad (10)$$

A.2. Reaction Order and Observed Kinetics

A typical kinetics trace will be presented to show the relationship between the observed data of a photochemical 1st order reaction and the “apparent” order of said reaction from the kinetics. Let us observe the decrease of an absorbing species “A” at a particular

wavelength (Figure A.1, arrow). Now let's plot the absorbance maxima of "A" as a function of time of irradiation (Figure A.2).

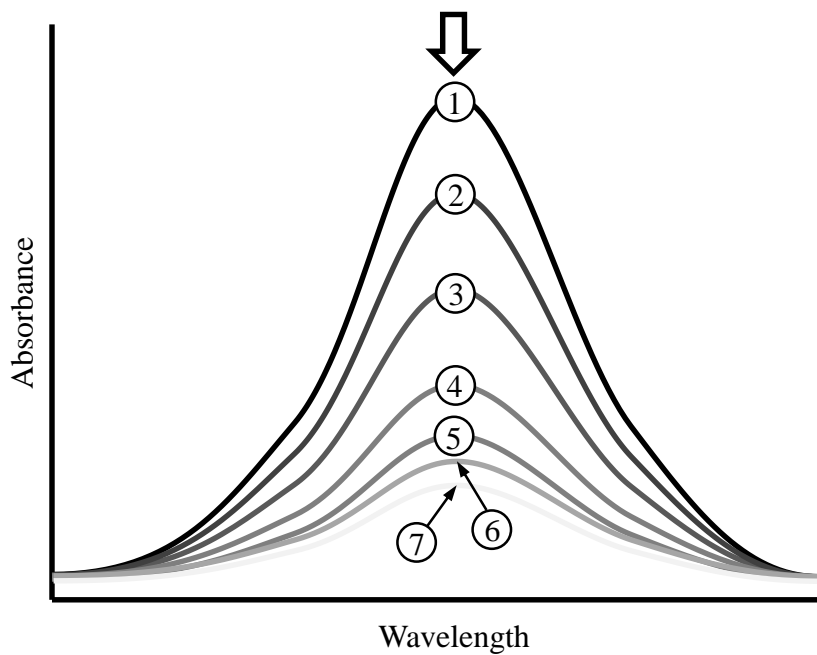


Figure A.1. Example absorbance data from 1st order photochemical reaction.

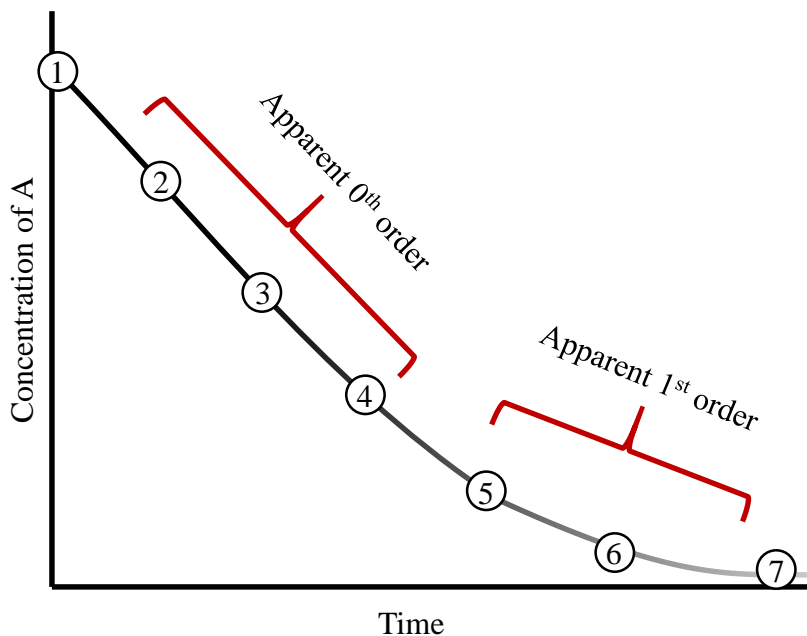


Figure A.2. Graph of concentration of “A” over time from absorbance data.

From Figure A.2 we can see that there is a 0th order and a 1st order regime. Why does this occur? It is necessary to explain this apparent discrepancy in the experimental data because almost all of the data used to determine kinetics in this dissertation contains this feature. We will have to work through some math to find the source of this oddity. This will require starting with the very beginning of where the experimental data is derived. Recall the definitions of absorbance (A, eq 11), transmittance (T, eq 12), and the Beer-Lambert law (eq 13).

$$A = -\log(T) \quad (11)$$

$$T = \frac{I}{I_0} \times 100 \quad (12)$$

$$A = \epsilon bc = \log\left(\frac{I_0}{I}\right) \quad (13)$$

In the Beer-Lambert law, “ ϵ ” is the molar extinction coefficient for the compound, “ b ” is the path length of the cell, and “ c ” is the concentration of the absorbing species in the solution. “ I_0 ” is the initial intensity of the light before entering the sample. “ I ” is the intensity of light after leaving the sample and “ I_A ” is the absorbed intensity of light. Hence the following equation is true (eq 14, note: the number 1 is colored red to prevent confusion):

$$I_A = I_0 - I = I_0 \left(1 - \frac{I}{I_0} \right) \quad (14)$$

We have now isolated the term I/I_0 to the far right of eq 14. We can now use a rearrangement of the Beer-Lambert law to replace it (eq 15, recall algebraic logarithm rules).

$$I_A = I_0 (1 - 10^{-\epsilon bc}) \quad (15)$$

From our quantum yield (eq 9) we can add in our newly defined definition of I_A (eq 15). Because we are looking at the disappearance of an absorbing species “A” our rate is in terms of $d[A]/dt$ (eq 16).

$$\frac{d[A]}{dt} = \Phi I_A = I_0 (1 - 10^{-\epsilon b[A]}) \quad (16)$$

Finally we have reached an equation that will explain the experimental results of Figure A.2. We will examine two extremes. When $\text{Abs} > 2$ (or $\epsilon bc > 2$), more than 99%

of the light entering the cell is absorbed. This means that the absorbance changes very little over time and the rate is essentially ΦI_A (or 0th order in [A]). However, when Abs $\ll 1$ (or $\epsilon bc \gg 1$), only a small fraction of the light is absorbed. The term $1 - 10^{-\epsilon b[A]}$ may be well approximated by $2.303\epsilon b[A]$. Then the rate equation is $\Phi I_0(2.303\epsilon b[A])$, or 1st order in [A]. Hence the apparent change in reaction order depending on the absorbance.

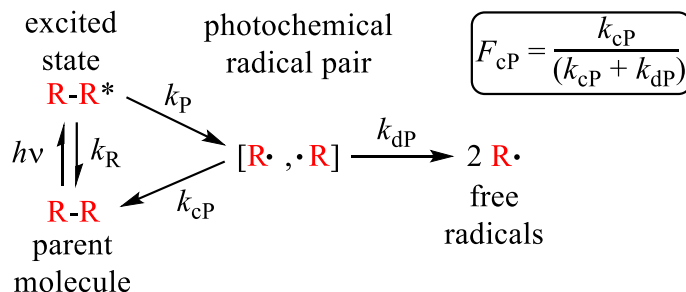
We haven't yet introduced how we take an experimental curve like Figure A.2 and produce a quantum yield. In this case we will be determining an observed quantum yield (Φ_{Obs}) with measured and known values (eq 17). We will use the slope of the 0th order portion of Figure A.2 [$d(A)/dt$], the measured volume of the solution being irradiated, the path length of the cell, the intensity of the light, the extinction coefficient of the absorbing species (ϵ), and a correction factor for non-absorbance (%A is the average % absorbance).

$$\Phi_{\text{Obs}} = \frac{-\left(\frac{d(A)}{dt}\right)(\text{volume})}{(\epsilon)(\text{path length})(\text{intensity})} \times \left(\frac{100}{\%A}\right) \quad (17)$$

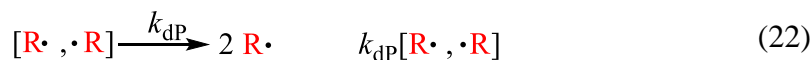
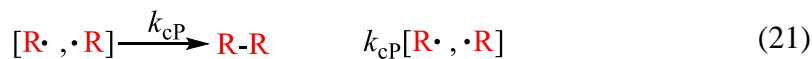
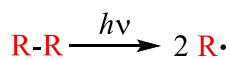
A.3 Photochemical Solvent Cage Effect Kinetics

The determination of useful kinetic equations for the solvent cage effect will now be presented. Although much more complicated than the 1st order derivation, many of the same algebraic manipulations are the same. Consider first the overall reaction

(Scheme A.1), and then the elementary steps of the reaction with corresponding rate expressions (eq 18-22). The overall reaction (Scheme A.1), also contains the radical solvent cage recombination efficiency (F_{cP}) definition. This is an important metric in describing the solvent cage effect and is ultimately what we are after.



Scheme A.1. Photochemical solvent cage effect



In the above equations (eq 18-22), we have k_R as non-radiative decay of the excited state, k_P as the rate of homolysis of the excited state, k_{cP} as the recombination of a radical caged pair, and k_{dP} as the diffusion of the radical pair out of the solvent cage. The production rate of the product would be $k_{dP}[R\cdot, \cdot R]$. Just like in the example of 1st order kinetics,

this is a problem because it would be very difficult to know the concentration of a short-lived intermediate. Again, we will apply the steady-state approximation on $[R\cdot, \cdot R]$ to yield a more useful equation (eq 23).

$$\begin{aligned}
 \text{Production rate of } [R\cdot, \cdot R] &= \frac{d[R\cdot, \cdot R]}{dt} = k_p[R-R^*] \\
 \text{Consumption rate of } [R\cdot, \cdot R] &= \frac{-d[R\cdot, \cdot R]}{dt} = k_{cP}[R\cdot, \cdot R] + k_{dP}[R\cdot, \cdot R] \\
 k_p[R-R^*] &= k_{cP}[R\cdot, \cdot R] + k_{dP}[R\cdot, \cdot R] \\
 \Rightarrow [R\cdot, \cdot R] &= \frac{k_p[R-R^*]}{k_{cP} + k_{dP}} \tag{23}
 \end{aligned}$$

Now we can replace an intermediate $[R\cdot, \cdot R]$ with an equation that now includes a different intermediate $[R-R^*]$. This seems counterproductive but we will again use the steady-state approximation to rid us of $[R-R^*]$ (eq 24).

$$\begin{aligned}
 \text{Production rate of } [R-R^*] &= \frac{d[R-R^*]}{dt} = I_A \\
 \text{Consumption rate of } [R-R^*] &= \frac{-d[R-R^*]}{dt} = k_R[R-R^*] + k_p[R-R^*] \\
 I_A &= k_R[R-R^*] + k_p[R-R^*] \\
 \Rightarrow [R-R^*] &= \frac{I_A}{k_R + k_p} \tag{24}
 \end{aligned}$$

We will now take the production rate of the product $k_{dP}[R\cdot, \cdot R]$ and add in eq 23 to replace $[R\cdot, \cdot R]$ and then eq 24 to replace $[R-R^*]$. This will give us an equation with no intermediates (eq 25).

$$\frac{d[R\cdot]}{2dt} = k_{dP}[R\cdot, \cdot R] = \frac{k_{dP}k_p[R-R^*]}{k_{cP} + k_{dP}} = \frac{k_{dP}k_p I_A}{(k_{cP} + k_{dP})(k_R + k_p)}$$

(25)

Now that there are no intermediates we can put eq 25 into terms that can be easily measured. We will start by defining a quantum yield for the pair of radicals (ϕ_{pair} , eq 26). This definition is the inherent quantum yield of the dimer excited state [R-R*].

$$\phi_{\text{pair}} = \frac{k_{\text{P}}}{k_{\text{R}} + k_{\text{P}}} \quad (26)$$

We use this ϕ_{pair} definition in eq 25 to yield a new equation (eq 27).

$$\text{rate} = \frac{d[\text{R}\cdot]}{2dt} = \frac{k_{\text{dP}}I_{\text{A}}\phi_{\text{pair}}}{k_{\text{cP}} + k_{\text{dP}}} \quad (27)$$

We will again define an overall observed quantum yield for the reaction (Φ_{Obs} , eq 28) to alleviate us from having to use I_{A} from the rate equation (eq 27). This ultimately yields us an equation that we can work with (eq 29).

$$\Phi_{\text{Obs}} = \frac{\text{rate}}{I_{\text{A}}} \quad (28)$$

$$\Phi_{\text{Obs}} = \frac{\text{rate}}{I_{\text{A}}} = \frac{k_{\text{dP}}\phi_{\text{pair}}}{k_{\text{cP}} + k_{\text{dP}}} \quad (29)$$

Remember at the very beginning of this section about F_{cP} (Scheme A.1)? This is ultimately what we are after to describe the solvent cage effect. We will have to use eq 29 to find it. F_{cP} is actually hiding in that equation. Consider the following transformation of eq 29 using the definition of F_{cP} (eq 29).

$$\Phi_{\text{Obs}} = \frac{k_{\text{dP}}\phi_{\text{pair}}}{k_{\text{cP}} + k_{\text{dP}}} = (1 - F_{\text{cP}})\phi_{\text{pair}} \quad (30)$$

If we are able to calculate a ϕ_{pair} for the reaction, we will be able to calculate F_{cP} using eq 30. To do this we will have to further manipulate eq 30 so we may extract ϕ_{pair} .

Consider the following transformations of eq 30 to yield eq 31.

$$\begin{aligned} \Phi_{\text{Obs}} &= \frac{k_{\text{dP}}\phi_{\text{pair}}}{k_{\text{cP}} + k_{\text{dP}}} = (1 - F_{\text{cP}})\phi_{\text{pair}} \\ \frac{1}{\Phi_{\text{Obs}}} &= \frac{k_{\text{cP}} + k_{\text{dP}}}{k_{\text{dP}}\phi_{\text{pair}}} \\ \frac{1}{\Phi_{\text{Obs}}} &= \frac{k_{\text{cP}}}{k_{\text{dP}}\phi_{\text{pair}}} + \frac{k_{\text{dP}}}{k_{\text{dP}}\phi_{\text{pair}}} \\ \frac{1}{\Phi_{\text{Obs}}} &= \frac{1}{\phi_{\text{pair}}} \left(1 + \frac{k_{\text{cP}}}{k_{\text{dP}}} \right) \end{aligned} \quad (31)$$

Diffusion out of the solvent cage (k_{dP}) is inherently related to the strength of the solvent cage. By increasing bulk viscosity (η) of the solution we can increase the strength of the solvent cage (and decrease k_{dP}). Conversely, decreasing bulk viscosity of the solution will decrease the strength of the solvent cage and increase k_{dP} . Bulk viscosity is the propensity of a solution to resist flow. Mathematically this can be represented as $k_{\text{dP}} \propto \eta^{-1}$. Care must be taken in the interpretation of this relationship as it is actually the microviscosity that dictates the cage effect.³ We can add small molecule viscosity enhancers (viscogens) such as paraffin oil to increase the bulk viscosity of the solution. This acts to change the microviscosity as well. However, polymeric viscosity enhancers will only increase the bulk viscosity and do very little to the microviscosity. If we use

our new relationship in eq 31 we can quickly see that if bulk viscosity is decreased to near zero we can eliminate the k_{cP} term (eq 32).

$$\frac{1}{\Phi_{\text{Obs}}} = \frac{1}{\phi_{\text{pair}}} \left(1 + k_{cP} \eta \right) \quad (32)$$

How do we measure something at zero viscosity? Experimentally we will increase the bulk viscosity of the solution being irradiated by changing the amount of viscogen. This will give us a series of points at different viscosities with corresponding Φ_{Obs} . We can then plot a graph of Φ_{Obs}^{-1} vs η . By extrapolation to zero viscosity (y-intercept) we can yield a value of ϕ_{pair} for that system (Figure A.3).

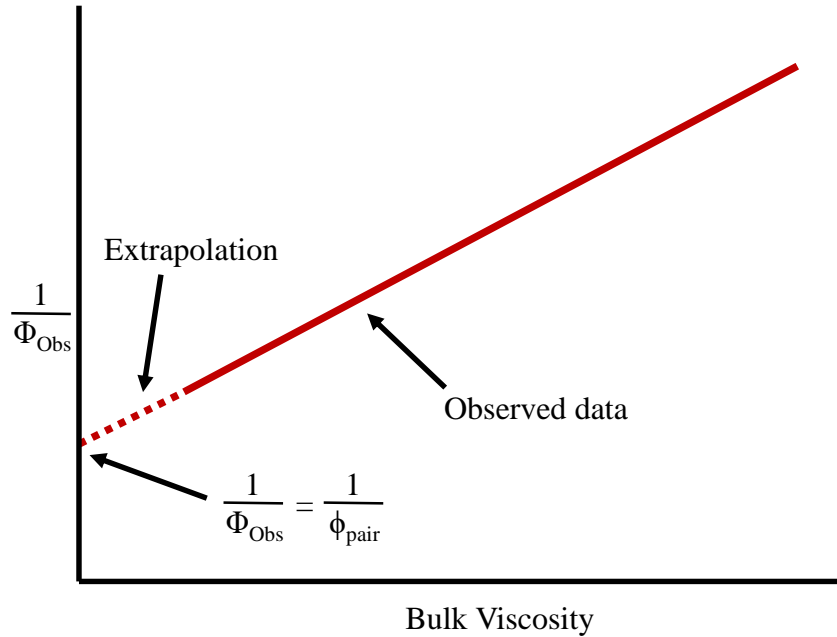


Figure A.3. Illustration of method for extrapolation to y-intercept.

APPENDIX B

SUPPORTING INFORMATION FOR CHAPTER II

Justin T. Barry, Daniel J. Berg, David R. Tyler*

Department of Chemistry and Biochemistry, University of Oregon, Eugene, OR

97403-1253

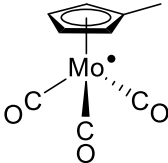
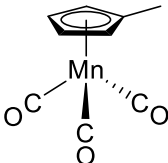
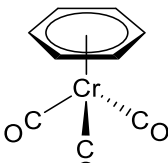
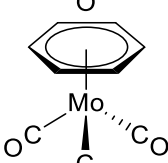
Appendix B of my dissertation is supporting information for a published paper. Reproduced with permission from *J. Am. Chem. Soc.* **2016**, *138*, 9389–9392. Copyright 2017 American Chemical Society.

Selection of the NMR probe

The typical lifetime for a caged radical pair is on the order of 5×10^{-12} s and is too short to be observed with NMR techniques.¹ Consequently, a probe molecule was needed to mimic the nature of the $[\text{Cp}'\text{Mo}(\text{CO})_3]$ radical in the different solvent systems. The probe should ideally have similar mass and size to the that of the $[\text{Cp}'\text{Mo}(\text{CO})_3]$ radical because $F_{\text{CP}} \propto \text{mass}^{1/2}/\text{radius}^2$.² A similar dipole moment would also mimic the potential electrostatic interactions between the solvent and radical. A sharp and well resolved peak, separated from the background, would also greatly increase the accuracy of the DOSY NMR experiments. An organometallic complex was sought having suitable parameters. Unfortunately, many transition metals contain large quadrupolar moments

and have multiple isotopes. Consider the example of Cp'Mn(CO)₃.³ The quadrupolar moment of ⁵⁵Mn caused broadening in the ¹H spectrum and in the ⁵⁵Mn spectrum that made quantification impossible. Two additional possibilities were the benzene complexes of C₆H₆Cr(CO)₃ and C₆H₆Mo(CO)₃. Both compare fairly well with the [Cp'Mo(CO)₃] radical in terms of size and mass (Table B.1). Although C₆H₆Mo(CO)₃ is a better match in terms of mass, C₆H₆Cr(CO)₃ was selected because ⁵³Cr has a much smaller quadrupolar moment (3 x 10⁻³⁰ Q/m² compared to 1.2 x 10⁻²⁹ and 1.1 x 10⁻²⁸ Q/m² for ⁹⁵Mo and ⁹⁷Mo respectively).

Table B.1. Comparison between radicals produced by photolysis and potential probe molecules. (Δ values are the difference of probe molecules from $[\text{Cp}'\text{Mo}(\text{CO})]$ radical)

Complex	Dipole (Debye)	Δ Dipole (Debye)	Mass (Da)	Δ Mass (Da)	Volume (\AA^3)	Δ Volume (\AA^3)
	[†] 3.9	0.00	255.06	0.00	*200.86	0.00
	*2.52	-1.38	204.06	-51.00	*202.28	1.42
	*2.53 ¥5.30	*-1.37 ¥1.40	214.14	-40.92	*194.05	-6.81
	*4.67 ¥5.85	*0.77 ¥1.95	258.10	3.00	*197.51	-3.35

*HF, 3-21G start from MMFF conformer (In collaboration with E. Adrian Henle)

[†] DFT B3LYP/3-21G(Mo)/6-31G* (Calculation performed by Dale Braden³)

¥ Experimentally determined values⁴

Instrumentation and Reagents

All samples were prepared in a darkened, nitrogen-filled glove box fitted with light emitting diodes in the red region (633 nm). Reagents were purified using standard procedures to exclude water and oxygen.⁵ Carbon tetrachloride (Acros, spectrophotometric grade 99+%), *n*-hexane (TCI, anhydrous), paraffin oil (Sigma-Aldrich, infrared grade), polystyrene (Aldrich, M_w 45,000), dimethylsiloxane (50 cSt, M_w ~3,780), polybutenes (Sigma-Aldrich, M_n 2,300, isobutylene > 90%), benzene chromium tricarbonyl (Strem, >98%) were degassed, and used as received. Toluene (Sigma-Aldrich, reagent grade), and 1,1-bis(3,4-dimethylphenyl)ethane (TCI, >90%) were dried with sodium and fractionally distilled under high vacuum. Hexamethyldisiloxane (Sigma-Aldrich, 98+%) was degassed and distilled under high vacuum. Liquid reagents were stored under activated molecular sieves (4 Å) (allowed to sit for at least 72 hours) before usage. Methylcyclopentadienylmolybdenum(I) tricarbonyl dimer (Sigma-Aldrich, 97%) was purified by recrystallization.

Determination of Bulk Viscosity

A Gay-Lussac pycnometer was used to determine the density of the solutions. The pycnometer was previously calibrated with 18 MΩ water at 25.0 °C. Solutions and the pycnometer were temperature equilibrated in a box that was regulated with a heat exchanger at 25.0 °C for at least 30 minutes prior to measurement. Three Ubbelohde type viscometers were used in this study (Cannon Instrument UB-50, UB-75, and UB-

100). A temperature regulated water tank was used to partially submerge the viscometers (regulated at 25.0 °C). The viscometers were calibrated using neat solvents of a varying and known viscosity (Table B.2). Measurements were performed in triplicate. Linear fits were determined for each viscometer (Figure B.1). Dynamic viscosities (referred to as bulk viscosities) were determined for each solvent system by measuring both the kinematic viscosity and the density (Figure B.2).

Table B.2. Literature densities and viscosities for calibration (25.0 °C).

Compound	Density (g/cm ³)	Dynamic Viscosity (cP)
diglyme	0.9384	0.989
tetraglyme	1.009	0.845
decane	0.7264	0.845
tetrahydrofuran	0.88	0.46
benzene	0.873	0.6
dimethylsulfoxide	1.095	1.99
<i>n</i> -hexane	0.6548	0.296
<i>n</i> -tetradecane	0.7591	2.077
2,6,10,14-tetramethylpentadecane	0.77911	5.4793

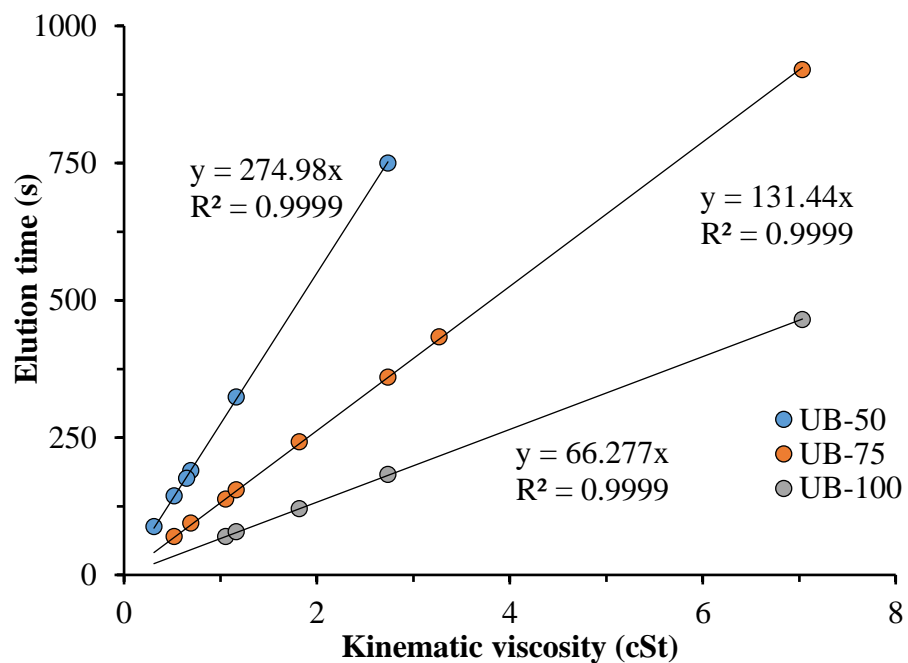


Figure B.1. Calibration regression of the viscometers.

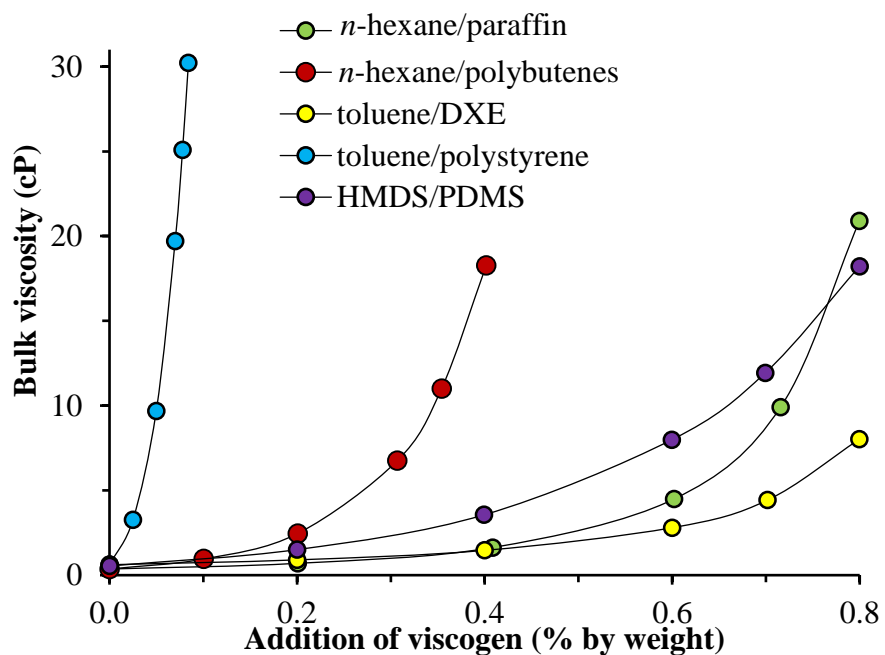


Figure B.2. Bulk viscosities of the solutions in relation to added viscogen amount (wt%). All samples included 20% wt. CCl₄.

Determination of microviscosity by NMR

Samples containing benzene chromium tricarbonyl were found to be oxygen and light sensitive in the presence of CCl_4 (noted by the loss of the C_6H_6 resonance accompanied with a brown precipitate). All samples were prepared in a darkened nitrogen glove box fitted with light emitting diodes in the red region (633 nm). The concentration of the benzene chromium tricarbonyl was 1.4 mM to mimic the concentration of $[\text{Cp}'\text{Mo}(\text{CO})_6]$ produced by photolysis of the $\text{Cp}'_2\text{Mo}_2(\text{CO})_6$ dimer. NMR samples contained a flame sealed internal lock capillary of acetone- d_6 and were subsequently flame sealed.

Diffusion ordered spectroscopy (DOSY) was performed on a 500 MHz Bruker spectrometer (^1H 500.23 MHz) equipped with a Prodigy Cyroprobe and using the **ledbpgp2s** pulse sequence. Pulse widths were individually calibrated to be 90° . (A typical experiment had a Δ (d20) of 0.06 s and a δ (p30) of 0.003 s with a varying gradient power from 5%-95%). Spin-lattice times were measured using the pulse sequence **tlir**. A methanol temperature probe was used to confirm the internal temperature (25 °C) of the probe prior to experimentation.⁶ Total temperature equilibrium time before DOSY measurements was 3-4 hours. A representative sample spectra is shown (Figure B.3).

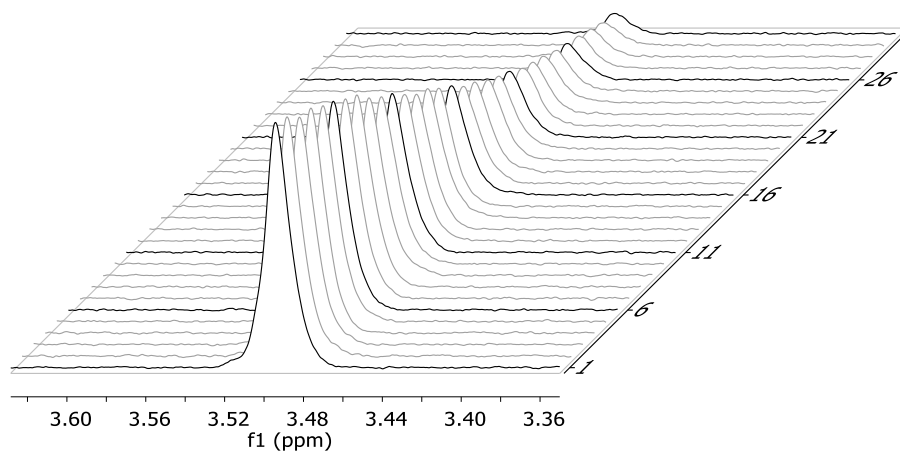


Figure B.3. DOSY plot of $C_6H_6Cr(CO)_3$ in 80% *n*-hexane and 20% CCl_4 (1.4 mM). The intermittent black line spectra are for visual aid only.

Determination of F_{CP}

An Oriel Merlin radiometry system was used to monitor the photoreaction of $Cp'_2Mo_2(CO)_6$. The irradiation source was a modified 50 mW frequency doubled Nd:YAG diode laser pointer module (DPSS-5, 532 nm, Beam of Light Technologies) with a Oriel 100 mm², NIST-calibrated silicon photodiode (model 70356) detector.⁷ The beam was chopped with a five-blade chopper (Oriel model 75163) operating at 30.0 Hz to eliminate electrical line noise. A custom built water-jacketed stir plate was regulated at 25.0 °C with a water recirculator. The entire system was regulated at 25.0 °C using an air-flow radiator and water recirculator. Each sample was prepared in a darkened glove box before being transferred in a Schlenk UV-vis cell.

The raw data is converted from transmittance to absorbance (Figure B.4). The linear portion is fitted (typically 200 data points) and the slope (dA/dt) is used in eq 1. The volume, path length, extinction coefficient, and intensity are measured quantities. The $100/\%A$ term is a correction for non-absorbance. The quantum yield measurements

are performed in triplicate for all samples. Calculation of F_{cP} requires the value Φ_{pair} (eq 2). Rearrangement of eq 2 yields eq 3. The rate k_d is inversely proportional to the viscosity of solution, such that, extrapolation to zero viscosity would yield a k_c/k_d term that is much smaller than 1 (as k_d becomes very large). At zero viscosity, $\Phi_{obsd} = \Phi_{pair}$. Plots of $1/\Phi_{obsd}$ vs. bulk viscosity (Figure B.5) are used to obtain Φ_{pair} by extrapolation to the y-intercept.

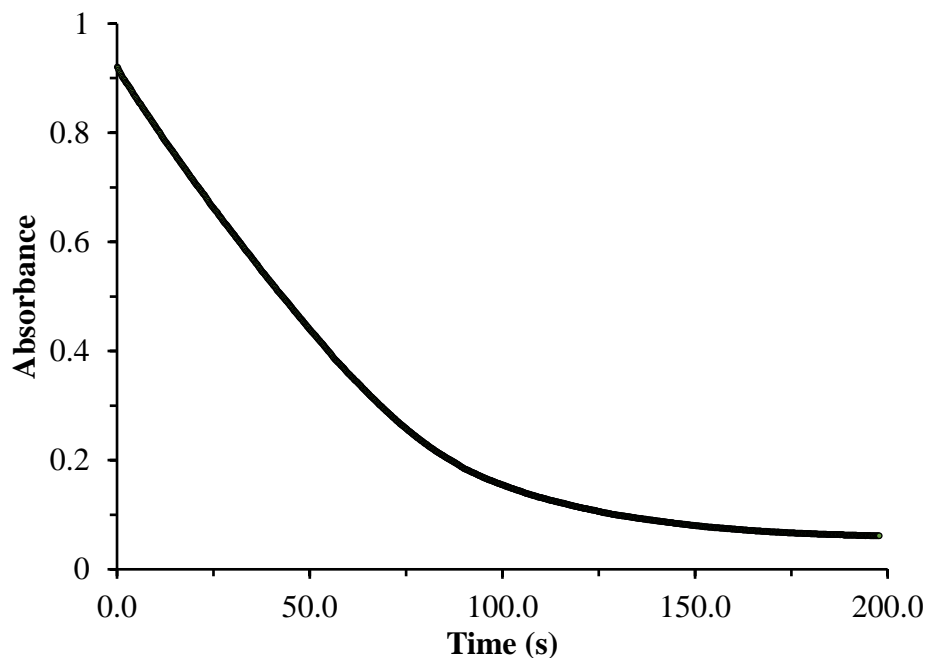


Figure B.4. Plot of absorbance decay of $Cp'_2Mo_2(CO)_6$ at 532 nm in 80% DXE and 20% CCl_4 .

$$\Phi_{obsd} = \frac{-\left(\frac{dA}{dt}\right)(\text{volume})}{(\epsilon)(\text{pathlength})(\text{intensity})} \times \frac{100}{\%A} \quad (1)$$

$$\Phi_{obsd} = \phi_{pair} \left(\frac{k_d}{k_c + k_d} \right) = \phi_{pair} (1 - F_{cP}) \quad (2)$$

$$\left(\frac{1}{\Phi_{obsd}} \right) = \left(\frac{1}{\phi_{pair}} \right) \left(1 + \frac{k_{cP}}{k_{dP}} \right) \quad (3)$$

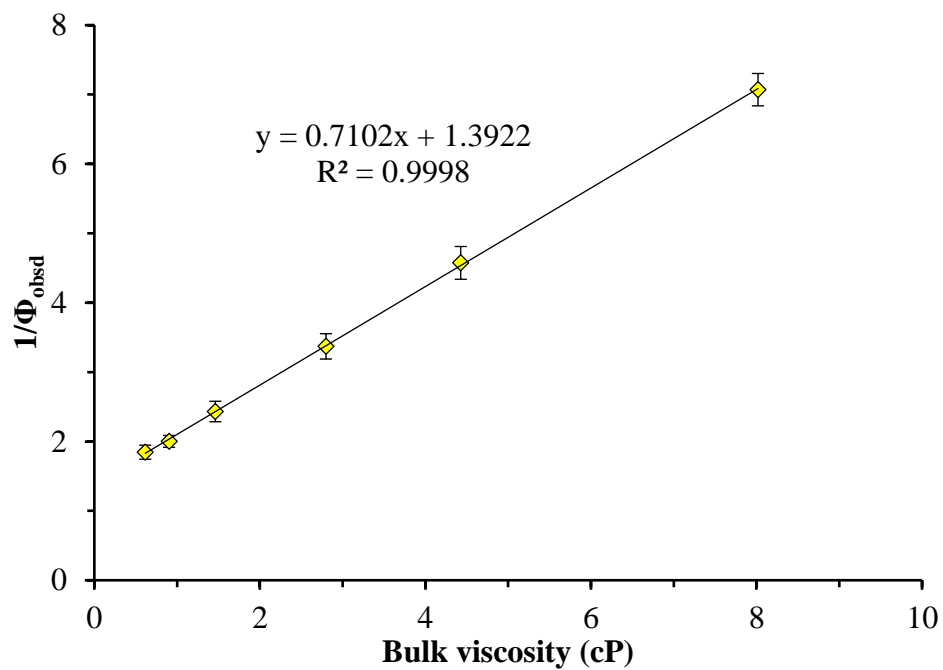


Figure B.5. Plot of quantum yields vs. bulk viscosity. The solvent was toluene with DXE added to increase bulk viscosity. All samples contain 20% wt. CCl₄. Samples were run in triplicate with error bars at $\pm 1\sigma$.

APPENDIX C

SUPPORTING INFORMATION FOR CHAPTER III

Justin T. Barry, Daniel J. Berg, David R. Tyler*

Department of Chemistry and Biochemistry, University of Oregon, Eugene, OR

97403-1253

Appendix C of my dissertation is supporting information for a published paper. Reproduced with permission from *J. Am. Chem. Soc.* **2017**, *139*, 14399-14405. Copyright 2017 American Chemical Society.

Description of solvents and reagents:

Solvents used in this study were further purified to remove any water.² Glyme (TCI Chemicals, >99.0%), tetraglyme (TCI Chemicals, >98.0%), toluene (Sigma-Aldrich, \geq 99.5%), and 1,1-bis(3,4-dimethylphenyl)ethane (TCI Chemicals, >90.0%) were refluxed with sodium metal and then distilled under reduced pressure. *N*-methyl-2-pyrrolidone (Sigma-Aldrich, >99.0%), and hexamethyldisiloxane (Sigma-Aldrich, 98+%) were distilled under reduced pressure. Paraffin (Fluka, infrared grade), *n*-hexane (TCI Chemical, anhydrous), polybutenes (Sigma-Aldrich, $M_n = 2300$, isobutylene > 90 %), polystyrene (Aldrich, $M_w = 45,000$), polydimethylsiloxane (Sigma-Adrich, 50 cSt, $M_w \sim 3780$), methan(ol-*d*₁) (Sigma-Aldrich, 99.5 atom % *D*), benzene chromium tricarbonyl (Strem, >98%), *N,N*-dimethylformamide (EMD Millipore, anhydrous, >99.8%) and carbon tetrachloride (Acros, spectrophotometric grade 99+%) were used without further

purification. Liquid reagents were degassed with N₂ or freeze-pump-thawed before bringing into the glove box and stored on activated molecular sieves (3 Å).

Methylcyclopentadienylmolybdenum(I) tricarbonyl dimer (Sigma-Aldrich, 97%) was purified by recrystallization.

Choice of DMF/CCl₄ for polarity study:

The range of polarities was chosen because of the miscibility of DMF and CCl₄ with the solvatochromic indicator (Nile Red). Solvatochromism is inherently a microscopic phenomenon that directly depends on the environment around the probe molecule. Nile Red is typically used as a stain for lipids in biological systems.³ It was thought that a very polar solution of methanol/CCl₄ would preferentially solvate Nile Red. This would have given inaccurate polarities of the bulk solutions under study. If there had been a significant dependence on polarity, the inaccurate polarities would have made the interpretation difficult.

Table C.1. Solvents and viscogens used in this study with relevant properties.

solvent	viscogen	bulk viscosity	microviscosity	solvent
		range (cP)	range (s/m ²) × 10 ⁹	type
<i>n</i> -hexane	paraffin	0.36-20.61	0.29-6.08	aliphatic
	polybutenes (<i>M_w</i> = 3200)	0.36-18.27	0.28-2.31	aliphatic (polymeric)
toluene	1,1-bis(3,4- dimethylphenyl)- ethane	0.61-8.01	0.57-5.05	aromatic
	polystyrene (<i>M_w</i> = 45,000)	0.61-30.22	0.60-0.83	aromatic (polymeric)
	paraffin	0.61-21.06	0.55-6.08	mixed
hexamethyl- disiloxane	polydimethyl- siloxane (<i>M_w</i> = 3800)	0.54-18.22	0.41-1.94	siloxane (polymeric)
glyme	tetraglyme	0.50-2.83	0.49-2.23	polar aprotic
methanol- <i>D</i> ₁	tetraglyme	0.66-2.86	0.59-2.22	mixed
<i>N</i> -methyl-2- pyrrolidone	1,1-bis(3,4- dimethylphenyl)- ethane	1.88-7.66	1.62-6.26	mixed

Table C.2. Literature densities and viscosities for calibration (25.0 °C). These data were reported in a prior communication.¹

compound	density (g/cm ³)	dynamic viscosity (cP)
diglyme	0.9384	0.989
tetraglyme	1.009	0.845
decane	0.7264	0.845
tetrahydrofuran	0.88	0.46
benzene	0.873	0.6
dimethylsulfoxide	1.095	1.99
<i>n</i> -hexane	0.6548	0.296
<i>n</i> -tetradecane	0.7591	2.077
2,6,10,14- tetramethylpentadecane	0.77911	5.4793

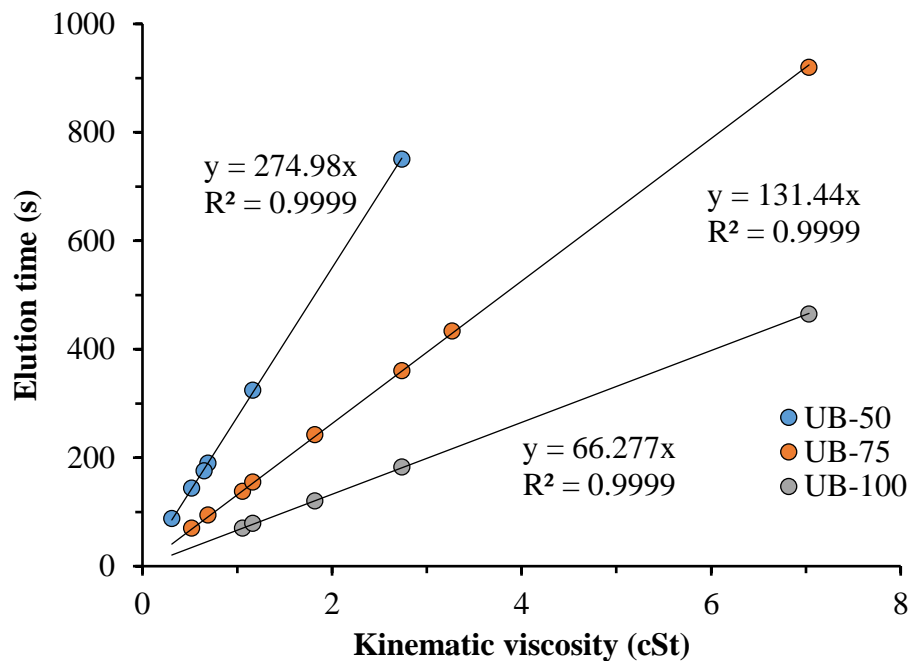


Figure C.1. Calibration regression of the viscometers used in this study. This data was reported in a prior communication.¹

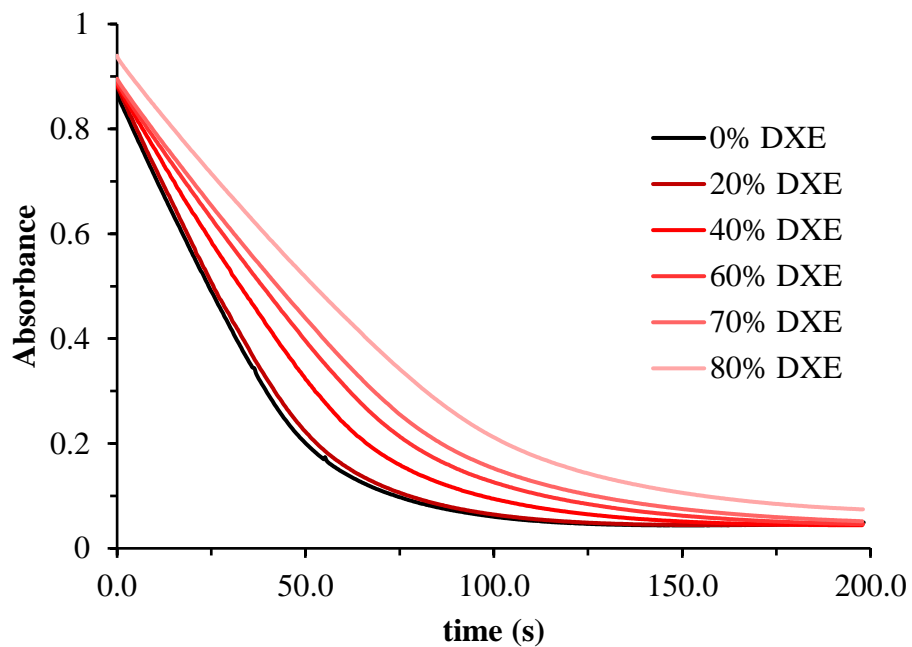


Figure C.2. Kinetic absorbance data for the toluene/DXE/ CCl_4 solvent system.

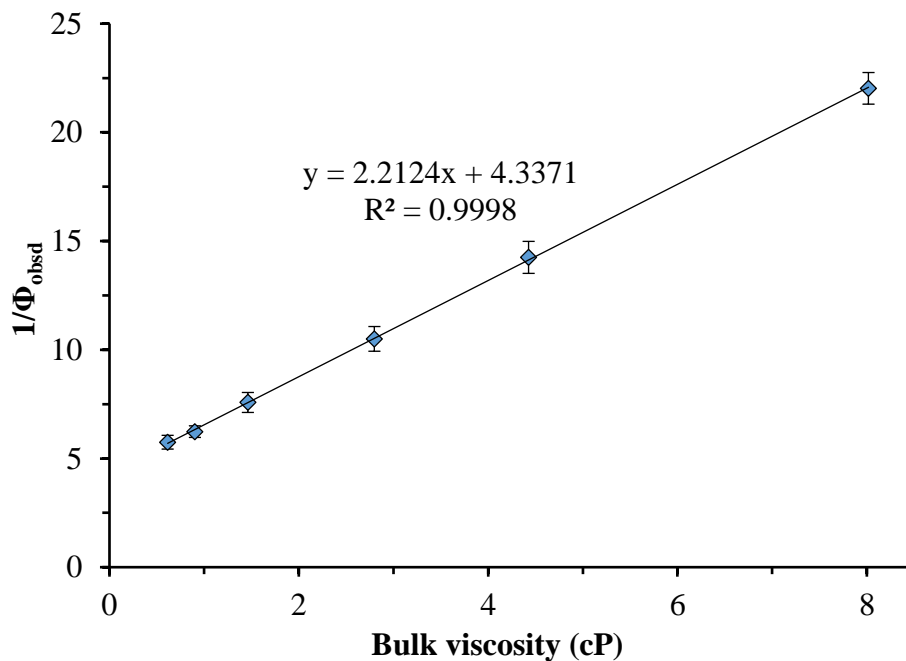


Figure C.3. Plot of $1/\Phi_{\text{obsd}}$ as a function of bulk viscosity for the toluene/DXE/ CCl_4 solvent system. Data points are in triplicate with error bars of 1σ .

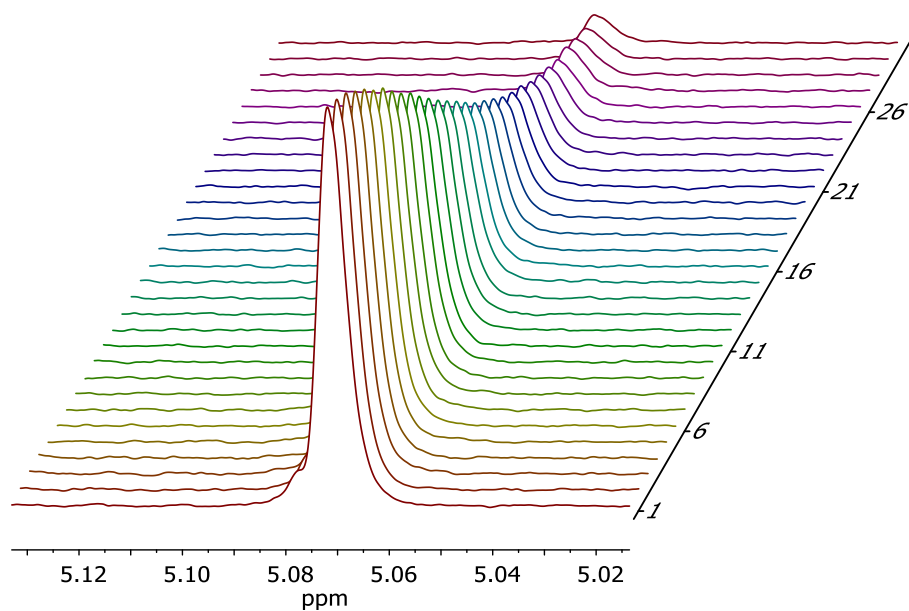


Figure C.4. Example ^1H -DOSY spectra of the $\text{C}_6\text{H}_6\text{Cr}(\text{CO})_3$ probe molecule in 80 vol% glyme and 20 vol% CCl_4 (part of the glyme/tetraglyme/ CCl_4 solvent series). Pulse sequence **ledbpgps**, $n_s = 8$, $d_1 = 10\text{s}$, 30 linear gradient slices.

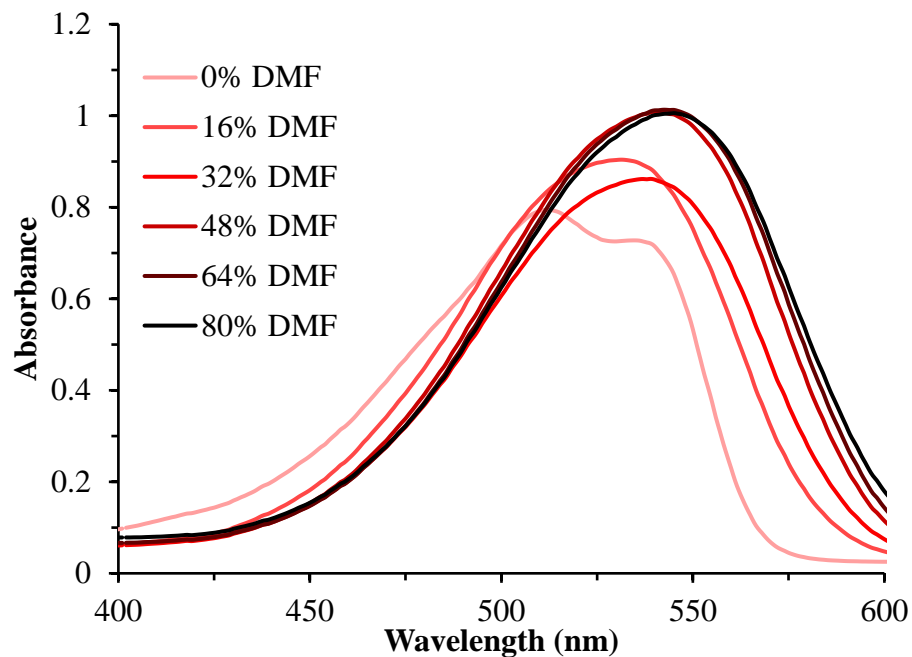


Figure C.5. UV-vis spectra of the solvatochromic indicator Nile red in the DMF/CCl₄ solvent system.

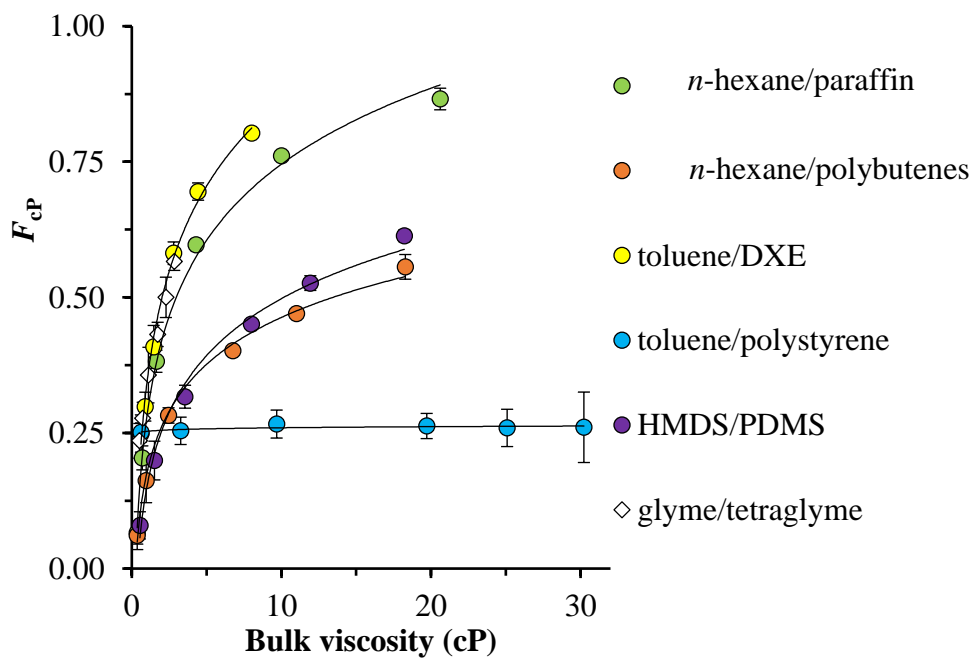


Figure C.6. A plot of F_{cp} as a function of bulk viscosity (cP). Each sample contains 20 wt% CCl₄; error bars are 1 σ ; and curves are only a visual aid.

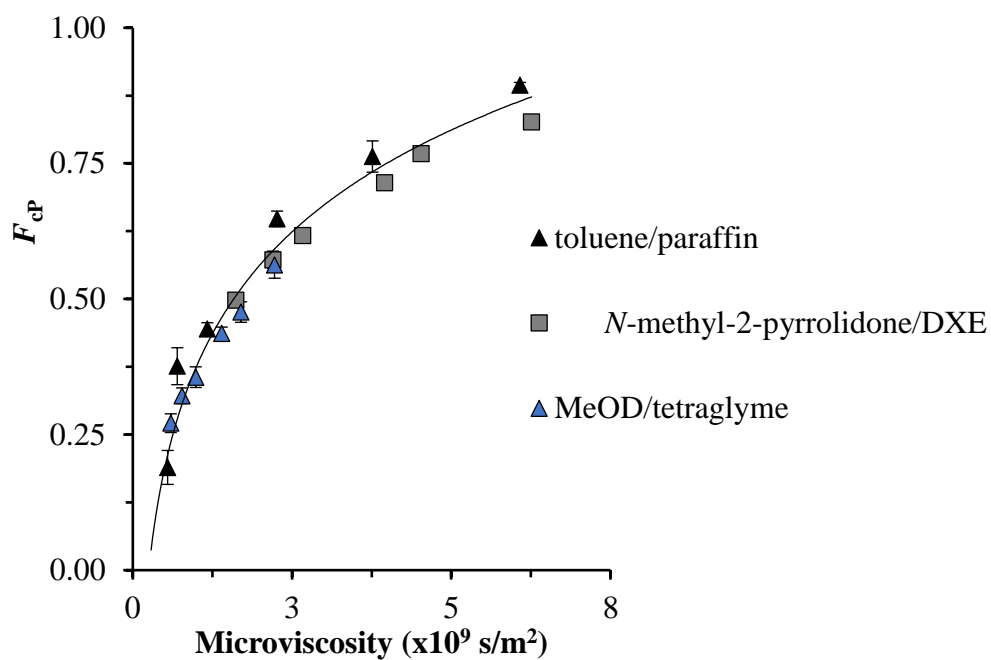


Figure C.7. A plot of F_{cp} as a function of microviscosity (s/m^2) for the mixed solvent systems (toluene/paraffin, *N*-methyl-2-pyrrolidone/1,1-bis(3,4-dimethylphenyl)ethane, methanol-*d*₁/tetraglyme). Each sample contains 20 wt% CCl₄; error bars are 1 σ ; and curves are only a visual aid.

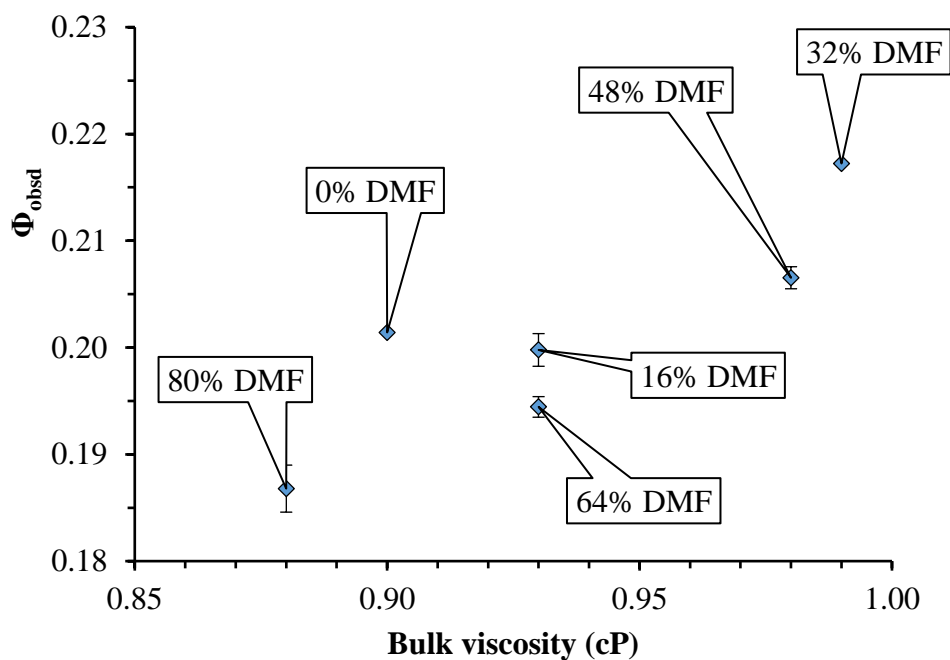


Figure C.8. A plot of Φ_{obsd} as a function of bulk viscosity in the solvent system dimethylformamide/ CCl_4 . Callouts on the data are for volume percentage dimethylformamide. Error bars are 1σ . Note that the range of Φ_{obsd} is only 0.19-0.22, whereas the range for *n*-hexane/paraffin/ CCl_4 spans 0.10-0.65.

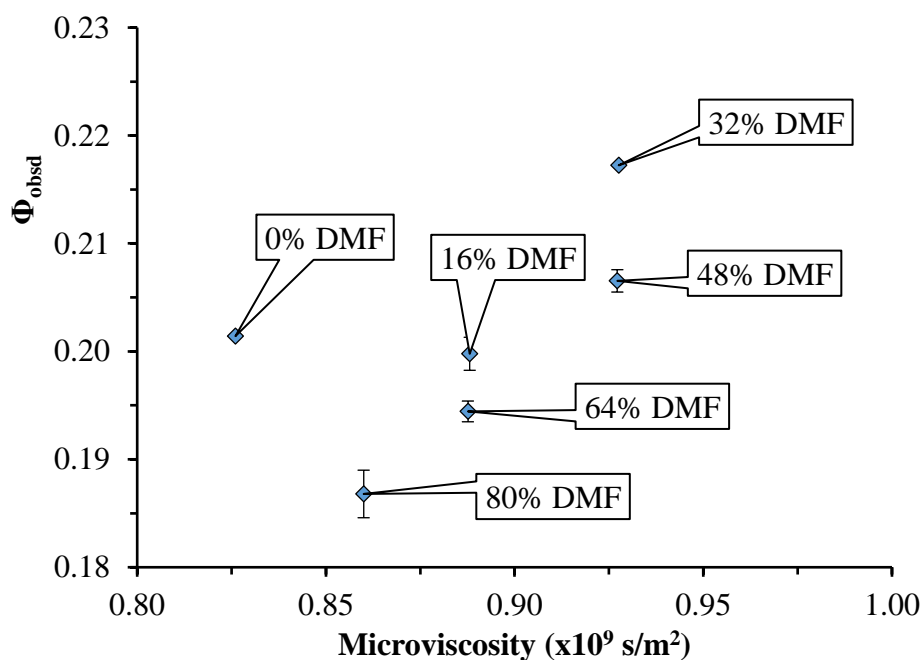


Figure C.9. A plot of Φ_{obsd} as a function of microviscosity in the solvent system dimethylformamide/ CCl_4 . Callouts on the data are for volume percentage dimethylformamide. Error bars are 1σ . Note that the range of Φ_{obsd} is only 0.19-0.22, whereas the range for *n*-hexane/paraffin/ CCl_4 spans 0.10-0.65.

APPENDIX D

SELECTED EXPERIMENTAL DETAILS FOR THE
SYNTHESIS OF AN ASYMMETRIC MOLYBDENUM DIMER
TO STUDY SIZE AND MASS DEPENDENCE ON F_{cP} OF
ASSYMETRIC RADICAL PAIRS IN A SOLVENT CAGE

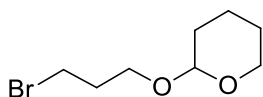
Justin T. Barry, David R. Tyler*

Department of Chemistry and Biochemistry, University of Oregon, Eugene, OR

97403-1253

Appendix D of my dissertation contains selected experimental details towards the synthesis of a molybdenum dimer of the type $R^1Cp(CO)_3Mo-Mo(CO)_3CpR^2$ (where $R^1 \neq R^2$).

Experimental Section



3-((tetrahydropyran-2-yl)oxy)-1-bromopropane

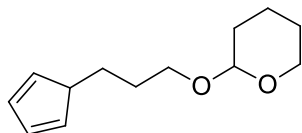
To a 250 mL round bottom, 47.86 g (0.344 mols) of bromopropanol was charged with 50 mL dichloromethane. The solution was cooled to 0 °C and 20 mg of pyridinium p-toluenesulfonate was added. Over the course of 30 minutes, 34.14 g (0.406 mols) of

3,4-dihydro-2*H*-pyran was added dropwise. The reaction was allowed to react for 6 hrs. Sodium bicarbonate was added and allowed to stir for 15 mins. The mixture was filtered over a coarse frit. The solution was then rinsed with aqueous sodium bicarbonate twice and with a brine solution once. Dried over sodium sulfate and then concentrated into a clear yellow oil (78.11 g, 97% yield). ¹H NMR (*d*₁-CDCl₃, 300 MHz, 25 °C): δ 4.59 (s, 1H), 3.85 (m, 2H), 3.52 (m, 4H), 2.12 (p, 2H), 1.70 (m, 6H)



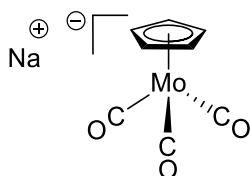
Sodium Cyclopentadienide

To a 250 mL round bottom, 168.2 g of molten dicyclopentadiene was added. Freshly chopped metallic sodium (10 g) was added under heavy flow of nitrogen. The mixture was refluxed at 160 °C for 6 hours. A white precipitate formed upon evolution of hydrogen gas. Upon completion, the mixture was filtered in a glove box and the product washed with hexanes. Yield was not obtained. Unreacted dicyclopentadiene was recovered for further reactions. ¹H NMR (*d*₆-DMSO, 300 MHz, 25 °C): δ 5.37 (s, 5H)



2-[(3-(1,3-cyclopentadien-1-yl)propyl)oxy]tetrahydro-2H-pyran

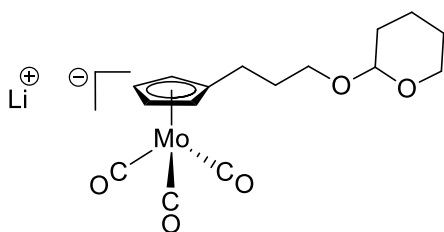
To a 100 mL round bottom, 7.47 g (33.4 mmols) of THP protected bromopropanol was added with 30 mL of THF. The solution was subjected to three freeze-pump-thaw cycles. The solution was cooled to $-78\text{ }^{\circ}\text{C}$ and 3.24 g (36.7 mmols) of sodium cyclopentadienide in 20 mL THF was cannula transferred in. The reaction was allowed to come to room temp at which a pink precipitate formed. Diethyl ether was added and the mixture was washed twice with water and once with a brine solution. The yellow solution was dried with sodium sulfate and concentrated to a viscous clear yellow oil (6.33 g, 90% yield).



NaCpMo(CO)₃

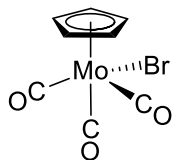
Under rigorous air free technique, 1.2701 g (14.4 mmols) sodium cyclopentadienide was charged into a single-neck 100 mL roundbottom with 40 mL THF and a stir bar. To a two-neck Schlenk adapted roundbottom, 4.0623 g (15.4 mmols) of molybdenum hexacarbonyl was added with 10 mL of THF and a stir bar. The two-neck flask was fitted with a reflux condenser and cooled to $0\text{ }^{\circ}\text{C}$ at which the sodium cyclopentadiene

solution was cannula transferred in. The mixture was refluxed at 80 °C for 15 hrs. The mixture turned a dark brown upon completion with some precipitate. The product was precipitated upon addition of hexanes and filtered. More hexanes were used to wash the white solid (NaCpMo(CO)₃·2THF, 5.7520 g, 70% yield). IR (THF) ν 1900, 1796, 1744 cm⁻¹.



LiCp'Mo(CO)₃

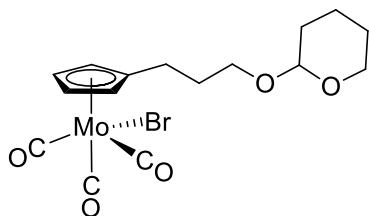
In a 100 mL one-neck round bottom, 2.9098g (13.9 mmols) of (1) was added with 50 mL THF. The solution was then freeze-pump-thawed three times. At -78 °C, 6.9 mL of 2.5 M n-buLi was added dropwise. Upon addition the solution turned a light orange. The solution was then cannula transferred into a two-neck Schlenk adapted 100 mL roundbottom with degassed molybdenum hexacarbonyl (4.0845 g, 15.5 mmols). The mixture was then refluxed at 80 °C for 15 hrs. The mixture turned a dark brown with some precipitate. All of the THF was removed *in vacuo* and the brown residue was redissolved in DCM. The product was then precipitated using hexanes and filtered to yield a white solid. Any THF present caused the product to oil. (4.0805 g, 74% yield). IR (THF) ν 1884, 1788, 1765 cm⁻¹.



CpMo(CO)₃Br

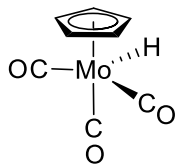
NaCpMo(CO)₃ was made *in situ* without isolation: 3.674 g (4.2 mmol) sodium cyclopentadienide, 1.2109 g (4.6 mmol) molybdenum hexacarbonyl. The solution was then cooled to 0 °C and 0.6662 g (4.2 mmol) bromine was added as a THF solution dropwise. The solution turned from dark brown to dark red. The solution was then precipitated with hexanes and filtered to yield a red solid (0.9938 g, 73% yield).

IR (THF) ν 2046, 1968 cm^{-1} .



Cp'Mo(CO)₃Br

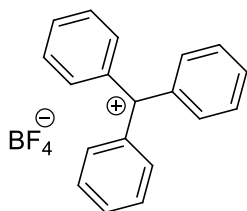
Cp'Mo(CO)₃Br was synthesized in a similar manner to CpMo(CO)₃Br. LiCp'Mo(CO)₃ was treated with 1 eq of bromine and used without workup. IR (THF) ν 2043, 1965 cm^{-1}



CpMo(CO)₃H

Sodium cyclopentadienide (2.1102 g, 23.9 mmols) was added to a 100 mL round bottom with 50 mL dimethylformamide. The resulting brown solution was cannula transferred into another Schlenk flask with degassed molybdenum hexacarbonyl (7.0001 g, 26.5 mmol). The reaction was refluxed at 120 °C for 24 hrs (reactions were usually complete in 6 hrs). DMF was distilled off resulting in a brown oil. Water was added to the brown oil to dissolve it, followed by the slow addition of acetic acid (9.6 mL) at 0 °C. A yellow precipitate formed immediately. The mixture was filtered and washed with water (5.2404 g, 82% yield). ¹H NMR (*d*₁-CDCl₃, 500 MHz, 25 °C): δ 5.42 (s, 5H), -5.56 (s, 1H); ¹³C NMR (*d*₁-CDCl₃, 500 MHz, 25 °C) δ 90.06 (s); IR (THF)

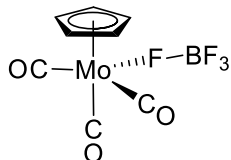
v 2023, 1931 cm⁻¹.



Trityl tetrafluoroborate

In a 100 mL Schlenk flask, triphenyl chloride (13.9622 g, 14.2 mmol) was dissolved in 50 mL of dry benzene. To the solution, 5.73 mL (14 mmol) of a 54% tetrafluoroboric

acid etherate was added dropwise at 0 °C. A yellow precipitate formed immediately and was filtered and washed with hexanes (11.4252 g, 69% yield). ¹H NMR (*d*₁-CDCl₃, 500 MHz, 25 °C): δ 8.22 (br, 3H), 7.87 (br, 6H), 7.70 (br, 6H).



To an improved Kjeldahl Schlenk flask, CpMo(CO)₃H (6.1450g, 24.9 mmols) was added to 50 mL of DCM. The yellow-brown solution was cooled to -78 °C and trityl tetrafluoroborate (8.5046 g, 25.8 mmols) in DCM was cannula transferred slowly down the side of the flask. During the course of the addition, the solution turned violet. After 1 hour, cold hexanes was added. The solution was then distilled at -78 °C under high vacuum to remove the DCM. A violet precipitate resulted that was washed with more cold hexanes. IR (THF) ν 2070, 1988 cm⁻¹

APPENDIX E

SUPPORTING INFORMATION FOR CHAPTER V

Justin T. Barry, David R. Tyler*

Department of Chemistry and Biochemistry, University of Oregon, Eugene, OR

97403-1253

Appendix E of my dissertation is the supporting information for a Chapter VI. This appendix details the kinetic derivations that are used in Chapter VI.

Derivation

The classic mechanistic model of the solvent cage effect (Figure E.1) will be modified for this derivation. First, the concentration of radical trap (CCl_4) will be significantly lowered so that free radicals can form collisional pairs (Figure E.2). Second, acronyms for some of the species will be used to cut down on clutter (Figure E.2).

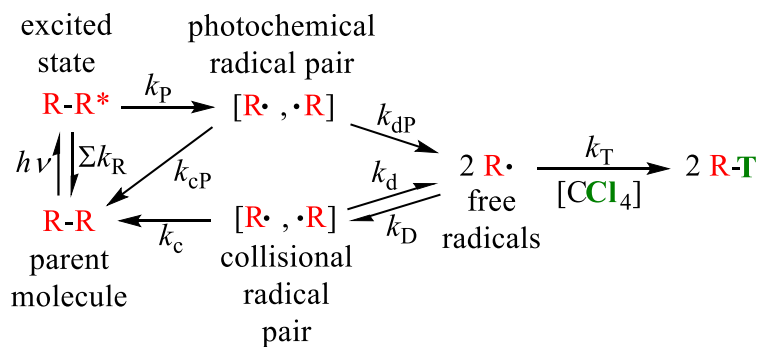


Figure E.1. Classical mechanistic model for the solvent cage effect.

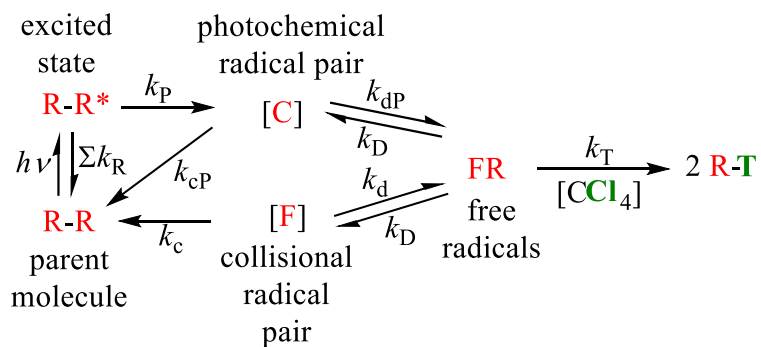


Figure E.2. Mechanistic model of the solvent cage effect used for this derivation.

SS of [random pair] [F]

$$\text{Production rate of [F]} = \frac{d[\text{F}]}{dt} = k_{\text{D}}[\text{FR}]^2$$

$$\text{Consumption rate of [F]} = \frac{-d[\text{F}]}{dt} = k_{\text{d}}[\text{F}] + k_{\text{c}}[\text{F}]$$

$$k_{\text{D}}[\text{FR}]^2 = k_{\text{d}}[\text{F}] + k_{\text{c}}[\text{F}]$$

$$\Rightarrow [\text{F}] = \frac{k_{\text{D}}[\text{FR}]^2}{k_{\text{d}} + k_{\text{c}}}$$

SS of [photochemical cage pair] [C]

$$\text{Production rate of [C]} = \frac{d[\text{C}]}{dt} = I_{\text{A}}\phi$$

$$\text{Consumption rate of [C]} = \frac{-d[\text{C}]}{dt} = k_{\text{d}}[\text{C}] + k_{\text{c}}[\text{C}]$$

$$I_{\text{A}}\phi = k_{\text{d}}[\text{C}] + k_{\text{c}}[\text{C}]$$

$$\Rightarrow [\text{C}] = \frac{I_{\text{A}}\phi}{k_{\text{d}} + k_{\text{c}}}$$

SS of [free radicals] [FR]

$$\text{Production rate of [FR]} = \frac{d[\text{FR}]}{dt} = k_{\text{d}}[\text{C}] + k_{\text{d}}[\text{F}]$$

$$\text{Consumption rate of [FR]} = \frac{-d[\text{FR}]}{dt} = 2k_{\text{t}}[\text{CCl}_4] + k_{\text{D}}[\text{FR}]^2$$

$$\Rightarrow [\text{FR}]^2 = \frac{k_{\text{d}}[\text{C}] + k_{\text{d}}[\text{F}] - 2k_{\text{t}}[\text{CCl}_4]}{k_{\text{D}}}$$

$$[\text{FR}]^2 = \frac{k_d[\text{C}]}{k_D} + \frac{k_d[\text{F}]}{k_D} - \frac{2k_t[\text{CCl}_4]}{k_D}$$

$$\text{identity } [\text{F}] = \frac{k_d[\text{FR}]^2}{k_d + k_c}$$

$$[\text{FR}]^2 = \frac{k_d[\text{C}]}{k_D} + \frac{k_d k_D [\text{FR}]^2}{k_D(k_d + k_c)} - \frac{2k_t[\text{CCl}_4]}{k_D}$$

$$[\text{FR}]^2 = \frac{k_d[\text{C}]}{k_D} + \frac{k_d[\text{FR}]^2}{(k_d + k_c)} - \frac{2k_t[\text{CCl}_4]}{k_D}$$

$$\text{identity } (1-F_c') = \frac{k_d}{(k_d + k_c)}$$

$$[\text{FR}]^2 = \frac{k_d[\text{C}]}{k_D} + (1-F_c')[\text{FR}]^2 - \frac{2k_t[\text{CCl}_4]}{k_D}$$

$$[\text{FR}]^2 - (1-F_c')[\text{FR}]^2 = \frac{k_d[\text{C}]}{k_D} - \frac{2k_t[\text{CCl}_4]}{k_D}$$

$$[\text{FR}]^2 - ([\text{FR}]^2 - F_c'[\text{FR}]^2) = \frac{k_d[\text{C}]}{k_D} - \frac{2k_t[\text{CCl}_4]}{k_D}$$

$$F_c'[\text{FR}]^2 = \frac{k_d[\text{C}]}{k_D} - \frac{2k_t[\text{CCl}_4]}{k_D}$$

$$[\text{FR}]^2 = \frac{k_d[\text{C}]}{F_c'k_D} - \frac{2k_t[\text{CCl}_4]}{F_c'k_D}$$

$$[\text{FR}] = \left(\frac{k_d[\text{C}]}{F_c'k_D} - \frac{2k_t[\text{CCl}_4]}{F_c'k_D} \right)^{1/2}$$

[C] is constant so entire term becomes "a"

$$a = \frac{k_d[\text{C}]}{F_c'k_D}$$

$$[\text{FR}] = \left(a - \frac{2k_t[\text{CCl}_4]}{F_c'k_D} \right)^{1/2}$$

$$2rate = k_t[CCl_4][FR]$$

$$[FR] = \left(a - \frac{2k_t[CCl_4]}{F_c'k_D} \right)^{1/2}$$

$$2rate = k_t[CCl_4] \left(a - \frac{2k_t[CCl_4]}{F_c'k_D} \right)^{1/2}$$

$$\frac{2rate}{k_t[CCl_4]} = \left(a - \frac{2k_t[CCl_4]}{F_c'k_D} \right)^{1/2}$$

$$\frac{2^2rate^2}{k_t^2[CCl_4]^2} = a - \frac{2k_t[CCl_4]}{F_c'k_D}$$

$$\frac{2^2rate^2F_c'k_D}{k_t^2[CCl_4]^2} = aF_c'k_D - 2k_t[CCl_4]$$

$$aF_c'k_D - \frac{2^2rate^2F_c'k_D}{k_t^2[CCl_4]^2} = 2k_t[CCl_4]$$

$$\frac{aF_c'k_D}{2} - \frac{2rate^2F_c'k_D}{k_t^2[CCl_4]^2} = k_t[CCl_4]$$

$$k_t[CCl_4] = \frac{aF_c'k_D}{2} - \frac{2rate^2F_c'k_D}{k_t^2[CCl_4]^2}$$

$$2rate = k_t[CCl_4][FR]$$

$$rate = \frac{aF_c'k_D}{2} - \frac{2rate^2F_c'k_D}{k_t^2[CCl_4]^2}$$

$$rate = \frac{aF_c'k_D}{2} - \frac{2rate^2F_c'k_D}{k_t^2[CCl_4]^2}$$

$$y = b - mx$$

plot *rate* vs $\frac{rate^2}{[CCl_4]^2}$

$$\text{slope} = \frac{2F_c' k_D}{k_t^2}$$

$$F_c' = \frac{\text{slope } k_t^2}{2k_D}$$

APPENDIX F

TABULATED CRYSTAL STRUCTURE DATA

Justin T. Barry, Sarah E. Brady, Lev M. Zahkarov, David R. Tyler*

Department of Chemistry and Biochemistry, University of Oregon, Eugene, OR

97403-1253

Appendix F of my dissertation reports the two crystal structures. Appropriate acknowledgements of work are made at the beginning of each structure.

Crystal Structure of 1,3-propanediol, 2-methyl-2-[[phenylsulfonyl]oxy]methyl-1,3-dibenzenesulfonate

This crystal structure was grown in collaboration with Sarah E. Brady during a rotation in the Prof. David R. Tyler lab. I conducted the synthesis, and grew the crystal. The crystal was solved by Dr. Lev M. Zahkarov. The goal was to produce the core pieces of star polymers. The tosylated alcohols would act as leaving groups for nucleophiles.

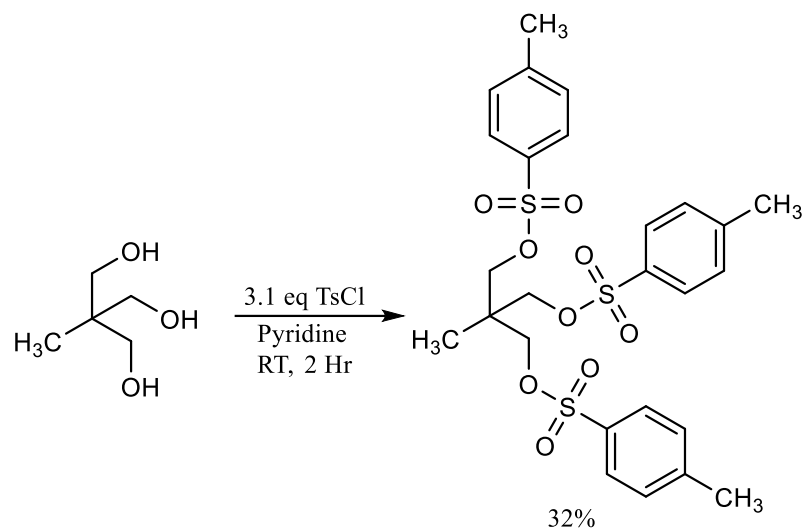


Figure F.1. Reaction to produce 1,3-propanediol, 2-methyl-2-[[[(phenylsulfonyl)oxy]methyl]-1,3-dibenzenesulfonate].

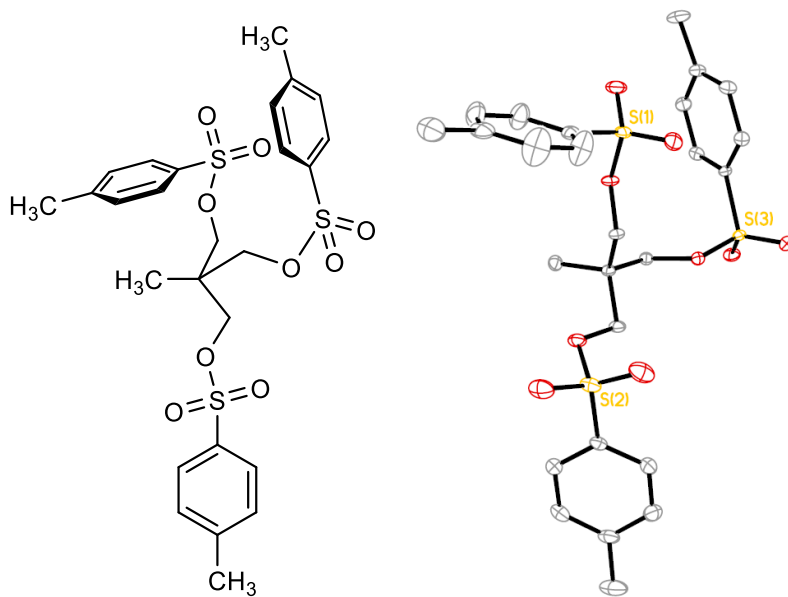


Figure F.2. Chemdraw sketch of the molecule next to the crystal structure ORTEP.

Table F.1. Crystal and structure refinement for 1,3-propanediol, 2-methyl-2-[[[(phenylsulfonyl)oxy]methyl]-1,3-dibenzenesulfonate (internal ID# mo_dt21_0m)

Identification code	mo_dt21_0m	
Empirical formula	C ₂₆ H ₃₀ O ₉ S ₃	
Formula weight	582.68	
Temperature	100(2) K	
Wavelength	0.71073 Å	
Crystal system	Monoclinic	
Space group	P2 ₁ /n	
Unit cell dimensions	a = 17.9114(14) Å	a = 90°.
	b = 5.8709(4) Å	b = 93.030(2)°.
	c = 25.958(2) Å	g = 90°.
Volume	2725.8(4) Å ³	
Z	4	
Density (calculated)	1.420 Mg/m ³	
Absorption coefficient	0.324 mm ⁻¹	
F(000)	1224	
Crystal size	0.37 x 0.23 x 0.14 mm ³	
Theta range for data collection	1.35 to 27.00°.	
Index ranges	-22 ≤ h ≤ 22, -7 ≤ k ≤ 7, -33 ≤ l ≤ 33	
Reflections collected	45449	
Independent reflections	5948 [R(int) = 0.0425]	
Completeness to theta = 27.00°	100.0 %	
Absorption correction	Semi-empirical from equivalents	
Max. and min. transmission	0.9549 and 0.8891	
Refinement method	Full-matrix least-squares on F ²	
Data / restraints / parameters	5948 / 0 / 463	
Goodness-of-fit on F ²	1.050	
Final R indices [I > 2σ(I)]	R1 = 0.0400, wR2 = 0.1095	
R indices (all data)	R1 = 0.0451, wR2 = 0.1192	
Largest diff. peak and hole	0.875 and -0.601 e.Å ⁻³	

Table F.2. Atomic coordinates and equivalent isotropic displacement parameters for [mo_dt21_0m]. $U(\text{eq})$ is defined as one third of the trace of the orthogonalized U^{ij} tensor.

	x	y	z	U(eq)
S(1)	7160(1)	7055(1)	1217(1)	16(1)
S(2)	7335(1)	6617(1)	-1231(1)	20(1)
S(3)	9870(1)	5548(1)	776(1)	12(1)
O(1)	7664(1)	8365(2)	833(1)	15(1)
O(2)	7301(1)	8181(2)	1699(1)	24(1)
O(3)	7283(1)	4660(2)	1168(1)	24(1)
O(4)	7596(1)	8326(2)	-788(1)	19(1)
O(5)	6618(1)	7459(3)	-1406(1)	30(1)
O(6)	7405(1)	4334(2)	-1045(1)	30(1)
O(7)	9195(1)	6185(2)	385(1)	13(1)
O(8)	9929(1)	3128(2)	736(1)	18(1)
O(9)	10499(1)	6961(2)	676(1)	17(1)
C(1)	8268(1)	8869(3)	35(1)	12(1)
C(2)	8080(1)	11419(3)	33(1)	16(1)
C(3)	7676(1)	7504(3)	305(1)	13(1)
C(4)	8320(1)	7945(3)	-512(1)	15(1)
C(5)	9034(1)	8615(3)	314(1)	13(1)
C(6)	6240(1)	7655(3)	985(1)	17(1)
C(7)	5817(1)	5976(4)	747(1)	42(1)
C(8)	5081(1)	6453(5)	582(1)	50(1)
C(9)	4772(1)	8575(4)	648(1)	28(1)
C(10)	5208(1)	10218(4)	892(1)	36(1)
C(11)	5945(1)	9778(4)	1060(1)	33(1)
C(12)	3977(1)	9063(6)	460(1)	41(1)
C(13)	7972(1)	7023(3)	-1715(1)	17(1)
C(14)	7932(1)	9014(3)	-2007(1)	21(1)
C(15)	8398(1)	9252(3)	-2415(1)	24(1)
C(16)	8895(1)	7523(4)	-2536(1)	24(1)
C(17)	8938(1)	5575(3)	-2228(1)	26(1)
C(18)	8479(1)	5310(3)	-1816(1)	23(1)
C(19)	9355(1)	7720(5)	-3005(1)	38(1)
C(20)	9545(1)	6293(3)	1379(1)	14(1)
C(21)	9740(1)	8399(3)	1594(1)	18(1)
C(22)	9437(1)	9014(3)	2055(1)	22(1)
C(23)	8948(1)	7581(3)	2300(1)	24(1)
C(24)	8781(1)	5459(3)	2084(1)	23(1)
C(25)	9070(1)	4804(3)	1621(1)	18(1)
C(26)	8577(2)	8368(4)	2777(1)	38(1)

Table F.3. Bond lengths [\AA] and angles [$^\circ$] for mo_dt21_0m.

S(1)-O(2)	1.4262(13)
S(1)-O(3)	1.4297(14)
S(1)-O(1)	1.5781(11)
S(1)-C(6)	1.7595(17)
S(2)-O(5)	1.4272(14)
S(2)-O(6)	1.4286(14)
S(2)-O(4)	1.5785(13)
S(2)-C(13)	1.7569(17)
S(3)-O(8)	1.4293(12)
S(3)-O(9)	1.4326(12)
S(3)-O(7)	1.5828(11)
S(3)-C(20)	1.7535(15)
O(1)-C(3)	1.4629(18)
O(4)-C(4)	1.4650(19)
O(7)-C(5)	1.4650(18)
C(1)-C(5)	1.525(2)
C(1)-C(3)	1.528(2)
C(1)-C(4)	1.529(2)
C(1)-C(2)	1.534(2)
C(2)-H(2A)	0.94(3)
C(2)-H(2B)	0.97(2)
C(2)-H(2C)	0.93(2)
C(3)-H(3A)	0.95(2)
C(3)-H(3B)	0.96(2)
C(4)-H(4A)	0.96(2)
C(4)-H(4B)	0.94(2)
C(5)-H(5A)	0.98(2)
C(5)-H(5B)	0.986(19)
C(6)-C(7)	1.371(3)
C(6)-C(11)	1.372(3)
C(7)-C(8)	1.392(3)
C(7)-H(7)	1.00(3)
C(8)-C(9)	1.378(3)
C(8)-H(8)	0.95(4)
C(9)-C(10)	1.373(3)
C(9)-C(12)	1.509(3)
C(10)-C(11)	1.392(3)
C(10)-H(10)	0.95(4)
C(11)-H(11)	0.92(3)
C(12)-H(12A)	0.87(4)
C(12)-H(12B)	0.91(4)
C(12)-H(14C)	0.96(5)
C(13)-C(18)	1.390(2)
C(13)-C(14)	1.393(2)
C(14)-C(15)	1.389(3)

C(14)-H(14)	0.91(2)
C(15)-C(16)	1.397(3)
C(15)-H(15)	0.98(2)
C(16)-C(17)	1.395(3)
C(16)-C(19)	1.511(3)
C(17)-C(18)	1.390(3)
C(17)-H(17)	1.00(2)
C(18)-H(18)	0.95(2)
C(19)-H(19A)	0.91(4)
C(19)-H(19B)	1.04(3)
C(19)-H(19C)	0.97(3)
C(20)-C(25)	1.393(2)
C(20)-C(21)	1.394(2)
C(21)-C(22)	1.387(2)
C(21)-H(21)	0.92(3)
C(22)-C(23)	1.391(3)
C(22)-H(22)	0.94(2)
C(23)-C(24)	1.392(3)
C(23)-C(26)	1.508(2)
C(24)-C(25)	1.386(2)
C(24)-H(24)	0.97(2)
C(25)-H(25)	0.95(2)
C(26)-H(26A)	0.95(3)
C(26)-H(26B)	1.02(4)
C(26)-H(26C)	0.92(3)
O(2)-S(1)-O(3)	120.78(8)
O(2)-S(1)-O(1)	104.34(7)
O(3)-S(1)-O(1)	109.20(7)
O(2)-S(1)-C(6)	108.99(8)
O(3)-S(1)-C(6)	108.19(8)
O(1)-S(1)-C(6)	104.09(7)
O(5)-S(2)-O(6)	119.64(9)
O(5)-S(2)-O(4)	103.78(8)
O(6)-S(2)-O(4)	109.39(8)
O(5)-S(2)-C(13)	109.42(8)
O(6)-S(2)-C(13)	108.73(9)
O(4)-S(2)-C(13)	104.83(7)
O(8)-S(3)-O(9)	120.06(7)
O(8)-S(3)-O(7)	104.16(7)
O(9)-S(3)-O(7)	109.18(7)
O(8)-S(3)-C(20)	110.00(7)
O(9)-S(3)-C(20)	108.56(7)
O(7)-S(3)-C(20)	103.60(7)
C(3)-O(1)-S(1)	117.38(10)
C(4)-O(4)-S(2)	118.64(10)
C(5)-O(7)-S(3)	116.67(9)

C(5)-C(1)-C(3)	111.12(12)
C(5)-C(1)-C(4)	108.00(12)
C(3)-C(1)-C(4)	108.51(13)
C(5)-C(1)-C(2)	106.82(12)
C(3)-C(1)-C(2)	110.83(13)
C(4)-C(1)-C(2)	111.53(13)
C(1)-C(2)-H(2A)	110.2(15)
C(1)-C(2)-H(2B)	110.5(12)
H(2A)-C(2)-H(2B)	111.6(19)
C(1)-C(2)-H(2C)	113.1(13)
H(2A)-C(2)-H(2C)	105.9(19)
H(2B)-C(2)-H(2C)	105.3(18)
O(1)-C(3)-C(1)	107.05(12)
O(1)-C(3)-H(3A)	108.6(12)
C(1)-C(3)-H(3A)	111.7(12)
O(1)-C(3)-H(3B)	107.8(12)
C(1)-C(3)-H(3B)	111.9(12)
H(3A)-C(3)-H(3B)	109.6(17)
O(4)-C(4)-C(1)	107.75(12)
O(4)-C(4)-H(4A)	107.2(12)
C(1)-C(4)-H(4A)	110.1(12)
O(4)-C(4)-H(4B)	106.6(12)
C(1)-C(4)-H(4B)	111.8(12)
H(4A)-C(4)-H(4B)	113.0(17)
O(7)-C(5)-C(1)	108.71(12)
O(7)-C(5)-H(5A)	107.8(11)
C(1)-C(5)-H(5A)	110.6(11)
O(7)-C(5)-H(5B)	109.2(10)
C(1)-C(5)-H(5B)	108.5(10)
H(5A)-C(5)-H(5B)	112.0(15)
C(7)-C(6)-C(11)	120.58(18)
C(7)-C(6)-S(1)	119.72(15)
C(11)-C(6)-S(1)	119.66(14)
C(6)-C(7)-C(8)	119.1(2)
C(6)-C(7)-H(7)	117.2(19)
C(8)-C(7)-H(7)	123.7(19)
C(9)-C(8)-C(7)	121.5(2)
C(9)-C(8)-H(8)	123(2)
C(7)-C(8)-H(8)	115(2)
C(10)-C(9)-C(8)	118.09(19)
C(10)-C(9)-C(12)	121.3(2)
C(8)-C(9)-C(12)	120.6(2)
C(9)-C(10)-C(11)	121.3(2)
C(9)-C(10)-H(10)	114(2)
C(11)-C(10)-H(10)	124(2)
C(6)-C(11)-C(10)	119.4(2)

C(6)-C(11)-H(11)	122(2)
C(10)-C(11)-H(11)	118(2)
C(9)-C(12)-H(12A)	114(2)
C(9)-C(12)-H(12B)	115(2)
H(12A)-C(12)-H(12B)	106(3)
C(9)-C(12)-H(14C)	117(3)
H(12A)-C(12)-H(14C)	105(4)
H(12B)-C(12)-H(14C)	99(4)
C(18)-C(13)-C(14)	121.30(16)
C(18)-C(13)-S(2)	119.51(14)
C(14)-C(13)-S(2)	119.11(13)
C(15)-C(14)-C(13)	118.91(17)
C(15)-C(14)-H(14)	118.7(15)
C(13)-C(14)-H(14)	122.3(15)
C(14)-C(15)-C(16)	120.94(17)
C(14)-C(15)-H(15)	115.4(15)
C(16)-C(15)-H(15)	123.6(15)
C(17)-C(16)-C(15)	118.89(17)
C(17)-C(16)-C(19)	120.61(19)
C(15)-C(16)-C(19)	120.45(19)
C(18)-C(17)-C(16)	121.01(17)
C(18)-C(17)-H(17)	119.8(14)
C(16)-C(17)-H(17)	119.2(14)
C(17)-C(18)-C(13)	118.89(17)
C(17)-C(18)-H(18)	120.2(14)
C(13)-C(18)-H(18)	120.9(14)
C(16)-C(19)-H(19A)	110(2)
C(16)-C(19)-H(19B)	111.0(18)
H(19A)-C(19)-H(19B)	107(3)
C(16)-C(19)-H(19C)	111.4(16)
H(19A)-C(19)-H(19C)	110(3)
H(19B)-C(19)-H(19C)	108(2)
C(25)-C(20)-C(21)	121.43(15)
C(25)-C(20)-S(3)	119.12(13)
C(21)-C(20)-S(3)	119.39(12)
C(22)-C(21)-C(20)	118.39(16)
C(22)-C(21)-H(21)	121.0(15)
C(20)-C(21)-H(21)	120.6(15)
C(21)-C(22)-C(23)	121.36(17)
C(21)-C(22)-H(22)	118.8(15)
C(23)-C(22)-H(22)	119.8(15)
C(22)-C(23)-C(24)	118.96(16)
C(22)-C(23)-C(26)	120.32(19)
C(24)-C(23)-C(26)	120.65(19)
C(25)-C(24)-C(23)	120.99(17)
C(25)-C(24)-H(24)	118.1(14)

C(23)-C(24)-H(24)	120.9(14)
C(24)-C(25)-C(20)	118.82(16)
C(24)-C(25)-H(25)	119.8(13)
C(20)-C(25)-H(25)	121.4(13)
C(23)-C(26)-H(26A)	111.5(19)
C(23)-C(26)-H(26B)	111(2)
H(26A)-C(26)-H(26B)	112(3)
C(23)-C(26)-H(26C)	106.1(18)
H(26A)-C(26)-H(26C)	113(3)
H(26B)-C(26)-H(26C)	103(3)

Symmetry transformations used to generate equivalent atoms:

Table F.4. Anisotropic displacement parameters ($\text{\AA}^2 \times 10^3$) for mo_dt21_0m. The anisotropic displacement factor exponent takes the form: $-2p^2[h^2 a^{*2}U^{11} + \dots + 2 h k a^* b^* U^{12}]$

	U11	U22	U33	U23	U13	U12
S(1)	16(1)	21(1)	12(1)	4(1)	7(1)	1(1)
S(2)	19(1)	28(1)	13(1)	1(1)	0(1)	-4(1)
S(3)	12(1)	15(1)	10(1)	-1(1)	3(1)	2(1)
O(1)	17(1)	19(1)	10(1)	0(1)	6(1)	-3(1)
O(2)	24(1)	37(1)	11(1)	1(1)	5(1)	3(1)
O(3)	25(1)	22(1)	26(1)	9(1)	11(1)	2(1)
O(4)	16(1)	30(1)	10(1)	-2(1)	-1(1)	3(1)
O(5)	19(1)	50(1)	20(1)	-2(1)	-3(1)	-2(1)
O(6)	37(1)	30(1)	24(1)	5(1)	1(1)	-12(1)
O(7)	14(1)	14(1)	12(1)	-1(1)	1(1)	1(1)
O(8)	20(1)	17(1)	16(1)	-1(1)	4(1)	5(1)
O(9)	13(1)	23(1)	16(1)	0(1)	5(1)	-1(1)
C(1)	12(1)	14(1)	10(1)	1(1)	4(1)	-1(1)
C(2)	15(1)	14(1)	18(1)	4(1)	4(1)	1(1)
C(3)	13(1)	15(1)	10(1)	-1(1)	4(1)	-2(1)
C(4)	12(1)	24(1)	10(1)	0(1)	2(1)	1(1)
C(5)	13(1)	13(1)	12(1)	1(1)	3(1)	0(1)
C(6)	15(1)	24(1)	14(1)	3(1)	6(1)	-1(1)
C(7)	24(1)	29(1)	73(2)	-13(1)	-4(1)	-3(1)
C(8)	25(1)	43(1)	81(2)	-14(1)	-11(1)	-9(1)
C(9)	17(1)	49(1)	20(1)	7(1)	8(1)	-1(1)
C(10)	31(1)	39(1)	38(1)	-4(1)	-4(1)	14(1)
C(11)	30(1)	31(1)	38(1)	-11(1)	-8(1)	7(1)
C(12)	17(1)	73(2)	34(1)	11(1)	4(1)	3(1)
C(13)	21(1)	21(1)	10(1)	-1(1)	-1(1)	0(1)
C(14)	24(1)	22(1)	18(1)	1(1)	0(1)	4(1)
C(15)	27(1)	28(1)	16(1)	6(1)	-2(1)	0(1)
C(16)	22(1)	38(1)	11(1)	-2(1)	-1(1)	0(1)
C(17)	28(1)	32(1)	20(1)	-6(1)	-1(1)	9(1)
C(18)	30(1)	21(1)	17(1)	1(1)	-2(1)	5(1)
C(19)	30(1)	68(2)	17(1)	-3(1)	5(1)	-1(1)
C(20)	15(1)	18(1)	9(1)	0(1)	3(1)	5(1)
C(21)	21(1)	18(1)	13(1)	1(1)	1(1)	1(1)
C(22)	32(1)	20(1)	14(1)	-3(1)	1(1)	6(1)
C(23)	30(1)	30(1)	12(1)	2(1)	6(1)	11(1)
C(24)	25(1)	26(1)	17(1)	6(1)	9(1)	4(1)
C(25)	19(1)	18(1)	16(1)	2(1)	4(1)	2(1)
C(26)	56(2)	42(1)	19(1)	-3(1)	19(1)	9(1)

Table F.5. Hydrogen coordinates ($\times 10^4$) and isotropic displacement parameters ($\text{\AA}^2 \times 10^3$) for mo_dt21_0m.

	x	y	z	U(eq)
H(2A)	8463(13)	12250(40)	-112(9)	29(6)
H(2B)	7989(11)	11940(40)	377(9)	18(5)
H(2C)	7644(12)	11770(40)	-165(9)	22(5)
H(3A)	7794(11)	5920(40)	317(8)	14(5)
H(3B)	7187(12)	7710(30)	144(8)	16(5)
H(4A)	8686(12)	8780(40)	-691(8)	16(5)
H(4B)	8403(11)	6370(30)	-513(8)	11(4)
H(5A)	9424(11)	9260(30)	107(8)	10(4)
H(5B)	9020(10)	9350(30)	655(7)	6(4)
H(7)	6056(18)	4460(60)	709(13)	67(10)
H(8)	4820(20)	5240(70)	412(14)	80(11)
H(10)	4970(20)	11660(60)	914(14)	73(10)
H(11)	6221(18)	10960(60)	1210(13)	60(9)
H(12A)	3640(20)	8440(70)	648(15)	77(11)
H(12B)	3860(20)	8620(70)	128(17)	82(12)
H(14)	7598(13)	10150(40)	-1948(9)	28(6)
H(14C)	3830(30)	10640(90)	430(20)	116(16)
H(15)	8361(13)	10710(40)	-2598(9)	30(6)
H(17)	9293(13)	4340(40)	-2311(9)	32(6)
H(18)	8503(13)	3950(40)	-1615(9)	28(6)
H(19A)	9090(20)	7170(60)	-3287(15)	77(11)
H(19B)	9481(18)	9420(60)	-3081(12)	59(9)
H(19C)	9823(15)	6910(40)	-2958(10)	37(7)
H(21)	10066(13)	9350(40)	1435(9)	30(6)
H(22)	9563(13)	10440(40)	2200(9)	30(6)
H(24)	8450(13)	4410(40)	2248(9)	29(6)
H(25)	8935(12)	3370(40)	1473(8)	20(5)
H(26A)	8307(17)	7170(60)	2926(12)	58(9)
H(26B)	8254(19)	9770(60)	2699(14)	69(10)
H(26C)	8954(16)	8930(50)	2997(11)	39(7)

Table F.6. Torsion angles [°] for mo_dt21_0m.

O(2)-S(1)-O(1)-C(3)	176.39(11)
O(3)-S(1)-O(1)-C(3)	45.97(13)
C(6)-S(1)-O(1)-C(3)	-69.38(12)
O(5)-S(2)-O(4)-C(4)	179.13(12)
O(6)-S(2)-O(4)-C(4)	50.36(13)
C(13)-S(2)-O(4)-C(4)	-66.09(13)
O(8)-S(3)-O(7)-C(5)	-175.74(10)
O(9)-S(3)-O(7)-C(5)	-46.34(12)
C(20)-S(3)-O(7)-C(5)	69.18(12)
S(1)-O(1)-C(3)-C(1)	-173.37(10)
C(5)-C(1)-C(3)-O(1)	58.99(16)
C(4)-C(1)-C(3)-O(1)	177.59(12)
C(2)-C(1)-C(3)-O(1)	-59.63(16)
S(2)-O(4)-C(4)-C(1)	-150.41(11)
C(5)-C(1)-C(4)-O(4)	-176.46(12)
C(3)-C(1)-C(4)-O(4)	62.98(16)
C(2)-C(1)-C(4)-O(4)	-59.38(16)
S(3)-O(7)-C(5)-C(1)	-166.20(10)
C(3)-C(1)-C(5)-O(7)	51.73(16)
C(4)-C(1)-C(5)-O(7)	-67.17(15)
C(2)-C(1)-C(5)-O(7)	172.74(12)
O(2)-S(1)-C(6)-C(7)	-140.69(18)
O(3)-S(1)-C(6)-C(7)	-7.6(2)
O(1)-S(1)-C(6)-C(7)	108.43(18)
O(2)-S(1)-C(6)-C(11)	37.12(18)
O(3)-S(1)-C(6)-C(11)	170.18(16)
O(1)-S(1)-C(6)-C(11)	-73.76(17)
C(11)-C(6)-C(7)-C(8)	0.0(4)
S(1)-C(6)-C(7)-C(8)	177.8(2)
C(6)-C(7)-C(8)-C(9)	0.5(5)
C(7)-C(8)-C(9)-C(10)	-1.1(4)
C(7)-C(8)-C(9)-C(12)	179.2(3)
C(8)-C(9)-C(10)-C(11)	1.1(4)
C(12)-C(9)-C(10)-C(11)	-179.1(2)
C(7)-C(6)-C(11)-C(10)	0.1(3)
S(1)-C(6)-C(11)-C(10)	-177.74(18)
C(9)-C(10)-C(11)-C(6)	-0.6(4)
O(5)-S(2)-C(13)-C(18)	-138.28(14)
O(6)-S(2)-C(13)-C(18)	-5.96(16)
O(4)-S(2)-C(13)-C(18)	110.95(14)
O(5)-S(2)-C(13)-C(14)	38.47(16)
O(6)-S(2)-C(13)-C(14)	170.79(14)
O(4)-S(2)-C(13)-C(14)	-72.31(15)
C(18)-C(13)-C(14)-C(15)	1.5(3)
S(2)-C(13)-C(14)-C(15)	-175.14(14)

C(13)-C(14)-C(15)-C(16)	0.7(3)
C(14)-C(15)-C(16)-C(17)	-2.4(3)
C(14)-C(15)-C(16)-C(19)	175.06(18)
C(15)-C(16)-C(17)-C(18)	2.0(3)
C(19)-C(16)-C(17)-C(18)	-175.46(18)
C(16)-C(17)-C(18)-C(13)	0.1(3)
C(14)-C(13)-C(18)-C(17)	-1.9(3)
S(2)-C(13)-C(18)-C(17)	174.74(14)
O(8)-S(3)-C(20)-C(25)	-30.37(15)
O(9)-S(3)-C(20)-C(25)	-163.57(13)
O(7)-S(3)-C(20)-C(25)	80.47(14)
O(8)-S(3)-C(20)-C(21)	152.39(13)
O(9)-S(3)-C(20)-C(21)	19.20(15)
O(7)-S(3)-C(20)-C(21)	-96.76(13)
C(25)-C(20)-C(21)-C(22)	-1.3(2)
S(3)-C(20)-C(21)-C(22)	175.86(13)
C(20)-C(21)-C(22)-C(23)	-0.1(3)
C(21)-C(22)-C(23)-C(24)	2.1(3)
C(21)-C(22)-C(23)-C(26)	-174.95(19)
C(22)-C(23)-C(24)-C(25)	-2.6(3)
C(26)-C(23)-C(24)-C(25)	174.42(19)
C(23)-C(24)-C(25)-C(20)	1.2(3)
C(21)-C(20)-C(25)-C(24)	0.8(2)
S(3)-C(20)-C(25)-C(24)	-176.38(13)

Symmetry transformations used to generate equivalent atoms:

Crystal data for $\text{RCp}_2\text{Mo}_2(\text{CO})_6$ [R = 1-(cyclopentadienyl)-2-phenyl-ethane]

This crystal structure was grown of a molybdenum dimer. This molecule was synthesized (Figure F.3) to eventually add a chromium tricarbonyl group to the phenyl moiety (Figure F.4). The purpose of this synthesis was two-fold; 1) to practice the thermal cracking of a Cp ligand in the presence of $\text{Mo}(\text{CO})_6$ to form a dimer, and 2) to form a novel organometallic complex to study.

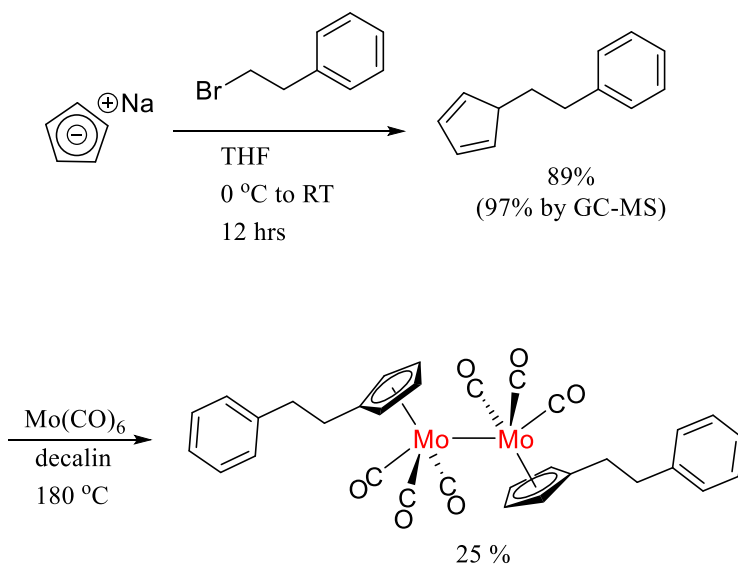


Figure F.3. Synthesis of the $\text{RCp}_2\text{Mo}_2(\text{CO})_6$ dimer [R = 1-(cyclopentadienyl)-2-phenyl-ethane].

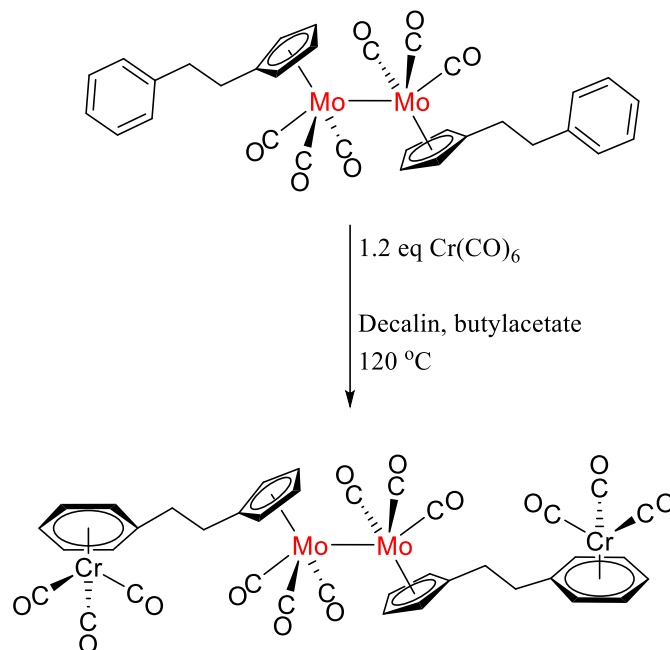


Figure F.4. Intended synthesis of a BzCr(CO)_3 appended molybdenum dimer complex.

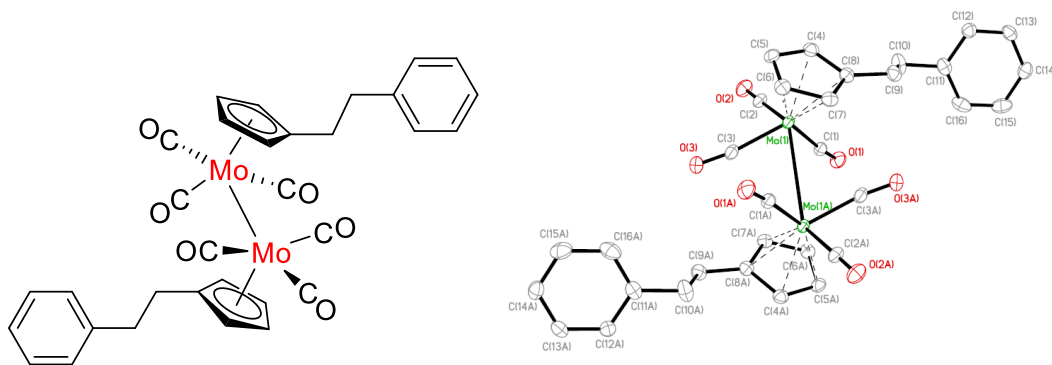


Figure F.5. Chemdraw sketch of molybdenum complex next to the crystal structure ORTEP.

Table F.7. Crystal and structure refinement for $\text{RCp}_2\text{Mo}_2(\text{CO})_6$ [R = 1-(cyclopentadienyl)-2-phenyl-ethane] (internal ID# cu_dt43_0m_a)

Identification code	cu_dt43_0m_a	
Empirical formula	C ₃₂ H ₂₆ Mo ₂ O ₆	
Formula weight	698.41	
Temperature	173(2) K	
Wavelength	1.54178 Å	
Crystal system	Triclinic	
Space group	P-1	
Unit cell dimensions	a = 8.0509(3) Å	a = 77.318(3)°.
	b = 9.6353(4) Å	b = 83.594(3)°.
	c = 9.9474(4) Å	g = 66.492(2)°.
Volume	690.09(5) Å ³	
Z	1	
Density (calculated)	1.681 Mg/m ³	
Absorption coefficient	7.813 mm ⁻¹	
F(000)	350	
Crystal size	0.070 x 0.050 x 0.030 mm ³	
Theta range for data collection	4.558 to 66.687°.	
Index ranges	-9 ≤ h ≤ 9, -11 ≤ k ≤ 11, -11 ≤ l ≤ 11	
Reflections collected	7868	
Independent reflections	2439 [R(int) = 0.0411]	
Completeness to theta = 66.687°	99.5 %	
Absorption correction	Semi-empirical from equivalents	
Max. and min. transmission	0.7528 and 0.6036	
Refinement method	Full-matrix least-squares on F ²	
Data / restraints / parameters	2439 / 0 / 233	
Goodness-of-fit on F ²	1.089	
Final R indices [I > 2σ(I)]	R1 = 0.0258, wR2 = 0.0660	
R indices (all data)	R1 = 0.0286, wR2 = 0.0675	
Extinction coefficient	n/a	
Largest diff. peak and hole	0.473 and -0.362 e.Å ⁻³	

Table F.8. Atomic coordinates and equivalent isotropic displacement parameters for $\text{RCp}_2\text{Mo}_2(\text{CO})_6$ [R = 1-(cyclopentadienyl)-2-phenyl-ethane]. $U(\text{eq})$ is defined as one third of the trace of the orthogonalized U^{ij} tensor.

	x	y	z	U(eq)
Mo(1)	4896(1)	8372(1)	788(1)	26(1)
O(1)	8999(3)	7877(3)	646(3)	46(1)
O(2)	6820(3)	5222(3)	-146(3)	48(1)
O(3)	3533(4)	9004(3)	-2178(3)	51(1)
C(1)	7468(4)	8149(3)	653(3)	33(1)
C(2)	6128(4)	6387(4)	190(4)	35(1)
C(3)	4082(4)	8859(4)	-1117(4)	36(1)
C(4)	4285(5)	6947(4)	2839(3)	36(1)
C(5)	2760(5)	7512(4)	1978(4)	38(1)
C(6)	2005(4)	9129(4)	1811(4)	35(1)
C(7)	3024(4)	9572(4)	2577(3)	34(1)
C(8)	4425(4)	8237(4)	3236(3)	33(1)
C(9)	5676(5)	8165(4)	4286(4)	38(1)
C(10)	7477(6)	6810(5)	4403(5)	52(1)
C(11)	8711(4)	6892(4)	5398(4)	40(1)
C(12)	8763(5)	6146(4)	6753(4)	38(1)
C(13)	9893(5)	6213(4)	7657(4)	41(1)
C(14)	10968(5)	7029(4)	7233(4)	44(1)
C(15)	10915(5)	7796(5)	5912(5)	55(1)
C(16)	9786(5)	7736(5)	4989(4)	52(1)

Table F.9. Bond lengths [Å] and angles [°] for cu_dt43_0m_a.

Mo(1)-C(2)	1.963(3)
Mo(1)-C(3)	1.969(4)
Mo(1)-C(1)	1.987(3)
Mo(1)-C(5)	2.302(3)
Mo(1)-C(4)	2.319(3)
Mo(1)-C(6)	2.330(3)
Mo(1)-C(7)	2.386(3)
Mo(1)-C(8)	2.405(3)
O(1)-C(1)	1.152(4)
O(2)-C(2)	1.143(4)
O(3)-C(3)	1.149(4)
C(4)-C(5)	1.427(5)
C(4)-C(8)	1.432(4)
C(4)-H(4)	0.97(3)
C(5)-C(6)	1.406(5)
C(5)-H(5)	0.99(4)
C(6)-C(7)	1.414(5)
C(6)-H(6)	0.83(3)
C(7)-C(8)	1.412(5)
C(7)-H(7)	0.91(3)
C(8)-C(9)	1.502(5)
C(9)-C(10)	1.510(5)
C(9)-H(9A)	0.96(5)
C(9)-H(9B)	0.99(4)
C(10)-C(11)	1.513(5)
C(10)-H(10A)	1.17(5)
C(10)-H(10B)	0.84(6)
C(11)-C(12)	1.377(5)
C(11)-C(16)	1.383(5)
C(12)-C(13)	1.377(5)
C(12)-H(12)	0.82(4)
C(13)-C(14)	1.364(5)
C(13)-H(13)	0.68(4)
C(14)-C(15)	1.354(6)
C(14)-H(14)	0.80(3)
C(15)-C(16)	1.388(6)
C(15)-H(15)	0.76(4)
C(16)-H(16)	0.95(4)
C(2)-Mo(1)-C(3)	77.55(14)
C(2)-Mo(1)-C(1)	78.00(12)
C(3)-Mo(1)-C(1)	106.52(13)
C(2)-Mo(1)-C(5)	89.79(13)
C(3)-Mo(1)-C(5)	101.03(13)
C(1)-Mo(1)-C(5)	146.43(14)
C(2)-Mo(1)-C(4)	85.72(13)

C(3)-Mo(1)-C(4)	134.22(12)
C(1)-Mo(1)-C(4)	111.18(13)
C(5)-Mo(1)-C(4)	35.96(12)
C(2)-Mo(1)-C(6)	123.14(12)
C(3)-Mo(1)-C(6)	95.86(13)
C(1)-Mo(1)-C(6)	152.60(13)
C(5)-Mo(1)-C(6)	35.35(12)
C(4)-Mo(1)-C(6)	58.96(12)
C(2)-Mo(1)-C(7)	143.41(12)
C(3)-Mo(1)-C(7)	122.66(13)
C(1)-Mo(1)-C(7)	117.75(12)
C(5)-Mo(1)-C(7)	58.34(12)
C(4)-Mo(1)-C(7)	58.09(11)
C(6)-Mo(1)-C(7)	34.87(11)
C(2)-Mo(1)-C(8)	115.71(13)
C(3)-Mo(1)-C(8)	153.95(12)
C(1)-Mo(1)-C(8)	98.42(12)
C(5)-Mo(1)-C(8)	58.85(11)
C(4)-Mo(1)-C(8)	35.23(11)
C(6)-Mo(1)-C(8)	58.10(12)
C(7)-Mo(1)-C(8)	34.29(11)
O(1)-C(1)-Mo(1)	173.4(3)
O(2)-C(2)-Mo(1)	178.7(3)
O(3)-C(3)-Mo(1)	171.8(3)
C(5)-C(4)-C(8)	108.1(3)
C(5)-C(4)-Mo(1)	71.37(19)
C(8)-C(4)-Mo(1)	75.67(19)
C(5)-C(4)-H(4)	127.4(19)
C(8)-C(4)-H(4)	124.4(19)
Mo(1)-C(4)-H(4)	122(2)
C(6)-C(5)-C(4)	107.7(3)
C(6)-C(5)-Mo(1)	73.41(18)
C(4)-C(5)-Mo(1)	72.67(18)
C(6)-C(5)-H(5)	125(2)
C(4)-C(5)-H(5)	127(2)
Mo(1)-C(5)-H(5)	117(2)
C(5)-C(6)-C(7)	108.3(3)
C(5)-C(6)-Mo(1)	71.24(18)
C(7)-C(6)-Mo(1)	74.74(18)
C(5)-C(6)-H(6)	129(2)
C(7)-C(6)-H(6)	123(2)
Mo(1)-C(6)-H(6)	118(2)
C(8)-C(7)-C(6)	108.9(3)
C(8)-C(7)-Mo(1)	73.60(18)
C(6)-C(7)-Mo(1)	70.39(18)
C(8)-C(7)-H(7)	128(2)

C(6)-C(7)-H(7)	123(2)
Mo(1)-C(7)-H(7)	121(2)
C(7)-C(8)-C(4)	106.9(3)
C(7)-C(8)-C(9)	126.5(3)
C(4)-C(8)-C(9)	126.3(3)
C(7)-C(8)-Mo(1)	72.12(18)
C(4)-C(8)-Mo(1)	69.10(18)
C(9)-C(8)-Mo(1)	129.4(2)
C(8)-C(9)-C(10)	115.8(3)
C(8)-C(9)-H(9A)	117(2)
C(10)-C(9)-H(9A)	101(3)
C(8)-C(9)-H(9B)	109(2)
C(10)-C(9)-H(9B)	109.6(19)
H(9A)-C(9)-H(9B)	104(3)
C(9)-C(10)-C(11)	112.5(3)
C(9)-C(10)-H(10A)	110(2)
C(11)-C(10)-H(10A)	105(2)
C(9)-C(10)-H(10B)	114(4)
C(11)-C(10)-H(10B)	114(4)
H(10A)-C(10)-H(10B)	100(5)
C(12)-C(11)-C(16)	118.1(3)
C(12)-C(11)-C(10)	120.4(4)
C(16)-C(11)-C(10)	121.4(4)
C(13)-C(12)-C(11)	120.5(3)
C(13)-C(12)-H(12)	124(3)
C(11)-C(12)-H(12)	116(3)
C(14)-C(13)-C(12)	120.7(4)
C(14)-C(13)-H(13)	121(3)
C(12)-C(13)-H(13)	119(3)
C(15)-C(14)-C(13)	119.9(4)
C(15)-C(14)-H(14)	115(3)
C(13)-C(14)-H(14)	125(3)
C(14)-C(15)-C(16)	120.0(4)
C(14)-C(15)-H(15)	121(4)
C(16)-C(15)-H(15)	119(4)
C(11)-C(16)-C(15)	120.8(4)
C(11)-C(16)-H(16)	118(2)
C(15)-C(16)-H(16)	121(2)

Symmetry transformations used to generate equivalent atoms:

Table F.10. Anisotropic displacement parameters ($\text{\AA}^2 \times 10^3$) for cu_dt43_0m_a. The anisotropic displacement factor exponent takes the form: $-2p^2 [h^2 a^*2U^{11} + \dots + 2 h k a^* b^* U^{12}]$

	U11	U22	U33	U23	U13	U12
Mo(1)	27(1)	29(1)	29(1)	-9(1)	1(1)	-15(1)
O(1)	31(1)	51(1)	58(2)	-8(1)	-7(1)	-18(1)
O(2)	50(1)	39(1)	61(2)	-22(1)	5(1)	-18(1)
O(3)	70(2)	60(2)	39(2)	-8(1)	-12(1)	-39(2)
C(1)	36(2)	33(2)	33(2)	-8(1)	-1(1)	-16(1)
C(2)	34(2)	36(2)	41(2)	-11(2)	2(1)	-20(1)
C(3)	38(2)	40(2)	39(2)	-14(2)	2(2)	-23(2)
C(4)	41(2)	37(2)	31(2)	-6(1)	5(1)	-18(2)
C(5)	41(2)	47(2)	38(2)	-9(2)	7(2)	-30(2)
C(6)	24(2)	46(2)	35(2)	-7(2)	3(1)	-13(2)
C(7)	32(2)	33(2)	34(2)	-7(1)	6(1)	-11(1)
C(8)	33(2)	36(2)	31(2)	-11(1)	5(1)	-13(1)
C(9)	43(2)	37(2)	32(2)	-12(2)	3(2)	-13(2)
C(10)	50(2)	50(2)	46(2)	-19(2)	-14(2)	-2(2)
C(11)	38(2)	38(2)	35(2)	-12(2)	-2(2)	-4(2)
C(12)	41(2)	35(2)	40(2)	-6(2)	-4(2)	-15(2)
C(13)	46(2)	36(2)	32(2)	-2(2)	-6(2)	-9(2)
C(14)	36(2)	45(2)	53(2)	-12(2)	-8(2)	-15(2)
C(15)	41(2)	55(2)	69(3)	-2(2)	9(2)	-26(2)
C(16)	45(2)	59(2)	39(2)	2(2)	8(2)	-16(2)

Table F.11. Hydrogen coordinates ($\times 10^4$) and isotropic displacement parameters ($\text{\AA}^2 \times 10^3$) for cu_dt43_0m_a.

	x	y	z	U(eq)
H(4)	5060(40)	5880(40)	3170(30)	31(9)
H(5)	2340(50)	6890(40)	1530(40)	48(11)
H(6)	1150(40)	9760(40)	1330(30)	22(8)
H(7)	2790(40)	10580(40)	2600(30)	32(9)
H(9A)	5250(60)	8080(50)	5230(50)	66(13)
H(9B)	5880(40)	9140(40)	4090(40)	36(9)
H(10A)	7260(60)	5660(50)	4850(50)	67(13)
H(10B)	7980(80)	6610(70)	3640(60)	110(20)
H(12)	8130(50)	5640(50)	6960(40)	52(12)
H(13)	9940(50)	5800(40)	8310(40)	33(11)
H(14)	11690(50)	7070(40)	7700(40)	35(10)
H(15)	11480(60)	8280(50)	5670(50)	68(15)
H(16)	9780(50)	8220(40)	4040(40)	48(11)

Table F.12. Torsion angles [°] for cu_dt43_0m_a.

C(8)-C(4)-C(5)-C(6)	1.8(4)
Mo(1)-C(4)-C(5)-C(6)	-65.6(2)
C(8)-C(4)-C(5)-Mo(1)	67.4(2)
C(4)-C(5)-C(6)-C(7)	-1.0(4)
Mo(1)-C(5)-C(6)-C(7)	-66.1(2)
C(4)-C(5)-C(6)-Mo(1)	65.1(2)
C(5)-C(6)-C(7)-C(8)	-0.1(4)
Mo(1)-C(6)-C(7)-C(8)	-63.9(2)
C(5)-C(6)-C(7)-Mo(1)	63.8(2)
C(6)-C(7)-C(8)-C(4)	1.2(3)
Mo(1)-C(7)-C(8)-C(4)	-60.7(2)
C(6)-C(7)-C(8)-C(9)	-171.9(3)
Mo(1)-C(7)-C(8)-C(9)	126.2(3)
C(6)-C(7)-C(8)-Mo(1)	61.9(2)
C(5)-C(4)-C(8)-C(7)	-1.8(3)
Mo(1)-C(4)-C(8)-C(7)	62.7(2)
C(5)-C(4)-C(8)-C(9)	171.3(3)
Mo(1)-C(4)-C(8)-C(9)	-124.2(3)
C(5)-C(4)-C(8)-Mo(1)	-64.5(2)
C(7)-C(8)-C(9)-C(10)	-155.8(3)
C(4)-C(8)-C(9)-C(10)	32.3(5)
Mo(1)-C(8)-C(9)-C(10)	-59.3(4)
C(8)-C(9)-C(10)-C(11)	175.4(3)
C(9)-C(10)-C(11)-C(12)	94.5(4)
C(9)-C(10)-C(11)-C(16)	-84.1(5)
C(16)-C(11)-C(12)-C(13)	-1.7(5)
C(10)-C(11)-C(12)-C(13)	179.6(3)
C(11)-C(12)-C(13)-C(14)	0.7(5)
C(12)-C(13)-C(14)-C(15)	0.6(6)
C(13)-C(14)-C(15)-C(16)	-0.7(6)
C(12)-C(11)-C(16)-C(15)	1.5(5)
C(10)-C(11)-C(16)-C(15)	-179.8(4)
C(14)-C(15)-C(16)-C(11)	-0.3(6)

Symmetry transformations used to generate equivalent atoms:

REFERENCES CITED

CHAPTER I

- (1) Grissom, C. B.; Chagovetz, A. M. *Z. Fuer Phys. Chem. Muenchen Ger.* **1993**, *182*, 181–188.
- (2) Lott, W. B.; Chagovetz, A. M.; Grissom, C. B. *J. Am. Chem. Soc.* **1995**, *117*, 12194–12201.
- (3) Woodward, J. R. *Prog. React. Kinet. Mech.* **2002**, *27*, 165–207.
- (4) Kaptein, R. *Adv. Free-Radic. Chem. Lond.* **1975**, *5*, 319–380.
- (5) Rembaum, A.; Szwarc, M. *J. Chem. Phys.* **1955**, *23*, 909–913.
- (6) Maleczka, R. E.; Geng, F. *J. Am. Chem. Soc.* **1998**, *120*, 8551–8552.
- (7) Tomooka, K.; Yamamoto, H.; Nakai, T. *Angew. Chem. Int. Ed.* **2000**, *39*, 4500–4502.
- (8) Griesser, M.; Dworak, C.; Jauk, S.; Hofer, M.; Rosspeintner, A.; Grabner, G.; Liska, R.; Gescheidt, G. *Macromol. Wash. DC U. S.* **2012**, *45*, 1737–1745.
- (9) Bosch, P.; Mateo, J. L.; Serrano, J. J. *Photochem. Photobiol. Chem.* **1997**, *103*, 177–184.
- (10) Wolff, E.-H. P.; Bos, A. N. R. *Ind. Eng. Chem. Res.* **1997**, *36*, 1163–1170.
- (11) Frounchi, M.; Farhadi, F.; Mohammadi, R. P. *Sci. Iran.* **2002**, *9*, 86–92.
- (12) Capek, I. *Adv. Colloid Interface Sci.* **2001**, *91*, 295–334.
- (13) De Kock, J. B. L.; Van Herk, A. M.; German, A. L. *J. Macromol. Sci. Polym. Rev.* **2001**, *C41*, 199–252.
- (14) Grogan, T. G.; Bag, N.; Traylor, T. G.; Magde, D. *J. Phys. Chem.* **1994**, *98*, 13791–13796.
- (15) Van Dijk, H. K.; Van der Haar, J.; Stufkens, D. J.; Oskam, A. *Inorg. Chem.* **1989**, *28*, 75–81.
- (16) Knoll, H.; De Lange, W. J. G.; Hennig, H.; Stufkens, D. J.; Oskam, A. **1992**, *430*, 123–132.

- (17) Balzani, V.; Scandola, F.; Graetzel, M., Ed.; Academic Press: New York, 1983; pp 1–48.
- (18) Clark, C. D.; Hoffman, M. Z. *Coord. Chem. Rev.* **1997**, *159*, 359–373.
- (19) Chesta, C. A.; Mohanty, J.; Nau, W. M.; Bhattacharjee, U.; Weiss, R. G. *J. Am. Chem. Soc.* **2007**, *129*, 5012–5022.
- (20) Levin, P. P.; Efremkin, A. F.; Kasparov, V. V.; Khudyakov, I. V. *J. Phys. Chem. A* **2016**, *120*, 7484–7489.
- (21) Turro, N. J.; Zimmt, M. B.; Lei, X. G.; Gould, I. R.; Nitsche, K. S.; Cha, Y. *J. Phys. Chem.* **1987**, *91*, 4544–4548.
- (22) Martin, J. C.; Dombchik, S. A. *Advances in Chemistry*; American Chemical Society, 1968; Vol. 75, pp 269–281.
- (23) Covert, K. J.; Askew, E. F.; Grunkemeier, J.; Koenig, T.; Tyler, D. R. *J. Am. Chem. Soc.* **1992**, *114*, 10446–10448.
- (24) Garr, C. D.; Finke, R. G. *J. Am. Chem. Soc.* **1992**, *114*, 10440–10445.
- (25) Krause, J. R.; Bidinosti, D. R. *Can. J. Chem.* **1975**, *53*, 628–632.
- (26) Landrum, J. T.; Hoff, C. D. *J. Organomet. Chem.* **1985**, *282*, 215–224.
- (27) Noyes, R. M. *J. Am. Chem. Soc.* **1955**, *77*, 2042–2045.
- (28) Noyes, R. M. *J. Am. Chem. Soc.* **1956**, *78*, 5486–5490.
- (29) Odian, G. *Principles of Polymerization, 4th Edition*; Wiley-Interscience: New York, 2004.
- (30) Lindfors, B. E.; Male, J. L.; Covert, K. J.; Tyler, D. R. *Chem. Commun. Camb.* **1997**, *17*, 1687–1688.
- (31) Male, J. L.; Lindfors, B. E.; Covert, K. J.; Tyler, D. R. *Macromolecules* **1997**, *30*, 6404–6406.
- (32) Male, J. L.; Lindfors, B. E.; Covert, K. J.; Tyler, D. R. *J. Am. Chem. Soc.* **1998**, *120*, 13176–13186.
- (33) Coolbaugh, T. S.; Coots, R. J.; Santarsiero, B. D.; Grubbs, R. H. *Inorganica Chim. Acta* **1985**, *98*, 99–105.
- (34) Tenhaeff, S. C.; Tyler, D. R. *Organometallics* **1991**, *10*, 473–482.

- (35) Noyes, R. M. A *J. Chem. Phys.* **1954**, *22*, 1349–1359.
- (36) Lindfors, B. E.; Nieckarz, G. F.; Tyler, D. R.; Glenn, A. G. *J. Photochem. Photobiol. Chem.* **1996**, *94*, 101–105.
- (37) Nieckarz, G. F.; Litty, J. J.; Tyler, D. R. *J. Organomet. Chem.* **1998**, *554*, 19–28.
- (38) Schutte, E.; Weakley, T. J. R.; Tyler, D. R. *J Am Chem Soc* **2003**, *125*, 10319–10326.
- (39) Poli, R.; Harvey, J. N. *Chem. Soc. Rev.* **2003**, *32*, 1–8.
- (40) Harris, J. D.; Oelkers, A. B.; Tyler, D. R. *J. Am. Chem. Soc.* **2007**, *129*, 6255–6262.
- (41) Koenig, T.; Fischer, H. *Free Radicals* **1973**, *1*, 157–189.
- (42) Oelkers, A. B.; Scatena, L. F.; Tyler, D. R. *J. Phys. Chem. A* **2007**, *111*, 5353–5360.
- (43) Oelkers, A. B.; Schutte, E. J.; Tyler, D. R. *Photochem. Photobiol. Sci.* **2008**, *7*, 228.
- (44) Oelkers, A. B.; Tyler, D. R. *Photochem. Photobiol. Sci.* **2008**, *7*, 1386–1390.

CHAPTER II

- (1) Franck, J.; Rabinowitsch, E. *Trans. Faraday Soc.* **1934**, *30*, 120–131.
- (2) Rabinowitch, E.; Wood, W. C. *Trans. Faraday Soc.* **1936**, *32*, 1381–1387.
- (3) Rabinowitch, E. *Trans. Faraday Soc.* **1937**, *33*, 1225–1233.
- (4) Koenig, T.; Fischer, H. *Free Radic.* **1973**, *1*, 157–189.
- (5) Koenig, T. W. *ACS Symp. Ser.* **1978**, *69*, 134–160.
- (6) Lorand, J. P. *Prog. Inorg. Chem.* **1972**, *17*, 207–325.
- (7) Rice, S. A. *Comprehensive Chemical Kinetics*; Elsevier: Amsterdam, Netherlands, 1985; Vol. 25.
- (8) Lott, W. B.; Chagovetz, A. M.; Grissom, C. B. *J. Am. Chem. Soc.* **1995**, *117*, 12194–12201.
- (9) Turro, N. J.; Kraeutler, B. *Acc. Chem. Res.* **1980**, *13*, 369–377.
- (10) Woodward, J. R. *Prog. React. Kinet. Mech.* **2002**, *27*, 165–207.

- (11) Kaptein, R. *Adv. Free-Radic. Chem. London* **1975**, *5*, 319–380.
- (12) Rembaum, A.; Szwarc, M. *J. Chem. Phys.* **1955**, *23*, 909–913.
- (13) Tanner, D. D.; Oumar-Mahamat, H.; Meintzer, C. P.; Tsai, E. C.; Lu, T. T.; Yang, D. *J. Am. Chem. Soc.* **1991**, *113*, 5397–5402.
- (14) Chowdhury, N.; Anoop, A.; Singh, N. D. P. *Synthesis* **2012**, *44*, 1745–1754.
- (15) Noyes, R. M. Z. *Fuer Elektrochem. Angew. Phys. Chem.* **1960**, *64*, 153–156.
- (16) Maleczka, R. E.; Geng, F. *J. Am. Chem. Soc.* **1998**, *120*, 8551–8552.
- (17) Tomooka, K.; Yamamoto, H.; Nakai, T. *Angew. Chem. Int. Ed.* **2000**, *39*, 4500–4502.
- (18) Watanabe, A.; Matsushita, M.; Masuda, A.; Igarashi, T.; Sakurai, T. *Heterocycles* **2009**, *78*, 2431–2437.
- (19) Griesser, M.; Dworak, C.; Jauk, S.; Hoefler, M.; Rosspointner, A.; Grabner, G.; Liska, R.; Gescheidt, G. *Macromolecules* **2012**, *45*, 1737–1745.
- (20) Bosch, P.; Mateo, J. L.; Serrano, J. J. *Photochem. Photobiol. A* **1997**, *103*, 177–184.
- (21) Wolff, E.-H. P.; Bos, A. N. R. *Ind. Eng. Chem. Res.* **1997**, *36*, 1163–1170.
- (22) Frounchi, M.; Farhadi, F.; Mohammadi, R. P. *Sci. Iran* **2002**, *9*, 86–92.
- (23) Capek, I. *Adv. Colloid Interface Sci.* **2001**, *91*, 295–334.
- (24) De Kock, J. B. L.; Van Herk, A. M.; German, A. L. *J. Macromol. Sci. Polym. Rev.* **2001**, *C41*, 199–252.
- (25) Garr, C. D.; Finke, R. G. *J. Am. Chem. Soc.* **1992**, *114*, 10440–10445.
- (26) Cole, A. G.; Yoder, L. M.; Shiang, J. J.; Anderson, N. A.; Walker, L. A.; Banaszak Holl, M. M.; Sension, R. J. *J. Am. Chem. Soc.* **2002**, *124*, 434–441.
- (27) Yoder, L. M.; Cole, A. G.; Walker, L. A.; Sension, R. J. *J. Phys. Chem. B* **2001**, *105*, 12180–12188.
- (28) Shiang, J. J.; Walker, L. A.; Anderson, N. A.; Cole, A. G.; Sension, R. J. *J. Phys. Chem. B* **1999**, *103*, 10532–10539.

- (29) Walker, L. A.; Shiang, J. J.; Anderson, N. A.; Pullen, S. H.; Sension, R. J. *J. Am. Chem. Soc.* **1998**, *120*, 7286–7292.
- (30) Grogan, T. G.; Bag, N.; Traylor, T. G.; Magde, D. *J. Phys. Chem.* **1994**, *98*, 13791–13796.
- (31) Van Dijk, H. K.; Van der Haar, J.; Stufkens, D. J.; Oskam, A. *Inorg. Chem.* **1989**, *28*, 75–81.
- (32) Knoll, H.; De Lange, W. J. G.; Hennig, H.; Stufkens, D. J.; Oskam, A. *J. Organomet. Chem.* **1992**, *430*, 123–132.
- (33) Balzani, V.; Scandola, F. In *Energy Resources Through Photochemistry and Catalysis*; Graetzel, M., Ed.; Academic Press: New York, 1983; pp 1–48.
- (34) Clark, C. D.; Hoffman, M. Z. *Coord. Chem. Rev.* **1997**, *159*, 359–373.
- (35) Berdzinski, S.; Horst, J.; Strassburg, P.; Strehmel, V. *ChemPhysChem* **2013**, *14*, 1899–1908.
- (36) Osawa, K.; Terazima, M.; Kimura, Y. *Chem. Phys. Lett.* **2013**, *564*, 21–25.
- (37) Okada, T.; Yago, T.; Takamasu, T.; Wakasa, M. *Phys. Chem. Chem. Phys.* **2012**, *14*, 3490–3497.
- (38) Nishiyama, Y.; Terazima, M.; Kimura, Y. *Chem. Phys. Lett.* **2010**, *491*, 164–168.
- (39) Khudyakov, I. V. *Res. Chem. Intermed.* **2013**, *39*, 781–804.
- (40) Xu, T.; Liu, Q.; Liu, Z.; Wu, J. *Energy Fuels* **2013**, *27*, 3148–3153.
- (41) Xu, J.; Weiss, R. G. *Photochem. Photobio. Sci.* **2005**, *4*, 210–215.
- (42) Cooper, H. L. R.; Groves, J. T. *Arch. Biochem. Biophys.* **2011**, *507*, 111–118.
- (43) Cooper, H. L. R.; Mishra, G.; Huang, X.; Pender-Cudlip, M.; Austin, R. N.; Shanklin, J.; Groves, J. T. *J. Am. Chem. Soc.* **2012**, *134*, 20365–20375.
- (44) Grause, G.; Karakita, D.; Ishibashi, J.; Kameda, T.; Bhaskar, T.; Yoshioka, T. *Polym. Degrad. Stab.* **2013**, *98*, 306–315.
- (45) Dondi, D.; Zeffiro, A.; Buttafava, A.; Marciano, C.; Bianchi, M.; Faucitano, A. *Polym. Degrad. Stab.* **2013**, *98*, 392–407.
- (46) Okamoto, M.; Tanaka, F. *J. Phys. Chem. A* **2006**, *110*, 10601–10606.

- (47) Bastos, E. L.; da Silva, S. M.; Baader, W. J. *J. Org. Chem.* **2013**, *78*, 4432–4439.
- (48) Das, R.; Dutta, B. K.; Maurino, V.; Vione, D.; Minero, C. *Environ. Chem. Lett.* **2009**, *7*, 337–342.
- (49) Houmam, A.; Hamed, E. M. *Phys. Chem. Chem. Phys.* **2012**, *14*, 113–124.
- (50) Perez-Benito, J. F. *Monatsh Chem.* **2013**, *144*, 49–58.
- (51) Khudyakov, I.; Zharikov, A. A.; Burshtein, A. I. *J. Chem. Phys.* **2010**, *132*, 014104/1.
- (52) Moscatelli, A.; Liu, Z.; Lei, X.; Dyer, J.; Abrams, L.; Ottaviani, M. F.; Turro, N. *J. Am. Chem. Soc.* **2008**, *130*, 11344–11354.
- (53) Abraham, S.; Ghosh, I.; Nau, W. M.; Chesta, C.; Pas, S. J.; Hill, A. J.; Weiss, R. G. *Photochem. Photobiol. Sci.* **2012**, *11*, 914–924.
- (54) Bhattacharjee, U.; Chesta, C. A.; Weiss, R. G. *Photochem. Photobiol. Sci.* **2004**, *3*, 287–295.
- (55) King, E. R.; Hennessy, E. T.; Betley, T. A. *J. Am. Chem. Soc.* **2011**, *133*, 4917–4923.
- (56) Paradine, S. M.; Griffin, J. R.; Zhao, J.; Petronico, A. L.; Miller, S. M.; Christina White, M. *Nat. Chem.* **2015**, *7*, 987–994.
- (57) An important point is that F_{CP} for a photochemically formed cage pair does not necessarily equal F_c for the same cage pair formed by thermolysis or by diffusional collision of two free radicals. In order to differentiate these cases, the photochemical cage effect is denoted F_{CP} .
- (58) Male, J. L.; Lindfors, B. E.; Covert, K. J.; Tyler, D. R. *J. Am. Chem. Soc.* **1998**, *120*, 13176–13186.
- (59) Nodelman, N.; Martin, J. C. *J. Am. Chem. Soc.* **1976**, *98*, 6597–6608.
- (60) Neuman, R. C. *J. Org. Chem.* **1972**, *37*, 495–496.
- (61) Owens, J.; Koenig, T. *J. Org. Chem.* **1974**, *39*, 3153–3154.
- (62) Lindfors, B. E.; Male, J. L.; Covert, K. J.; Tyler, D. R. *Chem. Commun.* **1997**, 1687–1688.
- (63) Male, J. L.; Yoon, M.; Glenn, A. G.; Weakley, T. J. R.; Tyler, D. R. *Macromolecules* **1999**, *32*, 3898–3906.

- (64) Oelkers, A. B.; Scatena, L. F.; Tyler, D. R. *J. Phys. Chem. A* **2007**, *111*, 5353–5360.
- (65) Oelkers, A. B.; Schutte, E. J.; Tyler, D. R. *Photochem. Photobiol. Sci.* **2008**, *7*, 228–234.
- (66) Oelkers, A. B.; Tyler, D. R. *Abstr. Pap. 229th ACS Natl. Meet. San Diego CA, March 13-17, 2005*, PHYS-331.
- (67) Covert, K. J.; Askew, E. F.; Grunkemeier, J.; Koenig, T.; Tyler, D. R. *J. Am. Chem. Soc.* **1992**, *114*, 10446–10448.
- (68) Schutte, E.; Weakley, T. J. R.; Tyler, D. R. *J. Am. Chem. Soc.* **2003**, *125*, 10319–10326.
- (69) Harris, J. D.; Oelkers, A. B.; Tyler, D. R. *J. Am. Chem. Soc.* **2007**, *129*, 6255–6262.
- (70) The trapping reaction is irreversible and a concentration of 2 M (~17.5 wt %) is sufficient to trap every free radical (see ref 67).
- (71) Ghose, R.; Fushman, D.; Cowburn, D. *J. Magn. Reson.* **2001**, *149*, 204–217.
- (72) In neat solutions (containing a natural abundance of ^1H) gradient attenuation of a signal (DOSY) gave reproducible results, whereas inversion recovery experiments (T_1) were hindered by large solvent peaks. Progressive saturation to measure T_1 is currently being explored.
- (73) Sekhar, A.; Latham, M. P.; Vallurupalli, P.; Kay, L. E. *J. Phys. Chem. B* **2014**, *118*, 4546–4551.
- (74) Waldeck, D. H. *Chem. Rev.* **1991**, *91*, 415–436.
- (75) Bowman, R. M.; Eissenthal, K. B. *Chem. Phys. Lett.* **1989**, *155*, 99–101.
- (76) Sun, Y. P.; Saltiel, J. *J. Phys. Chem.* **1989**, *93*, 8310–8316.
- (77) The use of either the translational or the rotational diffusion coefficients as an indicator of microviscosity is based on the observation that, in alkane solvents, the translational and rotational diffusion coefficients scale in a similar fashion to the chain length of the alkane.
- (78) Noyes, R. M. *J. Am. Chem. Soc.* **1955**, *77*, 2042–2045.
- (79) Noyes, R. M. *J. Am. Chem. Soc.* **1956**, *78*, 5486–5490.

- (80) $D = k_B T / 6\pi\eta_{\text{micro}} r$
- (81) Typical interpretations of the Stokes-Einstein equation are for bulk viscosity. It is generally agreed that for a pure solvent η and η_{micro} may be interchangeable. However, for a multicomponent solvent system it is important that D is for a particular molecule that experiences a particular microenvironment, η_{micro} .

CHAPTER III

- (1) Franck, J.; Rabinowitsch, E. *Trans. Faraday Soc.* **1934**, *30*, 120–130.
- (2) Rabinowitch, E. *Trans. Faraday Soc.* **1937**, *33*, 283–293.
- (3) Rabinowitch, E.; Wood, W. C. *Trans. Faraday Soc.* **1936**, *32*, 1381–1387.
- (4) Grissom, C. B.; Chagovetz, A. M. *Z. Phys. Chem.* **1993**, *182*, 181–188.
- (5) Lott, W. B.; Chagovetz, A. M.; Grissom, C. B. *J. Am. Chem. Soc.* **1995**, *117*, 12194–12201.
- (6) Griesser, M.; Dworak, C.; Jauk, S.; Hoefler, M.; Rosspeintner, A.; Grabner, G.; Liska, R.; Gescheidt, G. *Macromolecules* **2012**, *45*, 1737–1745.
- (7) Bosch, P.; Mateo, J. L.; Serrano, J. *J. Photochem. Photobiol. A* **1997**, *103*, 177–184.
- (8) Wolff, E.-H. P.; Bos, A. N. R. *Ind. Eng. Chem. Res.* **1997**, *36*, 1163–1170.
- (9) Frounchi, M.; Farhadi, F.; Mohammadi, R. P. *Sci. Iran* **2002**, *9*, 86–92.
- (10) Capek, I. *Adv. Colloid Interface Sci.* **2001**, *91*, 295–334.
- (11) De Kock, J. B. L.; Van Herk, A. M.; German, A. L. *J. Macromol. Sci. Polym. Rev.* **2001**, *C41*, 199–252.
- (12) Khudyakov, I. V.; Turro, N. J. *Des. Monomers Polym.* **2010**, *13*, 487–496.
- (13) Garr, C. D.; Finke, R. G. *J. Am. Chem. Soc.* **1992**, *114*, 10440–10445.
- (14) Meyer, J. W.; Hammond, G. S. *J. Am. Chem. Soc.* **1970**, *92*, 2187–2189.
- (15) Maleczka, R. E.; Geng, F. *J. Am. Chem. Soc.* **1998**, *120*, 8551–8552.
- (16) Tomooka, K.; Igarashi, T.; Nakai, T. *Tetrahedron* **1994**, *50*, 5927–5932.

- (17) Puri, M.; Biswas, A. N.; Fan, R.; Guo, Y.; Que, L. *J. Am. Chem. Soc.* **2016**, *138*, 2484–2487.
- (18) Woodward, J. R. *Prog. React. Kinet. Mech.* **2002**, *27*, 165–207.
- (19) Kaptein, R. *Adv. Free-Radic. Chem. London* **1975**, *5*, 319–380.
- (20) Chesta, C. A.; Mohanty, J.; Nau, W. M.; Bhattacharjee, U.; Weiss, R. G. *J. Am. Chem. Soc.* **2007**, *129*, 5012–5022.
- (21) Levin, P. P.; Efremkin, A. F.; Kasparov, V. V.; Khudyakov, I. V. *J. Phys. Chem. A* **2016**, *120*, 7484–7489.
- (22) Turro, N. J.; Zimmt, M. B.; Lei, X. G.; Gould, I. R.; Nitsche, K. S.; Cha, Y. *J. Phys. Chem.* **1987**, *91*, 4544–4548.
- (23) Hoijemberg, P. A.; Zerbs, J.; Reichardt, C.; Schwarzer, D.; Chesta, C. A.; Schroeder, J.; Aramendía, P. F. *J. Phys. Chem. A* **2009**, *113*, 5531–5539.
- (24) Berdzinski, S.; Horst, J.; Strassburg, P.; Strehmel, V. *ChemPhysChem* **2013**, *14*, 1899–1908.
- (25) Osawa, K.; Terazima, M.; Kimura, Y. *Chem. Phys. Lett.* **2013**, *564*, 21–25.
- (26) Okada, T.; Yago, T.; Takamasu, T.; Wakasa, M. *Phys. Chem. Chem. Phys.* **2012**, *14*, 3490–3497.
- (27) Nishiyama, Y.; Terazima, M.; Kimura, Y. *Chem. Phys. Lett.* **2010**, *491*, 164–168.
- (28) Khudyakov, I. V.; Serebrennikov, Y. A.; Turro, N. J. *Chem. Rev.* **1993**, *93*, 537–570.
- (29) Xu, J.; Weiss, R. G. *Photochem. Photobiol. Sci.* **2005**, *4*, 210–215.
- (30) Cooper, H. L. R.; Mishra, G.; Huang, X.; Pender-Cudlip, M.; Austin, R. N.; Shanklin, J.; Groves, J. T. *J. Am. Chem. Soc.* **2012**, *134*, 20365–20375.
- (31) Okamoto, M.; Tanaka, F. *J. Phys. Chem. A* **2006**, *110*, 10601–10606.
- (32) Xu, T.; Liu, Q.; Liu, Z.; Wu, J. *Energy Fuels* **2013**, *27*, 3148–3153.
- (33) Cooper, H. L. R.; Groves, J. T. *Arch. Biochem. Biophys.* **2011**, *507*, 111–118.
- (34) Grause, G.; Karakita, D.; Ishibashi, J.; Kameda, T.; Bhaskar, T.; Yoshioka, T. *Polym. Degrad. Stab.* **2013**, *98*, 306–315.

- (35) Dondi, D.; Zeffiro, A.; Buttafava, A.; Marciano, C.; Bianchi, M.; Faucitano, A. *Polym. Degrad. Stab.* **2013**, *98*, 392–407.
- (36) Bastos, E. L.; da Silva, S. M.; Baader, W. J. *J. Org. Chem.* **2013**, *78*, 4432–4439.
- (37) Das, R.; Dutta, B. K.; Maurino, V.; Vione, D.; Minero, C. *Environ. Chem. Lett.* **2009**, *7*, 337.
- (38) Houmam, A.; Hamed, E. M. *Phys. Chem. Chem. Phys.* **2011**, *14*, 113–124.
- (39) Perez-Benito, J. F. *Monatsh. Chem.* **2013**, *144*, 49–58.
- (40) Khudyakov, I.; Zharikov, A. A.; Burshtein, A. I. *J. Chem. Phys.* **2010**, *132*, 014104.
- (41) Moscatelli, A.; Liu, Z.; Lei, X.; Dyer, J.; Abrams, L.; Ottaviani, M. F.; Turro, N. *J. J. Am. Chem. Soc.* **2008**, *130*, 11344–11354.
- (42) Abraham, S.; Ghosh, I.; Nau, W. M.; Chesta, C.; Pas, S. J.; Hill, A. J.; Weiss, R. G. *Photochem. Photobiol. Sci.* **2012**, *11*, 914–924.
- (43) Bhattacharjee, U.; Chesta, C. A.; Weiss, R. G. *Photochem. Photobiol. Sci.* **2004**, *3*, 287–295.
- (44) King, E. R.; Hennessy, E. T.; Betley, T. A. *J. Am. Chem. Soc.* **2011**, *133*, 4917–4923.
- (45) Paradine, S. M.; Griffin, J. R.; Zhao, J.; Petronico, A. L.; Miller, S. M.; Christina White, M. *Nat. Chem.* **2015**, *7*, 987–994.
- (46) Khudyakov, I.; Levin, P.; Kuzmin, V. *Photochem. Photobiol. Sci.* **2008**, *7*, 1540–1543.
- (47) Levin, P.; Efremkin, A.; Khudyakov, I. *Photochem. Photobiol. Sci.* **2015**, *14*, 891–896.
- (48) It is important to note that our measurements are for a photochemical and not a thermal cage effect. The photochemical F_{CP} does not necessarily equal the thermal version F_c .
- (49) Koenig, T.; Fischer, H. *Free Radic.* **1973**, *1*, 157–189.
- (50) Lorand, J. P. *Prog. Inorg. Chem.* **1972**, *17*, 207–325.
- (51) Male, J. L.; Lindfors, B. E.; Covert, K. J.; Tyler, D. R. *J. Am. Chem. Soc.* **1998**, *120*, 13176–13186.

- (52) Harris, J. D.; Oelkers, A. B.; Tyler, D. R. *J. Organomet. Chem.* **2007**, *692*, 3261–3266.
- (53) Barry, J. T.; Berg, D. J.; Tyler, D. R. *J. Am. Chem. Soc.* **2016**, *138*, 9389–9392.
- (54) Nodelman, N.; Martin, J. C. *J. Am. Chem. Soc.* **1976**, *98*, 6597–6608.
- (55) Neuman, R. C. *J. Org. Chem.* **1972**, *37*, 495–496.
- (56) Owens, J.; Koenig, T. *J. Org. Chem.* **1974**, *39*, 3153–3154.
- (57) The determination of radical cage pair efficiencies typically requires arduous laboratory work. As an example, ¹⁸O labeling was required for monitoring cage efficiencies of diacetyl peroxide (see ref 58).
- (58) Martin, J. C.; Dombchik, S. A. *Adv. Chem. Ser.* **1968**, *75*, 269–281.
- (59) Covert, K. J.; Askew, E. F.; Grunkemeier, J.; Koenig, T.; Tyler, D. R. *J. Am. Chem. Soc.* **1992**, *114*, 10446–10448.
- (60) Lindfors, B. E.; Nieckarz, G. F.; Tyler, D. R.; Glenn, A. G. *J. Photochem. Photobiol. A* **1996**, *94*, 101–105.
- (61) Daglen, B. C.; Harris, J. D.; Dax, C. D.; Tyler, D. R. *Rev. Sci. Instrum.* **2007**, *78*, 074104/1-074104/4.
- (62) Wrighton, M. S.; Ginley, D. S. *J. Am. Chem. Soc.* **1975**, *97*, 4246–4251.
- (63) Tenhaeff, S. C.; Covert, K. J.; Castellani, M. P.; Grunkemeier, J.; Kunz, C.; Weakley, T. J. R.; Koenig, T.; Tyler, D. R. *Organometallics* **1993**, *12*, 5000–5004.
- (64) Harris, J. D.; Oelkers, A. B.; Tyler, D. R. *J. Am. Chem. Soc.* **2007**, *129*, 6255–6262.
- (65) Raiford, D. S.; Fisk, C. L.; Becker, E. D. *Anal. Chem.* **1979**, *51*, 2050–2051.
- (66) Deye, J. F.; Berger, T. A.; Anderson, A. G. *Anal. Chem.* **1990**, *62*, 615–622.
- (67) Sackett, D. L.; Wolff, J. *Anal. Biochem.* **1987**, *167*, 228–234.
- (68) Reichardt, C. *Chem. Rev.* **1994**, *94*, 2319–2358.
- (69) Khudyakov, I. V. *Res. Chem. Intermed.* **2013**, *39*, 781–804.

- (70) Noyes, R. M. *J. Chem. Phys.* **1955**, *23*, 1982.
- (71) Noyes, R. M. *J. Am. Chem. Soc.* **1956**, *78*, 5486–5490.
- (72) Male, J. L.; Lindfors, B. E.; Covert, K. J.; Tyler, D. R. *Macromolecules* **1997**, *30*, 6404–6406.
- (73) *CRC Handbook of Chemistry and Physics*, 82nd ed; Lide, D. R., Ed.; CRC Press: Boca Raton, 2001.
- (74) Dembo, M.; Glushko, V.; Aberlin, M. E.; Sonenberg, M. *Biochim. Biophys. Acta, Biomembr.* **1979**, *552*, 201–211.
- (75) Birks, J. B.; Lumb, M. D.; Munro, I. H.; Flowers, B. H.; S, F. R. *Proc. R. Soc. London Ser. A* **1964**, *280*, 289–297.
- (76) Abu-Zeid, M.-E. M. *Int. J. Quantum Chem.* **1972**, *6*, 279–293.
- (77) Smoluchowski, M. *Z. Phys. Chem.* **1918**, *92*, 129–168.
- (78) Oelkers, A. B.; Scatena, L. F.; Tyler, D. R. *J. Phys. Chem. A* **2007**, *111*, 5353–5360.
- (79) Terazima, M. *Acc. Chem. Res.* **2000**, *33*, 687–694.
- (80) Stickrath, A. B.; Carroll, E. C.; Dai, X.; Harris, D. A.; Rury, A.; Smith, B.; Tang, K.-C.; Wert, J.; Sension, R. J. *J. Phys. Chem. A* **2009**, *113*, 8513–8522.

CHAPTER IV

- (1) Levenson, R. A.; Gray, H. B. *J. Am. Chem. Soc.* **1975**, *97*, 6042–6047.
- (2) Harris, J. D.; Oelkers, A. B.; Tyler, D. R. *J. Organomet. Chem.* **2007**, *692*, 3261–3266.
- (3) Barry, J. T.; Berg, D. J.; Tyler, D. R. *J. Am. Chem. Soc.* **2017**, *139*, 14399–14405.
- (4) Covert, K. J.; Askew, E. F.; Grunkemeier, J.; Koenig, T.; Tyler, D. R. *J. Am. Chem. Soc.* **1992**, *114*, 10446–10448.
- (5) Wrighton, M. S.; Ginley, D. S. *J. Am. Chem. Soc.* **1975**, *97*, 4246–4251.
- (6) Daglen, B. C.; Harris, J. D.; Dax, C. D.; Tyler, D. R. *Rev. Sci. Instrum.* **2007**, *78*, 074104/1-074104/4.

- (7) Turro, N. J.; Scaiano, J. C.; Ramamurthy, V.; more, & O. *Principles of Molecular Photochemistry: An Introduction*, 1st edition.; University Science Books: Sausalito, Calif, 2008.
- (8) Oelkers, A. B.; Scatena, L. F.; Tyler, D. R. *J. Phys. Chem. A* **2007**, *111*, 5353–5360.

CHAPTER V

- (1) Wrighton, M. S.; Ginley, D. S. *J. Am. Chem. Soc.* **1975**, *97*, 4246–4251.
- (2) Covert, K. J.; Askew, E. F.; Grunkemeier, J.; Koenig, T.; Tyler, D. R. *J. Am. Chem. Soc.* **1992**, *114*, 10446–10448.
- (3) Tenhaeff, S. C.; Covert, K. J.; Castellani, M. P.; Grunkemeier, J.; Kunz, C.; Weakley, T. J. R.; Koenig, T.; Tyler, D. R. *Organometallics* **1993**, *12*, 5000–5004.
- (4) Coolbaugh, T. S.; Coots, R. J.; Santarsiero, B. D.; Grubbs, R. H. *Inorganica Chimica Acta* **1985**, *98*, 99–105.
- (5) Tenhaeff, S. C.; Tyler, D. R. *Organometallics* **1991**, *10*, 473–482.
- (6) Male, J. L.; Lindfors, B. E.; Covert, K. J.; Tyler, D. R. *J. Am. Chem. Soc.* **1998**, *120*, 13176–13186.
- (7) Noyes, R. M. *J. Am. Chem. Soc.* **1956**, *78*, 5486–5490.
- (8) Noyes, R. M. *J. Chem. Phys.* **1955**, *23*, 1982.
- (9) Stickrath, A. B.; Carroll, E. C.; Dai, X.; Harris, D. A.; Rury, A.; Smith, B.; Tang, K.-C.; Wert, J.; Sension, *J. Phys. Chem. A*, **2009**, *113*, 8513–8522.
- (10) Brady, S. The Synthesis of Linear and Nonlinear Photosensitive Organometallic Polymers Containing Mo-Mo Bonds: Evaluating the Effectiveness of Click Chemistry. **2013**.
- (11) Straub, T.; Haukka, M.; Pakkanen, T. A. *J. Organomet. Chem.* **2000**, *612*, 106–116.
- (12) Straub, T.; Haukka, M.; Brunner, M.; Koskinen, A. M. P.; Pakkanen, T. A. *J. Organomet. Chem.* **2005**, *690*, 674–677.
- (13) Tenhaeff, S. C.; Tyler, D. R. *Organometallics* **1991**, *10*, 1116–1123.

- (14) Beck Wolfgang; Schloter Klaus; Sünkel Karlheinz; Urban Günter; Forschner Thomas; Todaro Alicia; Cutler Alan. *Inorganic Synth.* **2007**.
- (15) Song, J. S.; Bullock, R. M.; Creutz, C. *J. Am. Chem. Soc.* **1991**, *113*, 9862–9864.

CHAPTER VI

- (1) Anslyn, E. V.; Dougherty, D. A. *Modern Physical Organic Chemistry*; University Science Books: Sausalito, CA, 2006.
- (2) Lyon, R. K.; Levy, D. H. *J. Am. Chem. Soc.* **1961**, *83*, 4290–4290.
- (3) Oelkers, A. B.; Schutte, E. J.; Tyler, D. R. *Photochem. Photobiol. Sci.* **2008**, *7*, 228.
- (4) Oelkers, A. B.; Tyler, D. R. *Photochem. Photobiol. Sci.* **2008**, *7*, 1386–1390.
- (5) Barry, J. T.; Berg, D. J.; Tyler, D. R. *J. Am. Chem. Soc.* **2016**, *138*, 9389–9392.
- (6) Barry, J. T.; Berg, D. J.; Tyler, D. R. *J. Am. Chem. Soc.* **2017**, *139*, 14399–14405.
- (7) Covert, K. J.; Askew, E. F.; Grunkemeier, J.; Koenig, T.; Tyler, D. R. *J. Am. Chem. Soc.* **1992**, *114*, 10446–10448.
- (8) Meyer, T. J.; Caspar, J. V. *Chem. Rev.* **1985**, *85*, 187–218.
- (9) Oelkers, A. B.; Scatena, L. F.; Tyler, D. R. *J. Phys. Chem. A* **2007**, *111*, 5353–5360.
- (10) Cox, B. G. *Modern Liquid Phase Kinetics*, 1 edition.; Oxford University Press: Oxford ; New York, 1994.
- (11) Zhang, X.; Meng, D.; Li, X.; Meng, L.; Sun, Z. *J. Organomet. Chem.* **2014**, *769*, 106–111.

APPENDIX B

- (1) Wrighton, M. S.; Ginley, D. S. *J. Am. Chem. Soc.* **1975**, *97*, 4246–4251.
- (2) Male, J. L.; Lindfors, B. E.; Covert, K. J.; Tyler, D. R. *J. Am. Chem. Soc.* **1998**, *120*, 13176–13186.
- (3) Braden, D. A. Ph.D. Dissertation, University of Oregon, 2000.

- (4) Aroney, M. J.; Clarkson, R. M.; Klepetko, R. J.; Masters, A. F.; Pierens, R. K. *J. Organomet. Chem.* **1990**, *393*, 371–378.
- (5) Armarego, W. L.; Chai, C. *Purification of Laboratory Chemicals*, 4th edition.; Butterworth-Heinemann: Oxford; Boston, 1997.
- (6) Raiford, D. S.; Fisk, C. L.; Becker, E. D. *Anal. Chem.* **1979**, *51*, 2050–2051.
- (7) Daglen, B. C.; Harris, J. D.; Dax, C. D.; Tyler, D. R. *Rev. Sci. Instrum.* **2007**, *78*, 074104/1–074104/4.

APPENDIX C

- (1) Barry, J. T.; Berg, D. J.; Tyler, D. R. *J. Am. Chem. Soc.* **2016**, *138*, 9389–9392.
- (2) Armarego, W. L. .; Chai, C. *Purification of Laboratory Chemicals*, 4th edition; Butterworth-Heinemann: Oxford; Boston, 1997.
- (3) Greenspan, P.; Mayer, E. P.; Fowler, S. D. *J. Cell Biol.* **1985**, *100*, 965–973.